183(4), 2020

COMBUSTION ENGINES

Łukasiewicz
Instytut Pojazdów
Szynowych
TABOR

Instytut badawczy branży taboru szynowego z dumą budowany na wiedzy i doświadczeniu pracowników oraz nowoczesnych zasobach technicznych

Badania i certyfikacja

Systemy sterowania

Projekty B+R+I

Pojazdy dwudrogowe

Usuwanie barier w mobilności

Standaryzacja i unifikacja taboru

Rozwój konstrukcji pojazdów hybrydowych

Efektywność energetyczna i ekologiczna pojazdów

Bezpieczeństwo transportu kolejowego

www.tabor.lukasiewicz.gov.pl
www.facebook.com/IPSTABOR
sekretariat@tabor.lukasiewicz.gov.pl
+48 61 653 40 01

PTNSS Supporting Members
Członkowie wspierający PTNSS

BOSMAL Automotive Research and Development Institute Ltd
Instytut Badań i Rozwoju Motoryzacji BOSMAL Sp. z o.o

Motor Transport Institute
Instytut Transportu Samochodowego

Institute of Aviation
Sieć Badawcza Łukasiewicz – Instytut Lotnictwa

Automotive Industry Institute
Sieć Badawcza Łukasiewicz – Przemysłowy Instytut Motoryzacji

The Rail Vehicles Institute TABOR
Sieć Badawcza Łukasiewicz – Instytut Pojazdów Szynowych TABOR

Industrial Institute of Agricultural Engineering
Sieć Badawcza Łukasiewicz – Przemysłowy Instytut Maszyn Rolniczych

AVL List GmbH

Solaris Bus & Coach S.A.

Air Force Institute of Technology
Instytut Techniczny Wojsk Lotniczych

Toyota Motor Poland Ltd. Sp. z o.o.

Military Institute of Armoured & Automotive Technology
Wojskowy Instytut Techniki Pancernej i Samochodowej

COMBUSTION ENGINES

A Scientific Magazine

2020, 183(4)

Year LIX

PL ISSN 2300-9896
PL eISSN 2658-1442

Editor:
Polskie Towarzystwo Naukowe Silników Spalinowych
43-300 Bielsko-Biała, Sarni Stok 93 Street, Poland
tel.: +48 33 8130402, fax: +48 33 8125038
E-mail: sekretariat@ptnss.pl
WebSite: http://www.ptnss.pl
Papers available on-line: http://combustion-engines.eu

Contents

Declaration of the original version
The original version of the Combustion Engines journal is the printed version.

Editorial:
Institute of Combustion Engines and Powertrains
Poznan University of Technology
60-965 Poznan, Piotrowo 3 Street
tel.: +48 61 2244505, +48 61 2244502
E-mail: papers@ptnss.pl

Prof. Jerzy Merkisz, DSc., DEng.
(Editor-in-chief)
Miłosław Kozak, DSc., DEng.
Prof. Jacek Pielecha, DSc., DEng.
(Editorial Secretary for Science)
Prof. Ireneusz Pielecha, DSc., DEng.
Wojciech Cieślik, DEng.
(Technical Editors)
Joseph Woodburn, MSci
(Proofreading Editor)
Wojciech Serdecki, DSc., DEng.
(Statistical Editor)
and Associate Editors

Editor
Polish Scientific Society of Combustion Engines
43-300 Bielsko-Biała, Sarni Stok 93 Street, Poland
tel.: +48 33 8130402, fax: +48 33 8125038
E-mail: sekretariat@ptnss.pl
WebSite: http://www.ptnss.pl

Subscriptions
Send subscription requests to the Publisher's address.
Cost of a single issue PLN 30 + VAT.

Preparation for print
ARS NOVA Publishing House
60-782 Poznań, Grunwaldzka 17/10A Street

Circulation: 100 copies

Printing and binding

Zakład Poligraficzny Moś i Łuczak, sp. j.,
Poznań, Piwna 1 Street

The journal is registered in the Polish technical journals content database – **BAZTECH** www.baztech.icm.edu.pl

The journal is listed in the international database **IC Journal Master List** – **Index Copernicus** www.indexcopernicus.com

Papers published in the
Combustion Engines
quarterly receive 20 points as stated by the Notification of the Minister of Science and Higher Education dated 31 July 2019.

Cover
I – Harley-Davidson Screamin' Eagle 131 Softail Engine (*fot. www.totalmotorcycle.com*); background (abstract-cool-orange-texture – *www.123freevectors.com*)
IV – Maserati Nettuno – Twin-Combustion Engine (*fot. it.motor1.com*)

Article citation info:
PIELECHA, I. Control algorithms for a Range Extender vehicle with an combustion engine. *Combustion Engines*. 2020, **183**(4), 3-10. https://doi.org/10.19206/CE-2020-401

Ireneusz PIELECHA

CE-2020-401

Control algorithms for a Range Extender vehicle with an combustion engine

The combination of two drive sources: the internal combustion engine and the electric motor in the hybrid drive system requires an appropriate control system to manage their operation. It relies on many variables, and the greater the degree of drive hybridization the greater is the degree of interdependence of the parameters involved. The article presents solutions of electric drive control algorithms with an additional power source in the form of an internal combustion engine (Range Extender). The results of simulation analyzes in the AVL Cruise program are presented, taking into account three control algorithms and two driving cycles. The obtained results indicate the necessity to take various input quantities into account in order to optimize the use of the combustion engine.

Key words: *control algorithms, Range Extender, electric motor, combustion engine, battery system*

1. Introduction

Battery electric vehicles (BEV), at present, do not constitute a large group of vehicles in operation, due to their limited range. However, their share in the overall number of means of transport continues to increase [9]. A partial solution to the limited range problem is the use of range extender systems (REX or Range-Extended Electric Vehicle – REEV) in the form of an internal combustion engine (coupled with an electric generator) or a fuel cell (producing electricity) to recharge the batteries [1]. Range extenders are built as series drivetrains in hybrid systems.

For longer distances, REVs utilize the ICE to keep the battery charged, but consume noticeably less fuel than conventional ICEVs for the following two reasons [4]:

– The engine of an E-REV is significantly smaller than that of a conventional ICEV – it only needs to meet average power demands because peak power is delivered by the battery pack. The engine of an ICEV, on the other hand, must also cover peak-power surges, e.g. accelerations.
– The engine of an E-REV operates at a constant, highly efficient, rotation speed; whereas that of an ICEV often runs at low or high rotation speeds during which, in both situations, its efficiency is low.

There are currently attempts to use microturbines [6] and Wankel engines powered by gasoline [14] or hydrogen [15] in range extender systems.

Traditional control of the battery charging system in hybrid drive systems (without *plug-in* technology) maintained a fairly narrow range of changes in the state of charge (SOC). The use of a *plug-in* system increases the discharge range of the battery (Fig. 1), but at the same time requires the use of higher capacity batteries.

In such a system, the batteries can operate in two modes: typical discharge mode (CD – *charge depleting*) and sustained charge mode (CS – *charge sustaining*).

The first battery mode is applicable when the internal combustion engine is not used (driving in electric mode). The second mode, after discharging to the minimum value set by the controller, keeps the batteries low. This reduces the fuel consumption of the internal combustion engine, ensuring SOC values that are compatible with the combustion engine and the electric motor.

Thanks to the two operating modes, it is possible to use the available battery capacity to a greater extent, and the sustained battery charge level (DOD – *depth on discharge*) – much lower than in traditional hybrid drive systems.

2. Range Extender drive system control conditions

Controlling series hybrid drive systems (such as the REX drive) is much simpler than controlling a parallel or mixed hybrid drive. Currently, there are many methods used for controlling such systems. The simplest solution is to turn on the internal combustion engine within a certain range of battery SOC changes. In REX systems, high battery discharge is maintained in the CS – charge sustaining mode. The discharge value ranges from 25% to even 13% [5].

A simplified representation of such control was presented by Jeong [5], who divided the operating range into four modes:

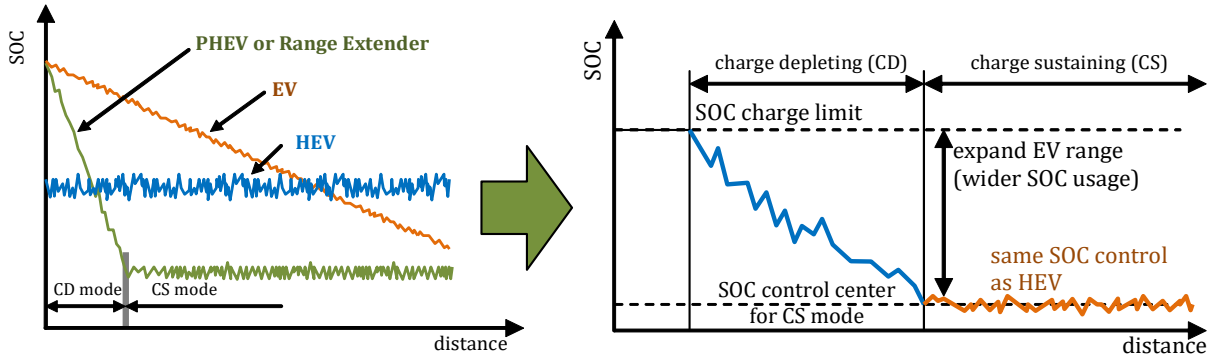

Fig. 1. Range Extender powertrain batteries discharge against purely electric (EV) and hybrid (HEV) drive modes [10, 13]

Received 25 July 2020; Received in revised form 25 August 2020; Accepted 25 August 2020
Available online 20 December 2020

1. Charge depletion – the range extender does not activate and the battery state of charge (SOC) is permitted to deplete without assistance except through brake regeneration.
2. Charge sustain – state of charge high.
3. Charge sustain – state of charge medium
4. Charge sustain – state of charge low.

Diversified SOC level (in the above operating ranges) leads to changes in the internal combustion engine operation: greater discharge results in increased engine speed and higher load values.

The analysis of the economic viability of the BMW i3 drive with an internal combustion engine system was conducted by Boretti [3]. Putting together several generations of the vehicle, the BMW i3 decided that the REX solution makes sense only when covering distances longer than the electric range. He showed that in the case of the BMW i3 BEV, increasing the battery's electrical capacity by 1 Ah translates into a range reduction of 0.88 km (0.55 miles) due to the increase in vehicle weight by 9.97 kg. While equipping an internal combustion engine into the BMW i3 increases its weight by 122.5 kg.

Although Range Extender drive systems have been available for several years, their operating strategies should still be verified. It is particularly important in the aspect of regenerative braking [7], as well as for the analysis of exhaust emissions and fuel consumption [8, 12].

3. Research aim

The analysis of the REX type drives presented in the article indicates their great diversity (in the form of the use of a battery and a secondary source of power, such as an internal combustion engine). The aim of this article is to determine the differences in the operating conditions of the internal combustion engine with the use of various control algorithms in various vehicle driving conditions.

4. Method

4.1. Test vehicle

The object of the research was a vehicle model whose characteristic parameters were presented in Table 1.

Table 1. Parameters characterizing the test vehicle with the internal combustion engine

Parameter	Unit	Value
Wheelbase	mm	2467
Frontal surface	m^2	1.97
Mass	kg	1700
Combustion engine type		3-cylinder SI, naturally aspirated
Fuel type	–	gasoline
Stroke volume	cm^3	800
Torque – Mo	Nm/rpm	95/4200
Power – Ne	kW/rpm	51.4/5780

It was assumed that the vehicle drive system should meet the following assumptions:

1. Electric motor with a maximum torque of 240 Nm at a rotational speed of 3000 rpm.
2. Generator adapted to work in line with the combustion engine: both with a torque of approximately 100 Nm in the rotational range of 3000–4000 rpm. This was assumed as a rotational speed that allows applying a significant load on both the generator and the internal combustion engine.

A 3-cylinder combustion engine with a displacement of 800 cm^3 was chosen, the characteristics of which are shown in Fig. 2. Additionally, the characteristics of the electric motor and generator were also presented in that figure.

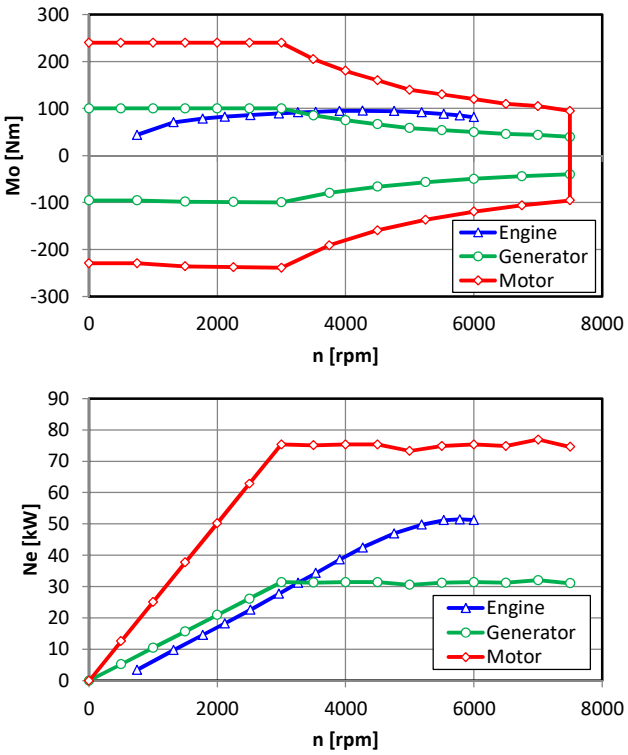

Fig. 2. Characteristics of the electric motor, generator and engine: a) torque, b) power

The selection of the battery was guided by the analysis of modern solutions used in such systems. Several batteries were analyzed from among which Li-Ion LNMCO cells ($LiNi_1/3Mn_1/3Co_1/3O_2$ – Lithium-Nickel-Mangan-Cobalt) [16] with parameters presented in Table 2 were selected.

Table 2. Technical parameters of the LNMCO batteries

Parameter	Unit	Value
Max charge	Ah	30
Nominal voltage	V	3.7
Maximum voltage	V	4.15
Minimum Voltage	V	3.4
Number of cells per row	pcs	80
Number of cells rows	pcs	1
Internal charge/discharge resistance	mOhm	1.5/1.4

4.2. Driving cycles

Research analyzes on the use of the internal combustion engine (and its operating conditions) were carried out using two standardized routes:

– in a NEDC test,
– in a WLTC test.

Characteristic parameters of these research tests were provided in Table 3.

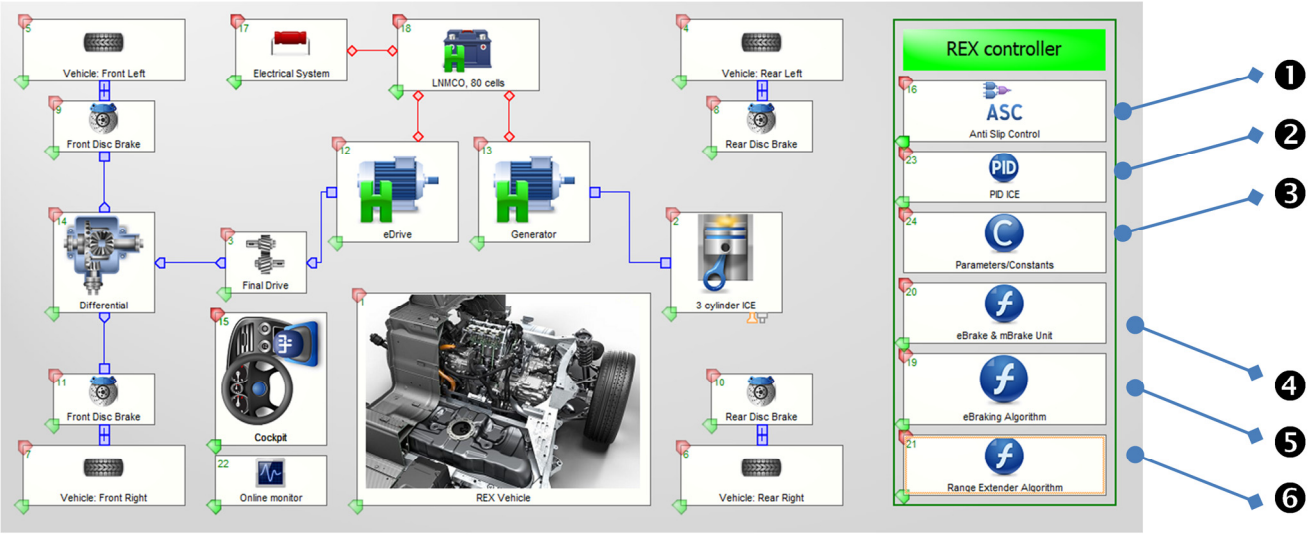

Fig. 3. Schematics of the analyzed REX type drive system

Table 3. Comparison of research tests used in simulations [11]

Parameter	NEDC Test	WLTC Test
Test cycle	Single test cycle	Dynamic cycle
Cycle time	1180 s	1800 s
Cycle distance	11 km	23.25 km
Average speed	34 km/h	46.5 km/h
Maximum speed	120 km/h	131 km/h
Driving phases	2 phases, 66% urban, 34% non-urban driving	4 phases, overall: 52% urban, 46% non-urban

5. Simulation model and REX drive system control

The REX drive simulation tests were carried out using the AVL Cruise software [2]. The program implements individual elements of the Range Extender drive system, assigning appropriate functions to the mechanical and electrical elements included in the simulation. Visualization of the mechanical and electrical diagram is shown in Fig. 3.

In addition to the typical elements of the drive system also the parameters controlling such a system were considered (shown in Fig. 3 on the right).

❶ **Anti Slip Control (ASC) system**. The system controls wheel slip by adjusting the torque value on each wheel separately. At first, the wheel with the highest value for the load transmitting factor (T_F) is selected.

$$T_F = \frac{F_L}{\mu \cdot F_N} \tag{1}$$

where: F_L – driving force, F_N – downwards force, μ – friction coefficient.

If this value greater than 1, the anti-slip control is activated and the load position will be reduced as long as the wheels have slip conditions (Fig. 4).

Fig. 4. Load transmission factor [2]

❷ **Internal combustion engine PID controller (PID ICE).** It is a regulator system that adjusts the changes in the engine speed to the set values.

The difference between target value and actual value is calculated by

$$\Delta C = C_{PID,des} - C_{PID,act} \tag{2}$$

If there is a limitation of the actual value by definition of a lower limit, the sign of ΔC is changed.

The controller output is defined by

$$C_{PID,out} = C_{PID.P} \cdot \Delta C + \\ + C_{PID.I} \cdot \int_0^t \Delta C(t)dt + \\ + C_{PID.D} \cdot \frac{d(\Delta C)}{dt} \tag{3}$$

In the current example: P = 10; I = 0 s; D = 1e–4 s^{-1}, thus

$$C_{PID,out} = C_{PID.P} \cdot \Delta C + C_{PID.D} \cdot \frac{d(\Delta C)}{dt} \tag{4}$$

❸ **Parameters/Constants**. The module contains values that limit process variables or typical constant values. There are, among others, quantities determining the battery state of charge (SOC), maximum pressure in the braking system and braking coefficients (front – BFF; rear – BFR) constituting a component of the braking torque:

$$M_B = 2p_B \cdot A_B \cdot \eta_B \cdot \mu_B \cdot r_B \cdot c_B \tag{5}$$

$$BFF = 2 \cdot A_{BF} \cdot \eta_{BF} \cdot \mu_{BF} \cdot r_{BF} \cdot c_{BF} \tag{6}$$

$$BFR = 2 \cdot A_{BR} \cdot \eta_{BR} \cdot \mu_{BR} \cdot r_{BR} \cdot c_{BR} \tag{7}$$

where: p_B – braking system pressure, A_B – the brake cylinder area; the area of the hydraulic cylinder (front – A_B = = 1800 mm^2; rear – A_B = 1500 mm^2, η_B – the efficiency considers the effects of the conversion of the hydraulic into the mechanical part of the brake (η_B = 0.99), m_B – the friction coefficient is between the brake drum, and respectively the friction disc or the brake shoes (m_B = 0.25), r_B – the radius where the braking force applies (front – r_B = 130 mm; rear – r_B = 110 mm), c_B – the specific brake factor is

a factor that depends on the design of the brake (disc brakes $c_B = 1$; drum brakes $c_B > 1$).

An overview of the values indicated above is presented in Table 4.

Table 4. Examples of values of parameters and constants

Parameter	Value	Unit	Method of determination
Brake factor front (BFF)	0.00011583	–	Equation (6)
Brake factor rear (BFR)	0.000081675	–	Equation (7)
SOC_{min}	13.5	%	Taken arbitrarily
SOC_{max}	16.0	%	Taken arbitrarily
Max brake pressure (BP_{max})	50	bar	Taken from [2]

❹ **eBrake & mBrake Unit**. The algorithm determines the conditions for the transition from eDrive to eBrake (Front & Rear). When calculating the braking torque of the electric motor (M_{EM}), one should take into account the gear ratio in the main gear ($i_{FD} = 6.21$) as well as the gear ratio in the gearbox (not present in this case; $i_G = 1$). Determining from equation (5) and using the i_{FD} gear ratio the current pressure in the brake system is calculated as:

$$p_B = \frac{M_{EM} \cdot i_{FD} \cdot i_G}{2 p_B \cdot A_B \cdot \eta_B \cdot \mu_B \cdot r_B \cdot c_B} \tag{8}$$

and taking the indicators of BFF (equation (6)) and BFR (equation (7)) as the sum of the braking coefficients:

$$p_B = \frac{M_{EM} \cdot i_{FD}}{BFF + BFR}. \tag{9}$$

the equivalent of the pressure in the braking system is obtained, which can be converted into electric braking (energy recuperation). If electric motor braking is used, then p_B (i.e. eBrake) takes negative values (negative torque value). In this case, electric braking will be used first, and if the braking performance requires additional pressures, then braking with the use of the hydraulic system will take place. If $M_{EM} > 0$, this motor transmits positive torque to the wheels of the vehicle.

❺ **eBraking Algorithm**. The algorithm determines the conditions for the transition from eDrive to eBrake. The necessary condition for the use of regenerative braking is the simultaneous fulfillment of two relationships (increase in pressure in the brake system and vehicle speed above a certain value):

$$\text{Brake Pressure} > 0 \text{ and Vehicle velocity} > 0.1 \text{ km/h} \tag{10}$$

In this case, braking is initiated, the control signal of which (activating the hydraulic braking) is defined as the ratio of the current brake pressure – BR to the maximum system pressure BR_{max}:

$$y = \frac{BR}{BR_{max}} \tag{11}$$

❻ **Range Extender Algorithm**. The last part of the REX drive control system concerns the algorithms for determining the internal combustion engine start-up algorithm. Three internal combustion engine operation algorithms have been implemented in the simulation program:

1. enabling the combustion engine to be started at one chosen operating point (n = 3000 rpm and Mo = 0.6 Mo_{max}) whenever the battery discharge level reaches the value of $SOC_{act} < SOC_{min}$; charging ends after reaching SOC_{max};
2. taking into account the first case, but also including the shutdown of the internal combustion engine, when the drive system experiences zero load (vehicle braking and no-load operation, such as at standstill);
3. algorithm depending on battery SOC and vehicle speed: after achieving $SOC_{act} < SOC_{min}$ the internal combustion engine operating conditions depend on the vehicle speed: based on three speed ranges (the boundary points between these ranges are at 20 km/h and 70 km/h); for which the internal combustion engine load changes at constant rotational speed, to 0.4; 0.6 and 0.8 Mo_{max}.

The block diagram of these algorithms is shown in Fig. 5.

Additionally, in order to secure a significant decrease in the battery SOC, a critical SOC restriction has been established. If the $SOC_{cr} < 13\%$ condition is met, the combustion engine will also be started: for mode 1 and 2 with standard settings, for mode 3 – the maximum settings contained in Fig. 5.

6. Testing the control algorithms in driving tests

6.1. Battery operating conditions and the function of the drive system control algorithms

The drive system tests were carried out on two test routes: for NEDC and WLTC.

By using a Li-Ion battery it becomes possible for the system to work in both CD and CS mode (shown in Fig. 1). The battery discharge (CD) mode is typical for electric vehicles. The study analyzed the battery recharging in the CS mode, therefore the initial value of the battery charge level was set at 15%. It is a value between SOC_{min} and SOC_{max}. The conditions of the algorithms' operation cause the recharging to start when the charge level drops below the minimum value.

6.2. Drive system operating conditions

The preliminary analysis of the test routes showed a much higher dynamics in the drive parameters in the WLTC test than in the NEDC test (Fig. 6). With similar maximum speeds in both tests, the typical NEDC acceleration was 0.7–1 m/s^2 (maximum – 1.1 m/s^2) – Fig. 6a. In the WLTC test, the maximum acceleration was slightly lower, amounting to 0.9–1 m/s^2. This was reflected in the operating conditions of the electric (drive) motor. In the NEDC test, the maximum torques were higher (up to 150 Nm, with M_{omax} = = 240 Nm) compared to the WLTC test (up to 100 Nm). However, the dynamics of torque value changes was greater during the WLTC test (Fig. 6b). Characteristically, during the regenerative braking, similar loads were obtained in both tests (about 75 Nm). In the WLTC test, speed values above 70 km/h were much more frequent than in the NEDC test, which indicates that the proposed drive system control algorithms should have a greater relevance in this test.

Data presented in Fig. 7 confirmed the presence of higher engine load values in the NEDC test. The electric motor worked in the first quadrant of the Mo–n characteristic, as a current generator – in the second quadrant. The

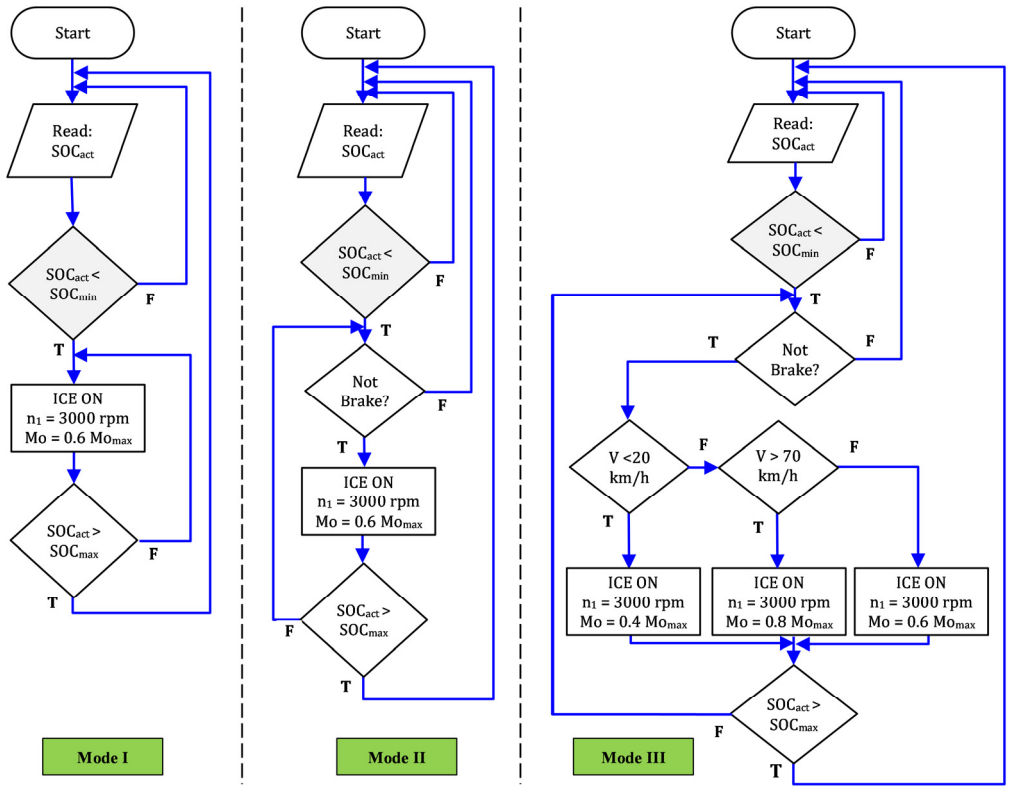

Fig. 5. The adopted control algorithms for the REX drive system

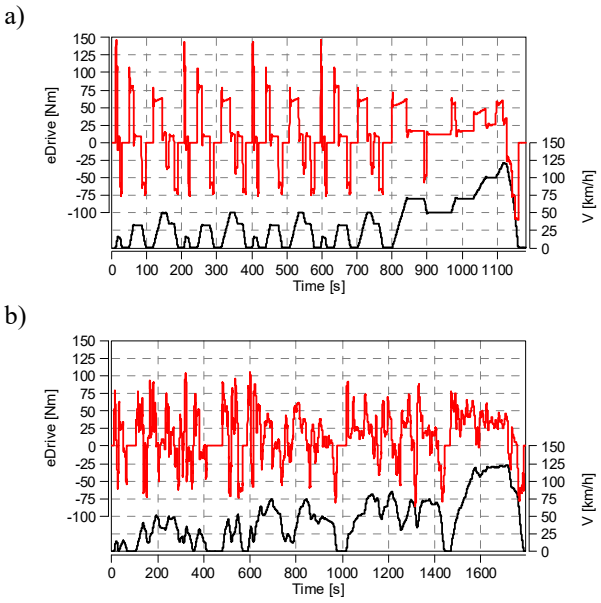

Fig. 6. The electric drive motor torque and vehicle speed characteristics obtained in the tests: a) NEDC, b) WLTC

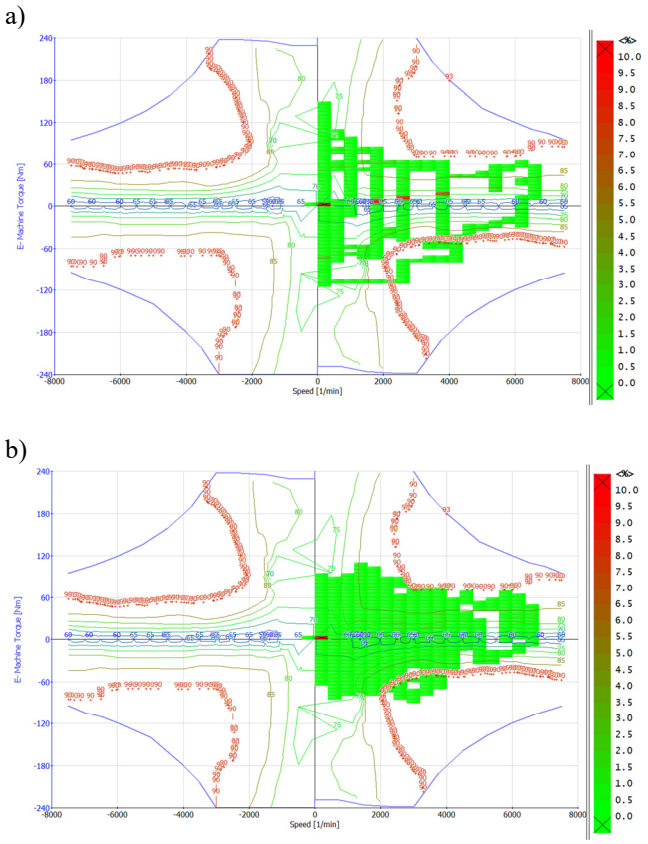

Fig. 7. Electric motor load : a) in the NEDC, b) in the WLTC

density of this engine's operating points in the WLTC test (Fig. 7b) showed significantly greater changes in its operation than in the NEDC test. Additionally, the adopted characteristics of the motor indicated that its use is in the efficiency range below 90%. This may indicate increased battery power consumption values. It follows that in selected tests the used combustion engine was too big (in terms of its torque and power). Operation of the vehicle in real conditions may result in the engine working within its high efficiency range. In both cited cases, the use of the braking torque in the efficiency range above 90% was observed,

which should indicate energy recovery with high efficiency of the engine's operation as a generator.

6.3. Comparative analysis of vehicle energy consumption

NEDC test

The following aspects were analyzed in the simulation: SOC, electric motor power, electric energy consumption and signals of the generator load (relative load) coupled with the internal combustion engine.

SOC analysis shows charging to SOC_{max} = 15% in the case of the first algorithm (mode I). As a result, the combustion engine was still running despite braking (Fig. 8). This indicates using the full allowable SOC range. However, the disadvantage of this solution was the much longer single use of the internal combustion engine.

The modified algorithm (mode II) contains a function that allows turning the internal combustion engine off when $SOC_{act} > SOC_{min}$ and vehicle braking occurs. Then the SOC does not need to reach the SOC_{max}. This means that regenerative braking takes priority over the operation of the internal combustion engine. On the other hand, such a strategy caused the actual battery charge range to decrease and the internal combustion engine had to operate more often. Such conditions could also be observed in Fig. 8, when the internal combustion engine was used much more often than during the operation in mode I.

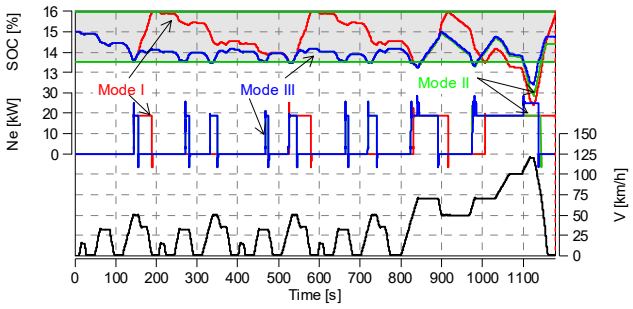

Fig. 8. Changes in SOC and internal combustion engine power in the NEDC test

Mode III places a differential load values on the internal combustion engine and the power generator during battery charging. As shown in Fig. 5, these values depend on the vehicle speed. This has a bearing on the discharge rate of the battery. Due to the low speed obtained during braking with the vehicle in the NEDC test, the first variant was practically not observed (low load of the combustion engine and generator at speeds below 20 km/h). However, in the case of high speed in this test, the use of an increased load on the battery charging system (internal combustion engine and generator) was observed in the final part of the test. Despite the different charging strategies, a significant drop in SOC at high driving speeds was observed. The introduced limitation in the form of SOC < 13% (which caused the combustion engine to always be on) – did not meet the conditions of maintaining SOC at the level of 13%. This was a result of, among others, the high energy consumption and different operating conditions of the internal combustion engine and generator in this respect (control mode I and II do not apply varied load values to the internal combustion engine).

Analyzing the current flow and electric energy consumption, a significant recharging of the battery was observed during the operation of the internal combustion engine, taking into account the first mode (red curve – electrical consumption – in Fig. 9). Where negative consumption values indicate current generation. This value was about 0.1 kWh and occurred in three instances of the combustion engine operation. Although a fourth such occurrence for the combustion engine begins to take place at t = = 1010 s, the demand was not compensated by the operation of the engine. Only after starting braking at 125 km/h, the increased recharge of the battery was observed. This means that such an approach, despite the initial recharging, does not provide an effective solution for ensuring a sufficient battery charge level.

Due to the only slightly differentiated algorithms of modes II and III, the NEDC test lacks significant changes in battery charging. The differences are discernable only at the end of the NEDC test.

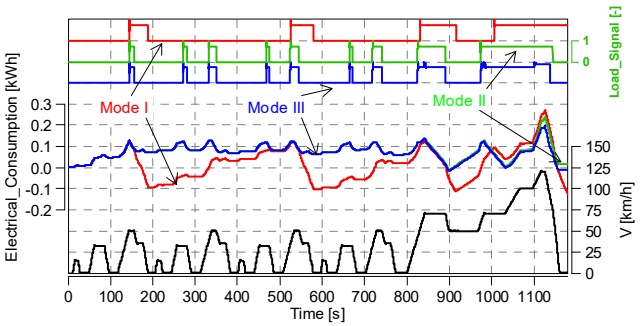

Fig. 9. Internal combustion engine load and electric energy consumption in the NEDC test

A summary of the above analyzes was reflected in the summary of SOC changes in the entire test (Table 5). It takes into account the battery charge limits in the NEDC test. The comparison shows that neither of the strategies was effective in reducing the battery energy level drop in the case of high driving speeds (related to high energy demand of the drive system). However, the smallest changes (the smallest SOC value drops) could be observed when using the algorithm in which the generator load keeps up with the changes in the battery SOC. In the case of mode I, a large SOC "margin" was obtained, but the fall below the critical value was also the largest. This means large fluctuations in the SOC value, which can significantly shorten the battery lifespan.

Table 5. SOC changes in the NEDC test in terms of different drive system control algorithms

Value	SOC [%]		
	Mode I	Mode II	Mode III
Min	11.36	11.87	12.40
Mean	14.60	13.98	14.02
Max	16.00	15.00	15.02

WLTC test

The conditions in the WLTC test were slightly different from the NEDC test, which should result in different SOC changes of the battery using different charging strategies.

Despite similar maximum speeds in the WLTC test, the profile of the entire test was more diverse. This resulted in the internal combustion engine being started much more often (Fig. 10).

Determination of SOC changes within the range <13.5;16>, indicates full utilization of this range only when using the algorithm of mode I. Using other algorithms, the battery SOC does not exceed about 15%. With mode I, the battery is charged only a few times throughout the WLTC test.

In other strategies, the use of the internal combustion engine was much more frequent. In the case of modes II and III, the changes in the middle and final parts of the test were much greater. This means that the SOC changes in the case of modes II and III were also greater. High driving speeds in the final part of the test have resulted in a different use of the internal combustion engine. The control algorithm III is much more effective than the others in terms of limiting the drop in the battery SOC.

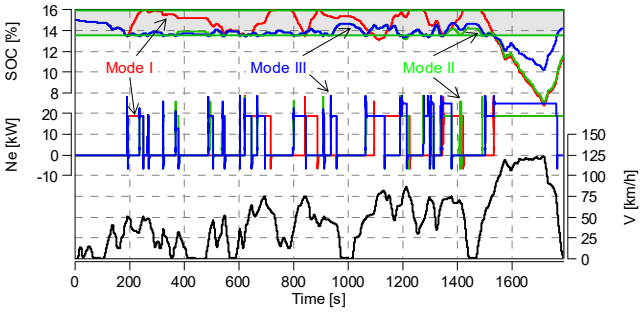

Fig. 10. Changes in SOC and internal combustion engine power in the WLTC test

The assessment of energy consumption (Fig. 11) shows high similarities of the energy flow compared to the NEDC test. However, the analysis of the IC engine load signal (*Load_signal*) shows its greater variability. Due to greater diversification of the driving profile, when the battery was recharged with the internal combustion engine on, the energy supplied to the battery reached the level of 0.2 kWh. This is approximately 100% more than in the NEDC test.

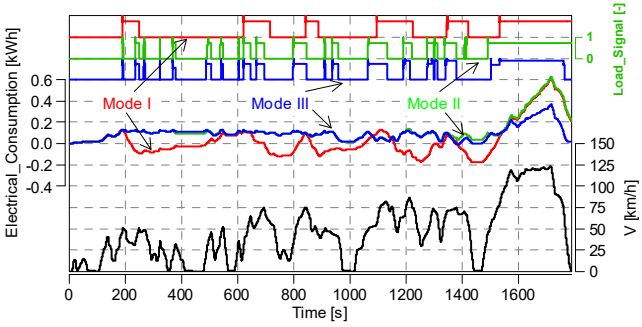

Fig. 11. Internal combustion engine load and electric energy consumption in the NEDC test

A comprehensive analysis of SOC changes in the WLTC test (Table 6) indicates a greater maximum discharge of the battery. With the control algorithms I and II, the obtained SOC had a minimum value of about 7%. This means it exceeded the critical value (SOC_{cr} = 13%) by about 50%. Such a drop in SOC value is very dangerous for the battery as it may lead to damage. The use of the third strategy results in the minimum SOC being around 10%. This is approximately only 30% below the critical level.

Table 6. SOC changes in the WLTC test in terms of different drive system control algorithms

Value	SOC [%]		
	Mode I	Mode II	Mode III
Min	6.77	7.00	10.15
Mean	14.22	13.37	13.68
Max	16.51	15.00	15.00

The comparison of the effectiveness of the REX drive control algorithms in the NEDC and WLTC tests was provided in Fig. 12. It shows that the simplest algorithms work quite well in the range of low maximum speeds. This was due to the limited energy required to drive the vehicle. The final SOC value in all control cases was above the critical minimum value (SOC_{cr} = 13%).

However, the simplest algorithms caused the critical SOC value to be dangerously exceeded during testing. This was more prominent when using the simpler system control algorithms (regardless of the drive test). Increasing the maximum speeds with a limited energy capacity of the battery requires using more complex control algorithms. The most advanced system presented in the paper allowed for a significant reduction of the battery SOC drop (regardless of the drive test). In the case of the NEDC test, the SOC_{cr} was exceeded by about 4% (which was qualified as being within the permissible error margin), while in the WLTC test – about 22%.

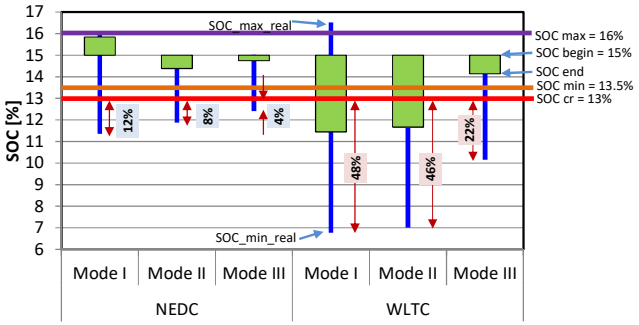

Fig. 12. Comparison of control algorithms in the Range Extender system in the two research tests

Conclusion

The presented research results of the control algorithms in the Range Extender drive system make it possible to draw the following conclusions:

1. The energy recovery systems and the conditions of cooperation between the internal combustion engine and the battery with different control algorithms for REX systems were successfully analyzed.
2. The control algorithms that take into account only the SOC limit values, do not properly control the battery charge in dynamic tests. It can only be effective under steady driving conditions or when driving in urban conditions while not reaching travel speeds over 80 km/h.
3. Using algorithms that use feedback from changes in the battery SOC allows for effective reduction of the range

of SOC changes. The advantage of such algorithms is that they keep the SOC in the acceptable range even during tests at higher driving speeds.

4. Using algorithms that take into account the thermal management of the internal combustion engine and various operating conditions of the internal combustion engine (rotational speed and load) could effectively enable predicting the energy flow changes in the battery system. At the same time, it can be used to avoid the state of "deep discharge", thus increasing the lifespan and durability of the whole system.

Acknowledgements

This work has been done under AVL University Partnership Program.

Nomenclature

CD	charge depleting
CS	charge sustaining
EV	electric vehicle
REEV	range-extended electric vehicle
HEV	hybrid electric vehicle
NEDC	New European Driving Cycle
REX	range extender
WLTC	World Harmonized Light Vehicle Test Cycle

Indexes

cr	critical
min	minimum
max	maximum
act	actual

Bibliography

[1] ANDWARI, A.M., PESIRIDIS, A., RAJOO, S. et al. A review of battery electric vehicle technology and readiness levels. *Renewable and Sustainable Energy Reviews*. 2017, **78**, 414-430. https://doi.org/10.1016/j.rser.2017.03.138

[2] AVL Cruise 2020 R1, User Manual. AVL 2020.

[3] BORETTI, A. Electric vehicles with small batteries and high-efficiency on-board electricity production. *Energy Storage*. 2019, **1**, e75. https://doi.org/10.1002/est2.75

[4] DELL, R.M., MOSELEY, P.T., RAND, D.A.J. Progressive Electrification of Road Vehicles (chapter 5). *Towards Sustainable Road Transport*. Academic Press 2014, 157-192. https://doi.org/10.1016/B978-0-12-404616-0.00005-0

[5] JEONG, J., LEE, W., KIM, N. et al. Control analysis and model validation for BMW i3 range extender. *SAE Technical Paper* 2017-01-1152. 2017. https://doi.org/10.4271/2017-01-1152

[6] JI, F., ZHANG, X., DU, F. et al. Experimental and numerical investigation on micro gas turbine as a range extender for electric vehicle. *Applied Thermal Engineering*. 2020, **173**, 115236. https://doi.org/10.1016/j.applthermaleng.2020.115236.

[7] KROPIWNICKI, J., FURMANEK, M. Analysis of the regenerative braking process for the urban traffic conditions. *Combustion Engines*. 2019, **178**(3), 203-207. https://doi.org/10.19206/CE-2019-335

[8] LIJEWSKI, P., KOZAK, M., FUĆ, P. et al. Exhaust emissions generated under actual operating conditions from a hybrid vehicle and an electric one fitted with a range extender. *Transportation Research Part D: Transport and Environment*. 2020, **78**, 102183. https://doi.org/10.1016/j.trd.2019.11.012

[9] MACIEJEWSKA, M., FUĆ, P., KARDACH, M. Analysis of electric motor vehicles market. *Combustion Engines*. 2019, **179**(4), 169-175. https://doi.org/10.19206/CE-2019-428

[10] NEMRY, F., LEDUC, G., MUÑOZ, A. Plug-in hybrid and battery-electric vehicles: State of the research and development and comparative analysis of energy and cost efficiency. *Joint Research Centre. Institute for Prospective Technological Studies*. Luxembourg 2009. ftp://ftp.jrc.es/pub/EURdoc/JRC54699_TN.pdf

[11] Regulation (EU) 2017/1151 Supplementing Regulation (EC) No 715/2007 of the European Parliament and of the Council on type-approval of motor vehicles with respect to emissions from light passenger and commercial vehicles (Euro 5 and Euro 6) and on access to vehicle repair and maintenance information, amending Directive 2007/46/EC of the European Parliament and of the Council, Commission Regulation (EC) No 692/2008 and Commission Regulation (EU) No 1230/2012 and repealing Commission Regulation (EC) No 692/2008. https://eur-lex.europa.eu/legal-content/EN/TXT/?uri=CELEX%3A32017R1151

[12] SOLOUK, A., TRIPP, J., SHAKIBA-HERFEH, M. et al. Fuel consumption assessment of a multi-mode low temperature combustion engine as range extender for an electric vehicle. *Energy Conversion and Management*. 2017, **148**, 1478-1496. https://doi.org/10.1016/j.enconman.2017.06.090

[13] TAKAOKA, T., ICHINOSE, H. The newly developed Toyota plug-in hybrid system. *31. Internationales Wiener Motorensymposium 2010*. Wien 2010.

[14] TURNER, M., TURNER, J., VORRARO, G. Mass benefit analysis of 4-stroke and Wankel range extenders in an electric vehicle over a defined drive cycle with respect to vehicle range and fuel consumption. *SAE Technical Paper* 2019-01-1282. 2019. https://doi.org/10.4271/2019-01-1282

[15] ZAMBALOV, S.D., YAKOVLEV, I.A., MAZNOY, A.S. Effect of multiple fuel injection strategies on mixture formation and combustion in a hydrogen-fueled rotary range extender for battery electric vehicles. *Energy Conversion and Management*. 2020, **220**, 113097. https://doi.org/10.1016/j.enconman.2020.113097

[16] ZHANG, C., JIANG, J., ZHANG, L. et al. A generalized SOC-OCV model for lithium-ion batteries and the SOC estimation for LNMCO battery. *Energies*. 2016, **9**, 900. https://doi.org/10.3390/en9110900

Prof. Ireneusz Pielecha, DSc., DEng. – Faculty of Civil and Transport Engineering, Poznan University of Technology.

e-mail: *ireneusz.pielecha@put.poznan.pl*

Article citation info:
MROZIK, M. Ecological comparative assessment of selected materials used for the construction of spark ignition engines. *Combustion Engines*. 2020, **183**(4), 11-14. https://doi.org/10.19206/CE-2020-402

Małgorzata MROZIK

CE-2020-402

Ecological comparative assessment of selected materials used for the construction of spark ignition engines

The aim of the article is to present the environmental effects of changes in material composition in selected internal combustion engines used in passenger cars using LCA analysis. The levels of energy consumption and emissions of pollutants related to material inputs occurring at the stage of engine production have been determined. The simplified LCA model presented in the paper shows the energy consumption and total CO_2 and SO_2 emissions on the basis of the mass of materials from which the engine is made. The research results presented in the paper give a picture of a modern passenger car engine on the basis of wear and the degree of recovery of materials used for its construction.

Key words: *engine, passenger car, life cycle analysis, eco-design, environmental protection*

1. Introduction

Along with the civilization development of the world, the awareness of the current environmental threats and the great need to counteract them increases. This is especially evident in the automotive field, where the environmental protection issues have recently become more and more focused. Currently, the ecological properties of vehicles, apart from the safety systems used, are very often considered to be determinants of technological progress in the automotive industry. Concerns about the negative impact of road transport on the environment are potentiated by the constantly growing number of cars in the world. Limiting the degradation of the environment by road transport is done by legal regulations, which are to contribute to the elimination of technologies harmful to the environment. Stricter environmental standards put the automotive industry under increasing pressure to reduce fuel consumption and exhaust emissions over the lifetime of a car. Hence, most of the research described in the world literature focuses on reducing energy consumption and emissions of toxic compounds and CO_2 directly related to the operation of the vehicle. Most often they relate to the environmental impact assessment of unconventional drives and alternative fuels. Nevertheless, the largest number of vehicles traveling on the road are still cars with classic spark-ignition combustion engines.

The main component of any vehicle is a car engine. Drives used in passenger vehicles are subject to diversification with the progress of civilization. Spark ignition (SI) engines are widely used in motor vehicles due to their many advantages. These include mainly: high reliability, durability, reduction of fuel consumption and minimization of their harmful impact on the natural environment. Obtaining the best performance indicators of an internal combustion engine has attracted the attention of designers and researchers from the first years of their creation. In the past, they were designed precisely for high performance. Currently, the most important stimulus for their development is low environmental impact. The aim is to minimize the emission of toxic substances and noise as well as low fuel consumption. Requirements for the ecological properties of engines are put forward both by the environmental protection authorities and by the users themselves, which proves a significant increase in the environmental awareness of the present society.

The modern power supply systems for SI engines differ significantly from the power systems from the end of the 20th century. Until the 1990s, the most widely used system was the carburetor. However, the introduction of Euro standards in Europe and the increase in fuel prices forced manufacturers to develop a modern petrol injection system. These systems allowed to reduce fuel consumption and emission of harmful exhaust components to the atmosphere. At the turn of the 70's and 80's, injection power and three-way exhaust gas catalysts were introduced in spark ignition engines. This caused a certain stagnation in their development, which lasted until the mid-90s. Contamination of the natural environment caused by the exploitation of means of transport is part of the global ecological problem and is the subject of many activities of governmental and non-governmental organizations, especially in the legislative sphere. This obviously forces manufacturers of SI engines to create new generations of vehicles in terms of design, technology and functionality. Therefore, the development of environmental protection requirements has become the main factor stimulating the development of modern designs of engines used in passenger vehicles [1, 2].

The traditional approach to the environmental assessment of a car consists mainly in determining the emissions of pollutants and CO_2 depending on the amount of fuel used by the vehicle. Existing emission standards are the result of this approach. The life cycle methodology (LCA) used in the work, described in ISO 14040 [3] and 14044 [4], expresses a contemporary approach to the problem of the impact of a car and its components on the environment. These standards define the method of comprehensive, quantitative determination of the environmental load, based on the inventory of environmental factors related to a facility, process or other activity over the entire cycle from the extraction of raw materials to their final management [5–7]. The LCA method, introduced since the 1970s [9, 10], is one of the most effective and reliable eco-balance tools that allow to assess the amount of energy consumption and the amount of emissions of hazardous substances and materials in all phases of the product's existence – starting from obtaining raw materials, and ending with the disposal of used

Received 21 September 2020; Received in revised form 6 October 2020; Accepted 10 October 2020
Available online 20 December 2020

up products. This forms the basis for estimating the options available to reduce these loads introduced into the environment.

The aim of the article is to present the environmental effects of changes in material composition in selected internal combustion engines used in passenger cars using the LCA method.

2. Modeling the life cycle of SI engine

2.1. Research objects

The subjects of the research were SI engines, which currently selected Hyundai and Ford vehicles are equipped with. These are petrol engines with similar operational characteristics, manufactured since 2005. Table 1 presents the basic technical data.

Table 1. Basic technical parameters of internal combustion engines tested

Engine specifications	Hyundai I30 1.4	Focus III 1.6 Eco-boost	Focus I 1.8	Fiesta 1.4
Year of construction	2016	2014	2005	2013
Cubic capacity	1396 cm³	1596 cm³	1796 cm³	1388 cm³
Engine type	petrol	petrol	petrol	petrol
Engine power	100 KM (74 kW) at 5500 rpm	150 KM (110 kW) at 5700 rpm	115 KM (85 kW) at 5750 rpm	96 KM
Maximum torque	137 Nm at 4200 rpm	240 Nm at 1900-3500 rpm	158 Nm at 3750 rpm	125 Nm at 4200 rpm
Number of cylinders	4	4	4	4
Arrangement of cylinders	in-line	in-line	in-line	in-line
Number of valves	16	16	16	16
Injection type	multi-point (MPI)	direct	multi-point (MPI)	multi-point (MPI)

2.2. LCA

The environmental safety of a car is currently one of the most important indicators determining the quality and competitiveness of a car on global markets. One of the priorities in the design of all technical facilities is currently to reduce their impact on the natural environment. This also applies to internal combustion engines. They are commonly seen as one of the sources of significant changes in the environment. Efforts undertaken so far to improve the environmental image of internal combustion engines were usually aimed at reducing the amount of exhaust fumes. However, the causes of environmental degradation related to internal combustion engines are much more complex. They are not limited to the consequences of the combustion process, but also result from the use of natural resources for the production of engines and from production processes, which are always accompanied by environmental impact. During the operation of internal combustion engines, noise is emitted and repairs are made, and after the end of the engine life it becomes important whether its parts can be recycled. These aspects should be taken into account by designers who comprehensively care about the environmental image of engines. Only then will their activities aimed at limiting the environmental impacts generated in the entire life cycle of internal combustion engines be consistent with contemporary trends in their design [8].

One of the most effective methods for the effective assessment of a product's environmental impact is the Life Cycle Assessment LCA. It is defined as a method of quantifying the environmental load, based on an inventory of environmental factors related to a facility, process or other activity in the cycle from the extraction of raw materials to their final use [9]. It is primarily used to determine the environmental impacts of the processes related to the entire contractual lifetime of the product, starting from the manufacturing of materials, through production, its use until its withdrawal from use. This approach is needed especially for passenger cars, and thus internal combustion engines, where special attention should be paid to the materials needed for their production. These mainly include metals, plastics, glass, rubber and ceramics, as well as fabrics and others. The production of these materials and then the components needed for the mass production of vehicles on an unprecedented scale requires the use of limited natural resources and energy in production processes, which is always accompanied by a negative impact on the environment [8].

The result of using the LCA method to analyze the environmental impacts of a facility is the eco-indicator in the form of a single number or an environmental profile, which is a characteristic indicating the size of the generated environmental loads within individual impact categories. Due to the simple and legible way of presenting the results, LCA is a method particularly appreciated by engineers dealing with the issues of environmental optimization of mechanical structures [9, 10].

2.3. Data sources

Life Cycle Inventory (LCI) data includes product data and process data. Product data is characterized by the tested car engines. According to the scope of the assessment, this is information about the parts and materials from which they were made. The data also includes information on fuel consumption and pollutant emissions during use, as well as information on the rates of material recovery and reuse in accordance with the applicable policy rules that regulate these issues [11, 12]. Process data, on the other hand, includes information on processing the processes in the production of materials and parts used to build internal combustion engines.

Material data on the tested engines of Ford and Hyundai vehicles was obtained during inventory studies carried out at a certified vehicle dismantling station in Szczecin, Poland and at an authorized Ford service center in Szczecin. As part of the tests at the dismantling station, the tested engines were disassembled into assemblies and individual parts. During the tests carried out at an authorized service point, the engines disassembled from the repaired cars and kept in stock were used. In order to prepare a list of materials used in cars, these materials were identified, weighed and their type was determined. Many small parts were made of one material and a similar technology. In this case, the parts list stated their total mass in kilograms. Missing material data on some components of the tested engines was obtained from the commercial IDIS database.

The list of parts prepared in this way, together with information on the weight of materials, was used to build the LCA model of the car engine. As the obtained parts are made of different components, in order to simplify the model and facilitate the presentation of the life cycle assessment results, the materials have been assigned to three groups:

- steel,
- aluminum,
- other materials.

Inputs include streams of the materials used in the engine, which come from the environment (primary production), and recycling (secondary production). The system outputs include pollutant emissions and the energy consumption associated with their generation.

For each material stream, the emission levels of substances were determined, such as CO, CO_2, CH_4, N_2O, NO_x, NMVOC which accompany primary and secondary production of materials. Data on the size of these emissions were obtained from the Ecoinvent 2.1 database, which is commonly used in life cycle tests [12]. The environmental impact of these variables was converted into emissions of carbon dioxide CO_2eq and sulfur dioxide SO_2. The Eco-Indicator EI99 E/A Europe method was used for the conversion. In the LCA studies, the total emission of CO_{2eq} and SO_2 was treated as an environmental impact category. On the other hand, energy consumption in material production processes was determined on the basis of the SimaPro and Greet databases.

3. The results of the comparative assessment

In order to perform a quantitative ecological comparative assessment of materials used in the construction of a car engine, an identification of the engine construction phase model was carried out on the basis of the collected research material covering 4 selected vehicles from two manufacturers belonging to segment B, which were produced in 2005-2016. This required determining the mass of the materials that make up each engine. The obtained material data reflects changes in the design of selected combustion engines of passenger cars. Table 2 presents the masses of materials from which the tested internal combustion engines are made. It was assumed that the level of energy consumption and emissivity in the construction phase of selected engines can be determined based on changes in the material structure.

Table 2. Material mass in kg

Engine	aluminum	steel, cast iron	other
Hyundai I30 1,4 petrol 80 kW	43.48	15.57	3.22
Focus III 1,6 ecoboost 110 kW	44.75	21.21	2.15
Focus I 1,8 petrol 85 kW	15.8	71.51	2.94
Fiesta 1,4 petrol 60 kW	13.9	76.33	2.9

The percentages of basic materials in the Hyundai I30 1.4 petrol 80 kW and Focus III 1.6 Ecoboost 110 kW engines are similar. They are characterized by a high (over 65%) share of aluminum. In turn, the Focus I 1.8 petrol 85 kW and Fiesta 1.4 petrol 60 kW engines are characterized by a very high (approx. 80%) share of steel and cast iron. This relationship is shown in Fig. 1.

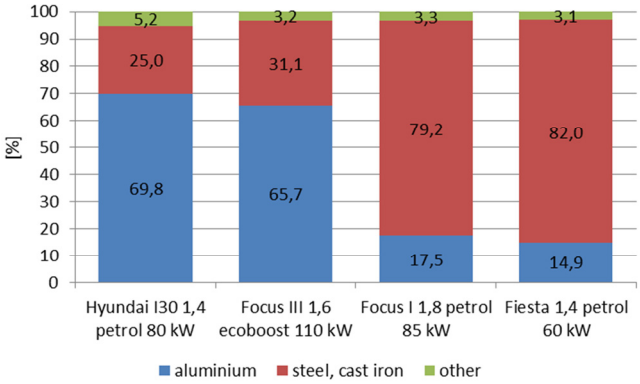

Fig. 1. Percentage of materials

Such distribution of materials in the presented engines results in a different percentage of energy expenditures and CO_2 and SO_2 emissions.

For energy expenditures (Fig. 2) in the Hyundai I30 1.4 petrol 80 kW and Focus III 1.6 Ecoboost 110 kW engines, aluminum had the greatest impact. Its share in energy expenditures was at the level of approx. 90%. In the Focus I 1.8 petrol 85 kW and Fiesta 1.4 petrol 60 kW engines, steel and cast iron accounted for slightly more than half of the share of energy expenditures (52.7–57.5%).

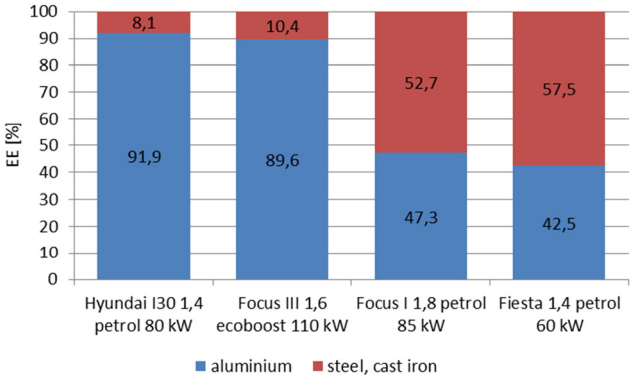

Fig. 2. Percentage of energy expenditure

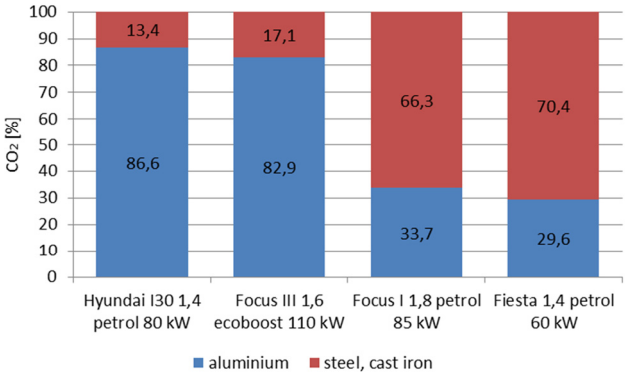

Fig. 3. Percentages of CO_2 emissions

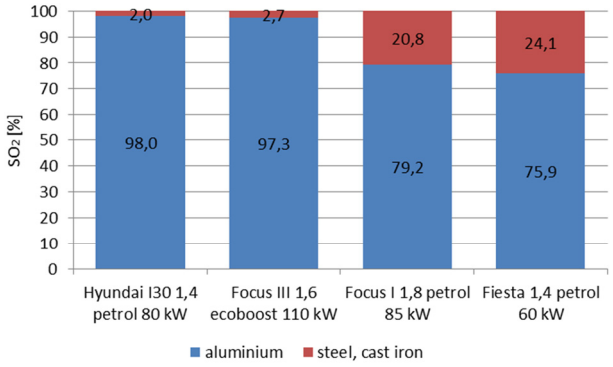

Fig. 4. Percentages of SO_2 emissions

For CO_2 and SO_2 emissions (Fig. 3 and Fig. 4) in the Hyundai I30 1.4 petrol 80 kW and Focus III 1.6 Ecoboost 110 kW engines, as well as for energy expenditures, aluminium had the greatest impact. Its share in CO_2 emissions was at the level of 82.9–86.6%, and in SO_2 emissions – at the level of 97.3–98.0%. In the Focus I 1.8 petrol 85 kW and Fiesta 1.4 petrol 60 kW engines, steel and cast iron accounted for most of the CO_2 emissions (66.3–70.4%), and aluminum for SO_2 (79.2–75.9 %).

3. Conclusion

The results presented in the paper present the environmental effects of changes in the material composition in Ford and Hyundai passenger car engines. The simplified LCA model of the engine presented in the paper shows the energy consumption and total CO_2 and SO_2 emissions on the basis of the obtained mass of materials. The changes in the use of materials are a signal of the technological progress that has taken place in the design of cars in recent times.

The selection of construction materials used in the construction of the tested internal combustion engines has a significant impact on the level of their environmental impact. There is a visible tendency to decrease the share of steel, cast steel and cast iron with a simultaneous increase in the share of other materials. This can be observed by systematically increasing the environmental loads associated with the use of other materials.

The percentages of basic materials in the tested engines are similar. The dominant material here is aluminum. In turn, the engines of the Focus I 1.8 petrol 85 kW and Fiesta 1.4 petrol 60 kW vehicles are characterized by a very high share of steel and cast iron.

Nomenclature

LCA	life cycle assessment
LCI	Life Cycle Inventory
CO_2	carbon dioxide
SO_2	sulphur dioxide
SI	spark ignition engine
NE	energy expenditures
NM	materials

Bibliography

[1] MERKISZ, J. Ekologiczne problemy silników spalinowych. *Wydawnictwo Politechniki Poznańskiej*. Poznań 1998.
[2] MERKISZ, J. Ekologiczne aspekty stosowania silników spalinowych. *Wydawnictwo Politechniki Poznańskiej*. Poznań 1995.
[3] International Organization for Standardization (ISO), 2006. 14040 – Environmental Management. Life Cycle Assessment. Principles and Framework.
[4] International Organization for Standardization (ISO), 2006. 14040 – Environmental Management. Life Cycle Assessment. Requirements and Guidelines.
[5] PN-EN ISO 14040. Zarządzanie środowiskowe – Ocena cyklu życia – Zasady i struktura. Polski Komitet Normalizacyjny, czerwiec 2006.
[6] PN-EN ISO 14040. Zarządzanie środowiskowe – Ocena cyklu życia – Wymagania i wytyczne. Polski Komitet Normalizacyjny, lipiec 2006.
[7] KULCZYCKA, J. Ekologiczna ocena cyklu życia (LCA) nową techniką zarządzania środowiskowego. *IGSMiE*, Kraków 2001.
[8] MERKISZ, J., KURCZEWSKI, P., LEWICKI, R. Wybrane aspekty prośrodowiskowego projektowania silników spalinowych. *Wydawnictwo Politechniki Poznańskiej*. Poznań 2007.
[9] Environmental Life Cycle Assessment of products, Part 1 – Guide, Part 2 – Backgrounds, NOH 1992.
[10] KOWALSKI, Z., KĘDZIERSKA, D., NOWAK, A.K. et al. LCA analysis of processing of the zinc and lead ores in Trzebionka Mining Works. *10th Conference on Environment and Mineral Processing, VŠB-TU Ostrava. Proceedings Part II*, 22-24.06.2006, 105-115.
[11] Directive 2000/64/EC of the European Parliament and of the Council, On the type-approval of motor vehicles with regard to their re-usability, recyclability and recoverability and amending Council Directive 70/156/EEC, 26 November 2005, Official Journal L 310.
[12] BIRAT, J., GUERIN, V., ROCCHIA, L. et al. 2004. Ecodesign of automobiles based on the environmental properties of body materials. *SAE Technical Paper*. 2004-01-0250.

Małgorzata Mrozik, DSc., DEng. – Faculty of Mechanical Engineering and Mechatronics, West Pomeranian University of Technology in Szczecin.
e-mail: *mmrozik@zut.edu.pl*

Article citation info:
NYGARD, A., BARTOSZEWICZ, J. Evaluation efficiency of low-power fans used in the means of transport. *Combustion Engines*. 2020, **183**(4), 15-20. https://doi.org/10.19206/CE-2020-403

Adam NYGARD
Jarosław BARTOSZEWICZ

CE-2020-403

Evaluation efficiency of low-power fans used in the means of transport

The article presents test results on low-power fans used in the means of transport. Fans evaluation was in the context of energy efficiency. Interest in scientific topics related to low-power fans has its source in the reports of the Chief Inspector of Environmental Protection on the state of the natural environment in Poland and European Union reports assessing our natural environment. The goal of the article is to compare experimental results with Minister of Economy Regulation of March 11th, 2014, which introduces changes in accordance to European Parliament and Council Directive 2009/125/WE, with regard to ecodesign requirements for fans driven by motors with an electric input power between 125 W and 500 kW.

Key words: *fans, low-power fans, evaluation efficiency, fan efficiency, transport*

1. Introduction

This article presents the continuation of tests on low-power centrifugal fans. Its purpose is to compare the results of tests with the Resolution of the Minister of Economy of 11 March 2014 implementing the changes in the performance of Directive 2009/125/EC of the European Parliament and of the Council with regard to ecodesign requirements for fans driven by motors with an electric input power between 125 W and 500 kW.

The directive was implemented to reduce electric energy consumption as a result of technology development and improvement of the design, rising the energy efficiency of fans used for gas transportation. This Directive concerns fans driven by electric motors. For the European market in 2016 energy consumption of fans described above was 344 TWh per year. With regard to the project being implemented by the European Union, requirements for fans were established. In its main part, the Directive presents information on how to calculate the minimum energy efficiency of a fan. The formula from Directive 2009/125/EC used to determine the minimum required energy efficiency that should be obtained by a fan (driven by motor with an electric input power between 125 W and 10 kW) is presented below:

$$\eta = 2.74 \cdot \ln(P_{el}) - 6.33 + N \quad (1)$$

where: η – energy efficiency, P_{el} – input power of the fan, N – energy efficiency grade (depending on the test methodology, type of fan and the efficiency) [1].

In connection with the earlier work of the authors who researched energy boilers [2–4] and aerodynamic analysis of gas flow by recirculation [5] including the combustion chamber. The previous article [6] presents the results of testing low-power centrifugal fans, which are used in low-power boilers

In this article presents test results on low-power centrifugal fans being a source of energy in pipeline transportation used in the means of transport.

Low-power fans are used in means of transport in ventilation, air conditioning and heaters [7]. The most commonly used air conditioners in the means of transport are integrated air conditioners installed during production, which we use in passenger cars, vans and trucks and who is part of the HVAC system (Heating, Ventilation, Air Conditioning) [8]. The integrated air conditioning system allows rising and lowering the air temperature in the vehicle's working space. Low-power fans meet the functional requirements of the project including the analysis of mass transport equations in ventilation systems, without the obligation to work with high efficiency. EU regulations impose the minimum efficiency that must be achieved by compression machines whose electrical power is greater than the defined minimum threshold given by a simple algebraic formula. As a result, almost all fans used in means of transport and mobile working machines are excluded from supervision. Compression machines are used to: increase the density of the gas medium, increase the pressure of the medium, force the flow, increase the temperature of the working medium and intensify the Joule-Thomson effect. The effect of the compression machine is to increase the pressure on the discharge side of the machine relative to the suction side. The ratio of pressure on the compressor discharge side to the pressure on the suction side is called compression. When the compression is less than 1.1 in relation to the suction side, we are talking about fans.

Figures 1–3 show selected cabin fans used to supply air to the cabin. Figure 1 presents the centrifugal fan installed in VW Jetta cars with 1.4 TSI engines with 150 HP output produced from 2014.

Fig. 1. Fan installed in VW Jetta [9]

Figure 2 presents the fan used in Mercedes-Benz CLS Coupe 220 BlueTEC manufactured from 2014 with 127 kW engine power.

Received 22 June 2020; Received in revised form 9 October 2020; Accepted 11 October 2020
Available online 15 December 2020

Fig. 2. Fan installed in Mercedes-Benz CLS Coupe 220 BlueTEC [9]

Figure 3 shows the fan diagram installed in the BMW 3 Series (F30 and F80) 318d produced from 2014 with a 112 kW engine power.

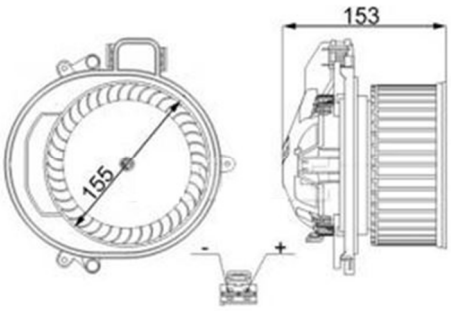

Fig. 3. Fan installed in BMW 3 Series [9]

Figures 4 and 5 show examples of fans used for cooling heat exchangers installed in various means of transport and mobile working machines. Figure 4 shows the SPAL 002-B46-02 fan, which has the following parameters:
– voltage: 24 V,
– current: 6.2 A,
– power: 148.8 W,
– air flow: 620 m³/h.

Fig. 4. Fan SPAL 002-B46-02 [10]

Figure 5 shows the SPAL 005-A45-02 fan, which has the following parameters:
– voltage: 12 V,
– current: 13.3 A,
– power: 160 W,
– air flow: 610 m³/h.

Fig. 5. Fan SPAL 005-A45-02 [10]

2. Test method

The subject of research were low-power fans used in transport, ventilation, air-conditioning and heaters. The fans were powered by electric motors. Nine fans with electric power from 10 W to 125 W were tested to verify the application of the directive for fans with less than 125 W input power.

Figure 6 presents the scheme of a measurement stand built in the Chair of Thermal Engineering of Poznan University of Technology.

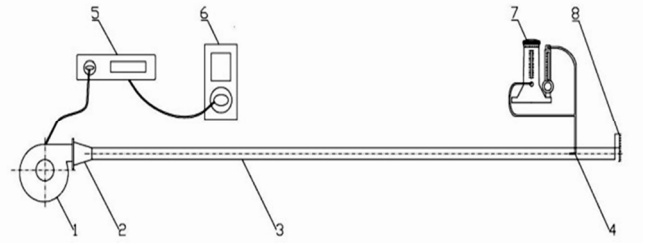

Fig. 6. Scheme of a measurement stand: 1 – fan, 2 – confusor, 3 – measuring channel, 4 – Prandtl probe, 5 – fan's operation regulator, 6 – wattmeter, 7 – compensation micro-manometer, 8 – flap valve

The measurement stand was built based on the guidelines contained in Polish standards [11, 12, 13, 14] and the directive. In the directive four measurement categories defining the arrangement of measurements and the inlet and outlet conditions of the fan were distinguished:
– "measurement category A" – the fan is measured with free inlet and outlet conditions,
– "measurement category B" – the fan is measured with free inlet and with a duct fitted to its outlet,
– "measurement category C" – the fan is measured with a duct fitted to its inlet and with free outlet conditions,
– "measurement category D" – the fan is measured with a duct fitted to its inlet and outlet.

Fans were tested using the arrangement where the fan is measured with free inlet and with a duct fitted to its outlet (measurement category B). Conducted tests allowed to measure and calculate the following quantities describing fans under tests: Δp_c – total pressure increase, P_{el} – electric power consumed by the fan, η – total efficiency of the fan, $\dot{V}$ – volume flow of the air flowing through the fan.

Based on the analysis of the measuring equipment used and the method of determining the characteristic parameters describing the operation of the fan, the relative error is for the following values:
– increase in total pressure – 1%,
– electric power consumed by the fan – 1.5%,
– air volume flow – 1%.

3. Results

Figures from 7 to 17 present characteristics of nine fans of electric power lower than 125 W.

Figures 7 and 8 present examples characteristics made for the fan F1 who were made for different values of motor speed n (100%, 72% and 45% of the maximum speed). Measurements were for relative quantities compared with the volume flow. The electric input power of the fan F1 was 37 W. The volume flow for speeds under test was as follows:

– for n = 100%, the volume flow increases from 29 m^3/h to 155 m^3/h,
– for n = 72%, the pressure decreases from 29 m^3/h to 106 m^3/h,
– for n = 45%, the pressure decreases from 20 m^3/h to 89 m^3/h.

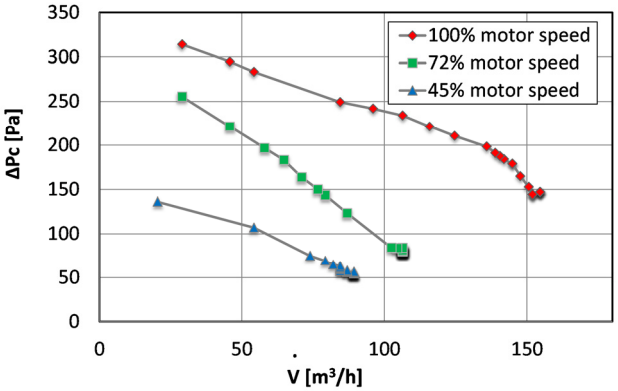

Fig. 7. Characteristics of ΔPc for fan F1

In Figure 7 we may notice the decrease of pressure with the increase of air volume flow. This dependence repeats for all motor speeds. For subsequent motor speeds, the pressure decrease was as follows:
– for n = 100% the pressure decreased from 314 Pa to 147 Pa,
– for n = 72% the pressure decreased from 255 Pa to 80 Pa,
– for n = 45% the pressure decreased from 136 Pa to 54 Pa.

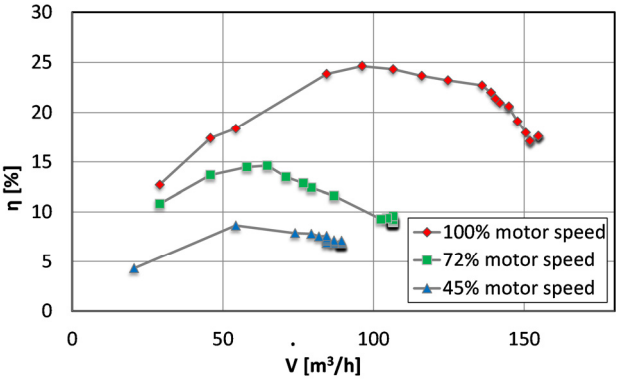

Fig. 8. Characteristics of η for fan F1

Figure 8 presents the efficiency characteristics. The fan had the highest efficiency during testing at maximum motor speed. Efficiency for motor speed n = 100% increases with the volume flow from 13% to 25% and for the volume flow equal to 155 m^3/h, it starts to decrease to 18%. Efficiency for motor speed n = 72% increases with the volume flow from 11% to 15% and for the volume flow equal to 65 m^3/h, it starts to decrease to 9%. Efficiency for motor speed n = 45% increases with the volume flow from 4% to 9% and for the volume flow equal to 54 m^3/h, it starts to decrease to 7%.

Figures from 9 to 17 present characteristics of total pressure increase, efficiency and power varying in a function of air volume flow. Graphs show the increase in the input electric power and the decrease in total pressure increase with the volume flow increase.

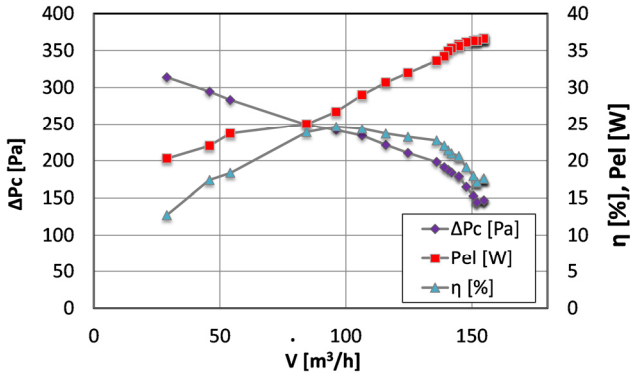

Fig. 9. Characteristics of fan F1 for 100% motor speed

Figure 9 presents the characteristics of fan F1 for 100% motor speed. The volume flow ranges from 29 m^3/h to 155 m^3/h. With its increase, the pressure decreases from 314 Pa to 147 Pa and the power consumption increases from 20 W to 37 W. With the increase of volume flow, the efficiency increases from 13% to 25% and for the volume flow equal to 155 m^3/h, it starts to decrease to 18%.

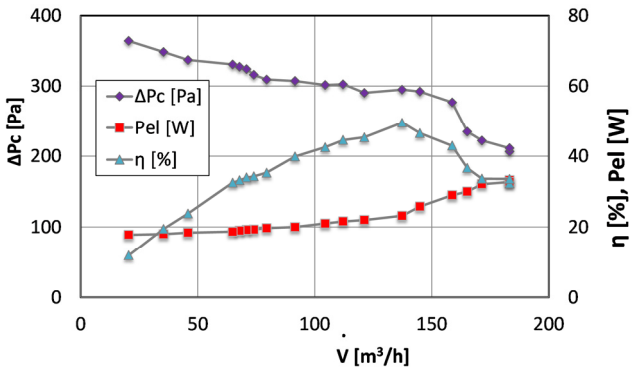

Fig. 10. Characteristics of fan F2 for 100% motor speed

Figure 10 presents the characteristics of fan F2 for 100% motor speed. The volume flow ranges from 20 m^3/h to 183 m^3/h. With its increase, the pressure decreases from 364 Pa to 206 Pa and the power consumption increases from 18 W to 33 W. With the increase of volume flow, the efficiency increases from 12% to 50% and for the volume flow equal to 137 m^3/h, it starts to decrease to 32%.

Figure 11 presents the characteristics of fan F3 for 100% motor speed. The volume flow ranges from 20 m^3/h to 171 m^3/h. With its increase, the pressure decreases from 325 Pa to 183 Pa and the power consumption increases from 18 W to 33 W. With the increase of volume flow, the efficiency increases from 11% to 34% and for the volume flow equal to 130 m^3/h, it starts to decrease to 27%.

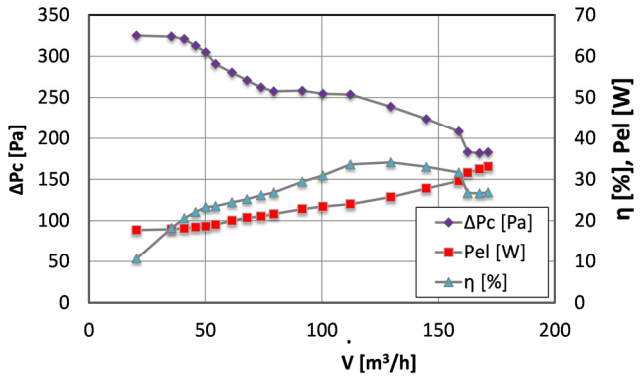

Fig. 11. Characteristics of fan F3 for 100% motor speed

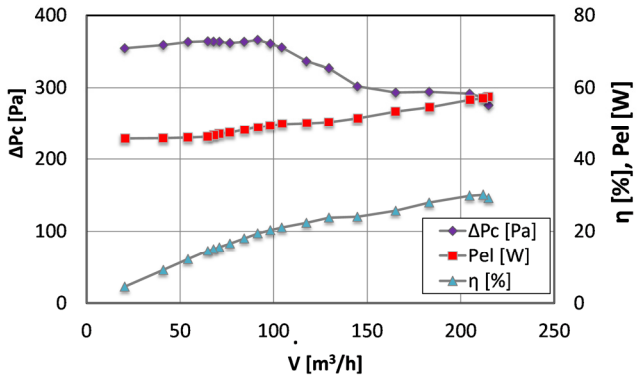

Fig. 12. Characteristics of fan F4 for 100% motor speed

Figure 12 presents the characteristics of fan F4 for 100% motor speed. The volume flow ranges from 20 m^3/h to 215 m^3/h. With its increase, the pressure decreases from 354 Pa to 276 Pa and the power consumption increases from 46 W to 58 W. With the increase of volume flow, the efficiency increases from 11% to 34%.

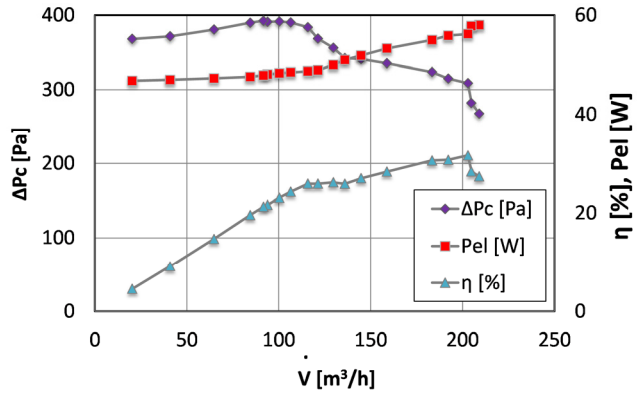

Fig. 13. Characteristics of fan F5 for 100% motor speed

Figure 13 presents the characteristics of fan F5 for 100% motor speed. The volume flow ranges from 20 m^3/h to 209 m^3/h. With its increase, the pressure decreases from 368 Pa to 268 Pa and the power consumption increases from 47 W to 58 W. With the increase of volume flow, the efficiency increases from 5% to 32%.

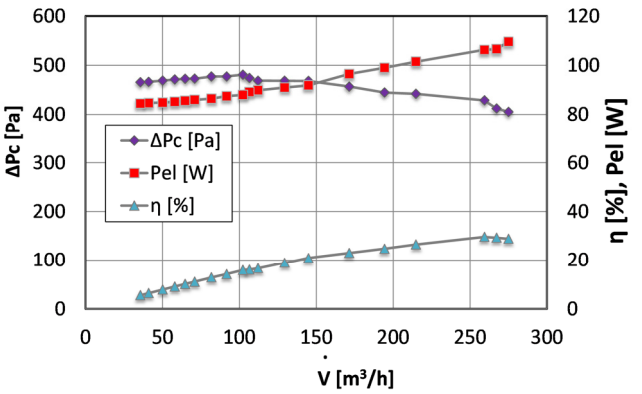

Fig. 14. Characteristics of fan F6 for 100% motor speed

Figure 14 presents the characteristics of fan F6 for 100% motor speed. The volume flow ranges from 35 m^3/h to 275 m^3/h. With its increase, the pressure decreases from 466 Pa to 406 Pa and the power consumption increases from 85 W to 110 W. With the increase of volume flow, the efficiency increases from 6% to 30%.

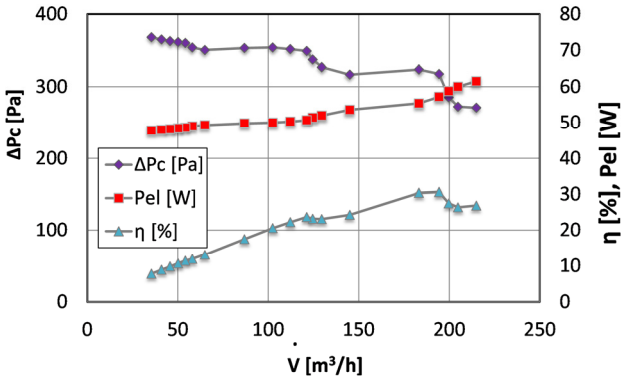

Fig. 15. Characteristics of fan F7 for 100% motor speed

Figure 15 presents the characteristics of fan F7 for 100% motor speed. The volume flow ranges from 35 m^3/h to 215 m^3/h. With its increase, the pressure decreases from 368 Pa to 271 Pa and the power consumption increases from 48 W to 62 W. With the increase of volume flow, the efficiency increases from 8% to 31% and for the volume flow equal to 194 m^3/h, it starts to decrease to 26%.

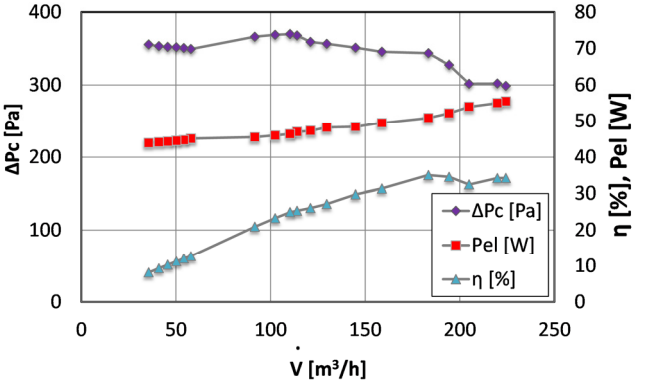

Fig. 16. Characteristics of fan F8 for 100% motor speed

Figure 16 presents the characteristics of fan F8 for 100% motor speed. The volume flow ranges from 35 m^3/h to 224 m^3/h. With its increase, the pressure decreases from 355 Pa to 299 Pa and the power consumption increases from 44 W to 56 W. With the increase of volume flow, the efficiency increases from 8% to 34%

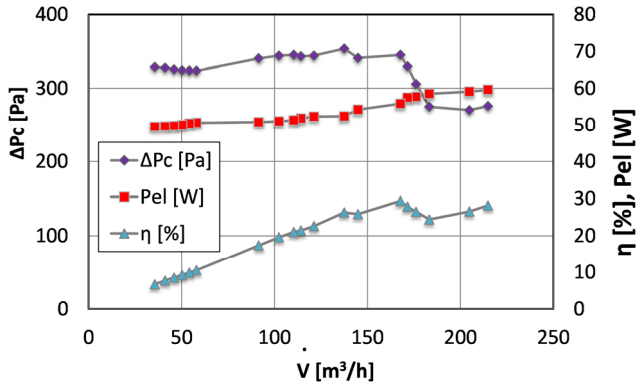

Fig. 17. Characteristics of fan F9 for 100% motor speed

Figure 17 presents the characteristics of fan F9 for 100% motor speed. The volume flow ranges from 35 m^3/h to 215 m^3/h. With its increase, the pressure decreases from 329 Pa to 276 Pa and the power consumption increases from 50 W to 60 W. With the increase of volume flow, the efficiency increases from 7% to 29%.

4. Conclusions

Table 1 presents a comparison of the following technical parameters fans: electric power consumed by the fan, total pressure increase, volume flow of the air flowing through the fan, total efficiency of the fan.

Table 1. Comparison of technical parameters fans

Fan symbol	Electric power P_{el} [W]	Total pressure increase ΔPc [Pa]	Volume flow of the air $\dot{V}$ [m^3/h]	Efficiency η [%]
F1	37	314	155	25
F2	33	364	183	50
F3	33	325	171	34
F4	58	366	215	30
F5	58	392	209	32
F6	110	481	275	30
F7	62	368	215	31
F8	56	370	224	35
F9	60	354	215	29

Table 2 presents a summary of the results for electrical power and fan efficiency.

Figure 18 shows a comparison of the efficiency obtained as a result of test measurements and the efficiency calculated on the basis of the formula in the directive.

Table 2. Summary of results for fans' efficiencies

Fan symbol	Electric power P_{el} [W]	Efficiency obtained in test η_1 [%]	Efficiency calculated based on the Directive η_2 [%]
F1	37	25	46
F2	33	50	45
F3	33	34	45
F4	58	30	47
F5	58	32	47
F6	110	30	49
F7	62	31	47
F8	56	35	47
F9	60	29	47

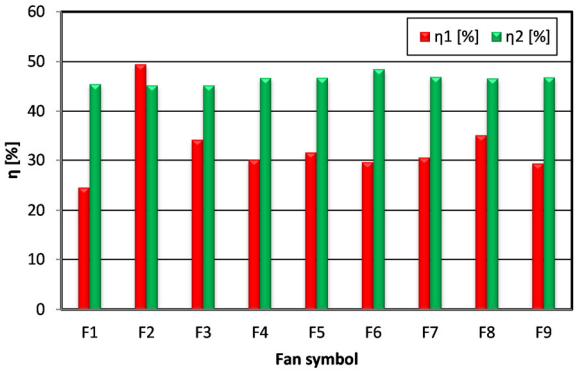

Fig. 18. Comparison results of the evaluation of efficiency

The purpose of the continuation of research in this article was to compare the results of research on nine centrifugal fans used in means of transport in terms of efficiency achieved and the requirements of the Regulation of the Minister of Economy of 11 March 2014 introducing changes in performance Directive 2009/125/EC of the European Parliament and of the Council [1] regarding ecodesign requirements for fans driven by motor with an electrical input between 125 W and 500 kW. After testing the nine fans, we can see that only one fan with the F2 symbol would meet the minimum energy efficiency requirements described in the directive. The other eight do not meet the requirements. Therefore, an appropriate resolution should be prepared covering the requirements for fans of this class, based on the results of tests on already existing fans, and it is justified to formulate an application to the Polish Committee for Standardization in order to verify the above-mentioned resolution. The results obtained indicate that there is a need to develop new guidelines. They should relate to the performance of low power fans with less than 125 W input power that is not covered by European Parliament Directive 2009/125/EC.

Acknowledgements

This work was supported by the 0712/SBAD/5148.

Nomenclature

η	energy efficiency
P_{el}	input power of the fan
N	energy efficiency grade
ΔPc	total pressure increase
$\dot{V}$	volume flow of the air

Bibliography

[1] Commission Regulation of the European Union No. 327/2011.

[2] URBANIAK, R., BARTOSZEWICZ, J., KŁOSOWIAK, R. et al. Main causes of NO_x emissions by low-power boilers. *Polish Journal of Environmental Studies.* 2015, **24**(5), 2223-2230. https://doi.org/10.15244/pjoes/40938

[3] NYGARD, A., BARTOSZEWICZ, J., BIEŃCZAK, K. Identyfikacja nieprawidłowej eksploatacji kotłów na paliwo stałe. *Przemysł chemiczny.* 2019, **98**(8), 1281-1282. https://doi.org/10.15199/62.2019.8.14

[4] KOCZYK, H. Heating technology practice. *SYSTHERM.* Poznan 2009.

[5] BARTOSZEWICZ, J., KŁOSOWIAK, R., BOGUSŁAWSKI, L. The analysis of the flow structure in a jet at variable geometry of the reverse chamber. *International Journal of Heat and Mass Transfer.* 2012, **11**, 3239-3245. https://doi.org/10.1016/j.ijheatmasstransfer.2012.02.050

[6] BARTOSZEWICZ, J., NYGARD, A., URBANIAK, R. Characteristics of fans used in low-power boilers. *Journal of Power Technologies.* 2017, **97**(1), 69-74.

[7] FORTUNA, S. Fans. *The Publishing house of AGH*. Krakow 1999.

[8] FODEMSKI, T. Thermal measurements. part I and II, *WNT*, Warsaw 2006.

[9] EUautoczęści. [online] www.euautoczesci.pl/katalog-czesci/ogrzewanie_wentylacja, accessed: 04.06.2020

[10] SPAL Automotive USA. [online] www.spalusa.com/products/fans, accessed: 04.06.2020

[11] Polish standard No. PN-81/M-42367.

[12] Polish standard No. PN-M-43011.

[13] Polish standard No. PN-93/M-53950/01.

[14] Polish standard No. PN-81/M-42366.

Adam Nygard, MEng. – Institute of Thermal Energy, Poznan University of Technology.
e-mail: *adam.nygard@put.poznan.pl*

Prof. Jarosław Bartoszewicz, DSc., DEng. – Institute of Thermal Energy, Poznan University of Technology.
e-mail: *jaroslaw.bartoszewicz@put.poznan.pl*

Article citation info:
ANDRYCH-ZALEWSKA, M. Simulation tests of selected gas flow parameters through combustion engine valves. *Combustion Engines*. 2020, **183**(4), 21-28. https://doi.org/10.19206/CE-2020-404

Monika ANDRYCH-ZALEWSKA

CE-2020-404

Simulation tests of selected gas flow parameters through combustion engine valves

The article presents the numerical analysis of a single-cylinder gasoline engine with indirect injection and spark ignition. The goal is to recognize and analyze gas flow through inlet and outlet valves and channels. These data were obtained from the simulation of a four-cycle engine cycle without combustion of the fuel-air mixture. The simulation was carried out in ANSYS, using a dedicated IC Engine module. After the simulation, the result was analyzed on the cross-sectional plane of both the valves and the combustion chamber. This method provided the necessary and concise representation of the flow characteristics. Five separate stages are presented – two describing the different displacement of the valve for each inlet and exhaust stroke and one representing the phenomenon of overlapping. The type of flow, its speed and tendency to create turbulence are described.

Key words: *simulation, engines, Ansys, gas flow*

1. Introduction

The road internal combustion engines have been defining the modern world for the last century. They are integral and essential part of the marine and overland spedition. While becoming more and more undesirable in environmentally conscious society, they still play overwhelmingly dominant role in today's private transportation. ICEs (Internal Combustion Engine) triumph is founded on the characteristics of petroleum fuels. Even in XXI century, petroleum distillates are the best widely available energy carriers. While ICEs are being burdened with a wide range of flaws, such as low efficiency, complex design, extensive maintenance required or noise, they are still the most reliable and feasible source of motion available. These features, along with the long history of automotive experiences, make the ICEs still the most popular option [1, 2].

At the end of the 20th century, when the geopolitical situation was more or less stabilized, issues of global warming and climate change were revealed. It was pointed out that the means of transport have a significant impact on the emission of harmful compounds to the environment. With the introduction of Euro regulations aimed at reducing emissions of harmful compounds from vehicles, automotive manufacturers have received an ultimatum – either you are investing in technology that reduces these emissions, or your vehicles will not be allowed on the roads of the countries signing the agreements [1, 2, 11, 13].

There are two main methods for reducing engine exhaust emissions. The first, best prevention or reduction of their formation, i.e. the formation of processes in the cylinder, which include: design factors, fuel injection systems, suitable fuels. Second, reducing emissions by non-engine methods (aftertreatment), i.e. the use of a combination of catalytic reactors and particulate filters, such as TWC – Three Way Catalyst [6, 20].

To reach satisfying and acceptable emission rates while maintaining high efficiency of combustion process, advanced simulation technics are being used. CFD analysis is inherent component of engine design process. Not only it enables engineers to analyze the flow of gases within the entire engine assembly, including intake/exhaust manifolds and ports, but also to have the direct insight into combustion chamber and behavior of gas throughout every stroke [3, 7, 17].

With the use of analytical calculations and material science it is possible to design given components of an engine with a proper mechanical properties and safety factor. However, those methods cannot answer questions concerning the actual flows occurring inside the engine. Parameters describing cross sectional area of intake/exhaust ports can give scalar information about the volume efficiency of the canals, while omitting valuable information about the flow of the medium. This example can be translated to almost every gas/fluid operating part of the engine, starting with intake system, cooling system, exhaust system, with the emphasis on the exhaust manifold, where the timing of exhaust pulses is vital to the proper, unobstructed expulsion of the exhaust fumes.

The mechanism of provision of fresh air/fuel mixture to the cylinder, with the following expulsion of exhaust fumes throughout the 4-stroke cycle should also be considered from this perspective. It is obvious that while poppet valves are the main solution used in present ICEs to seal the chamber during specified periods of time, they are hardly the best one. Their shape accompanied by the specific motion of their operation has huge impact on the flow of the air/fuel mixture, seriously affecting the process of combustion chamber refilling and gas expulsion. This is the reason why CFD analysis of combustion chamber during full engine cycle is often used – it provides essential information about the characteristics of flow and the thermodynamic processes taking place, e.g. compression.

The goal of this thesis is the analysis of the engine cycle by the means of numerical simulation and further comparison of it with the previously designed engine parameters. With the help of virtual model of engine cycle, flow phenomena occurring during valve movement, including valve overlap, will be closely observed and researched. With the results in form of cross sectional diagrams of flow type and velocity, theoretical parameters of the engine will be investigated and compared to their simulation correspondents.

2. Researched engine

The simulation is conducted for single-piston port injection SI engine, realizing 4-stroke cycle. Two exhaust and two intake valves are regulated by double overhead camshaft system driven by a timing belt. Cooling of the cylinder is conducted directly through wet sleeve cylinder liner,

Received 12 September 2020; Received in revised form 27 October 2020; Accepted 27 October 2020
Available online 15 December 2020

with additional coolant channels in cylinder head. Outer liquid cooling system is responsible for heat transfer and maintaining stable operational temperature of the engine. Design of the analyzed engine in the Fig. 1.

Parameters of the tested engine are presented in Table 1.

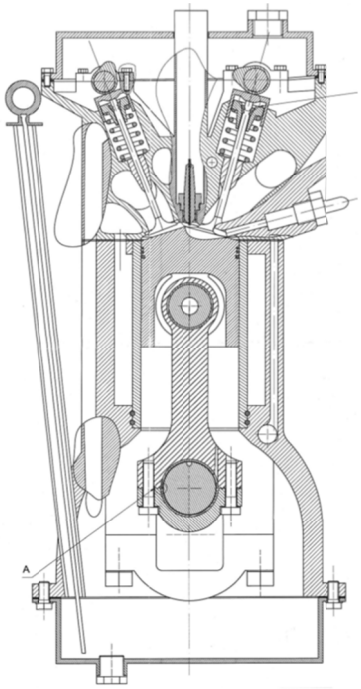

Fig. 1. Cross section of engine assemble [10]

Table 1. Design parameters of the engine [10]

Mechanical parameters		
Parameter	Value [unit]	Description
l	147 mm	Length of connecting rod
r	38.2 mm	Crank radius
D	85 mm	Cylinder bore
V_s	432.5 cm^3	Engine displacement
S	76.4 mm	Piston stroke
H_i	8.5 mm	Intake valve displacement
H_e	7.5 mm	Exhaust valve displacement
General parameters		
Parameter		Value
Realized thermodynamic cycle		Otto cycle (gasoline SI engine)
Injection		Port injection
Cooling		Liquid
Valvetrain system		DOHC
Air/fuel ratio		14.4:1
Parameter	Value [unit]	Description
N	25 kW	Power
n	7000 rpm	Maximum revolutions per minute
i	1	Number of cylinders
ε	9	Compression ratio
η	30.93%	Overall efficiency
–	4	Number of valves per cylinder
P_i	91 kPa	Intake manifold pressure
P_e	115 kPa	Pressure in exhaust system
P_0	101 kPa	Ambient pressure
T_0	300 K	Ambient temperature
g_e	264.5 g/kWh	Fuel consumption

3. Simulation assumptions

The due to complexity of simulation and limitations related to computing power of available computer, several assumptions and simplifications have to be introduced.

- Elimination of face radiuses – all inner surfaces of combustion chamber are modelled with sharp edges. Localized curvatures introduce high surface complexity, resulting in local mesh congestions. Increased number of mesh cells in these areas results in time-consuming calculations without much of an impact on the general analysis results. Model simplified in such a fashion, characterizes with satisfying credibility and optimal computation speed.
- Full air tightness – combustion chamber is fully sealed during compression and power stroke. It is assumed that piston ring seals are fully effective. With the blow-by loses ignored, there are no gas leakages piston throughout the cycle.
- Crevice volume omitted – crevice restricted by piston, cylinder and fire ring wall has no volume. While crevice does not have noticeable impact on the compression parameters, it introduces unwanted complications in the simulation model.
- Ambient temperature of the engine – all mechanical elements have negligible thermal conductivity and capacity. The temperature of the neighboring elements is stable and equal to ambient temperature throughout the cycle. No energy is introduced into the gas through the heat transfer from the boundary objects.
- Stable intake/exhaust pressure – no cyclic variations in intake/exhaust pressure are occurring throughout the cycle. In case of intake manifold, those can be effects of vacuum valve switching. In case of exhaust system, phenomenon of back pressure can severely restrict expulsion of gases.
- Ideal gas as a working medium – while simulating air/fuel mixture behavior, the ideal gas is used as a simulated medium. As the simulation does not cover the combustion, fuel addition in the air will only unnecessarily complicate simulation.
- No combustion – as the 4-stroke cycle is simulated with a use of a cold flow method, no combustion is taking place.
- Lengthened port channels – port channels are much longer to achieve equalized and even flow.
- Symmetry – due to the symmetry of the combustion chamber, only it's half will be calculated, to limit the necessary computing power.
- No spark plug – spark plug has been eliminated due to introduction of unnecessary complexity to the combustion chamber geometry.

Initially, dimensions are taken from the technical documentation [10] and each essential component of combustion chamber is modelled. Some undimensioned parts of complex shape, as intake/exhaust ports, are modelled with a personal input. With emphasis on the inner surfaces of combustion chamber, outer boundaries are omitted as they are not needed in the simulation. The model of the combustion chamber assembly is shown in Fig. 2.

To conduct the cold flow simulation, inner volume of combustion chamber and intake/exhaust ports is required (Fig. 3). This volume is restricted by: piston face, cylinder lining, cylinder head niche, seating faces of four poppet valves and the intake/exhaust porting.

The piston must be positioned in TDC (Top Dead Center), and the valves must be positioned in the closed position. Additionally, bodies of the intake and exhaust valves should be included into the file with the combustion chamber volume extract. Due to the ANSYS requirements, valve seating face has to be moved from the cylinder head seating face by a small margin, in this case 0.1 mm. This eliminates discontinuity in the flow phase by spreading apart boundaries of valve body and the cylinder head seating face [15, 18].

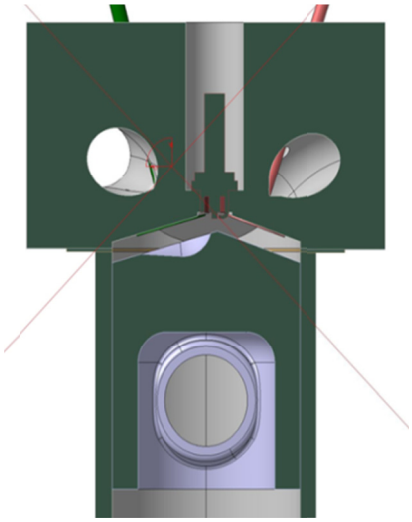

Fig. 2. Model of combustion chamber assembly

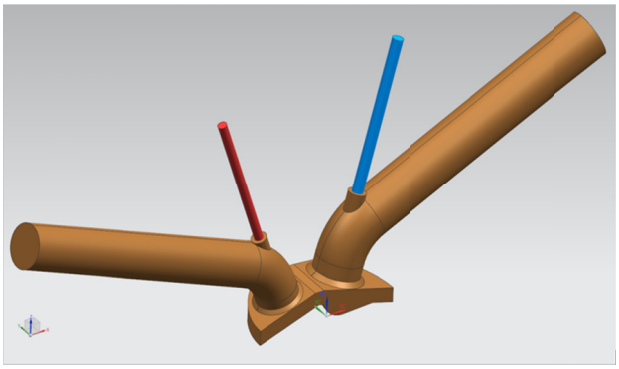

Fig. 3. Model of combustion chamber assembly

4. Design methodology

4.1. Style for figures

The simulation will be conducted in the ANSYS Products software, using IC Engine module. As the flow of the gas is directly dependent from crankshaft angle (phase of the engine cycle), transient simulation must be conducted. Due to variable volume of the combustion chamber and cyclic motion of the valves, dynamic mesh must be introduced. IC Engine module has integrated tools for automatic dynamic mesh construction, although they are unreliable and require extensive manual calibration. The model preparation consists of 5 main steps:

1. Model decomposition
2. Mesh parametrization
3. Mesh generation
4. Application of boundary conditions
5. Simulation process

Input model is split into array of characteristic sections required by the program. These parts carry individual information about the type of it's mesh and the meshing order (Table 2).

Table 2. In-program nomenclature of the decomposed bodies [9]

No.	Fluid Zone Name	Mesh requirement
1	fluid – ch	any mesh
2	fluid – valveID – ib	mesh with at least one layer at the top
3	fluid – valveID – port	any mesh
4	fluid – valveID – vlayer	layered mesh
5	fluid – crevice	any mesh

Section 1 recreates closed combustion chamber. Section 2 involves volume directly adhered to the valve stem. Section 3 recreates the intake/exhaust port volume. Section 4 recreates the seal created by valve being fully closed. Section 5 recreates crevice existing between piston cylindrical face, cylinder lining and fire ring (Figs. 4, 5).

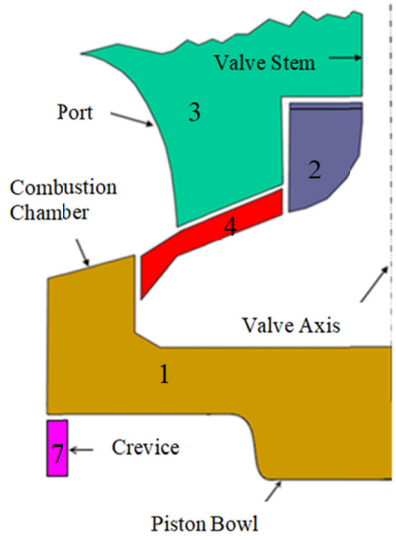

Fig. 4. Separate sections created in decomposition process [9]

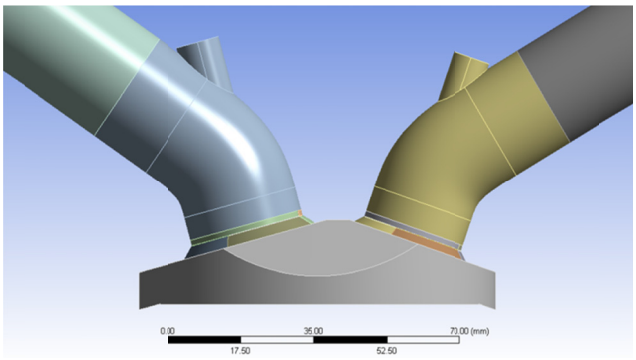

Fig. 5. Separate sections created in decomposition process [9]

First step of the meshing process is mesh parametrization. While whole sequence is automatic, user has possibility to configure mesh parameters of every decomposed body in terms of sizing, inflation and spacing. During mesh generation, ANSYS meshes decomposed body in set order, following previously mentioned parameters [5, 8, 12]. Mesh of whole geometry is shown in figure 6 and cross section of the valve mesh in Fig. 7.

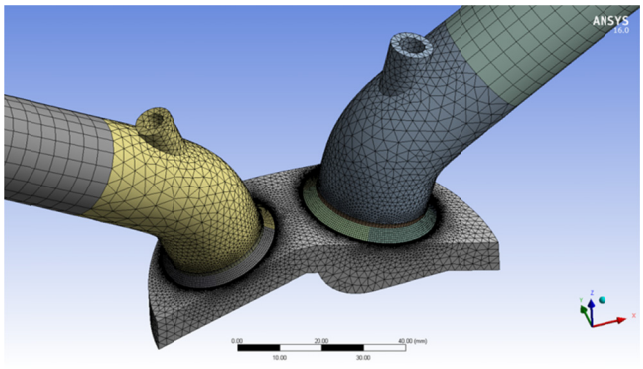

Fig. 6. Mesh of whole geometry

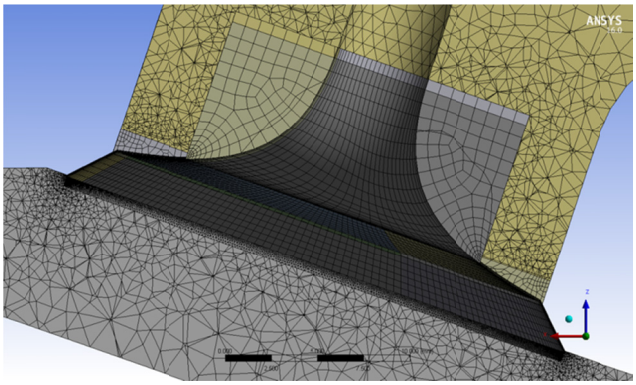

Fig. 7. Cross section of the valve mesh

Unfortunately, automatically generated mesh features a huge amount of mesh defects, yielding very poor mesh quality, essential for a successful simulation. Further mesh refinement of sections adjacent to valves, deletion of port inflation and modification of meshing methods results in mesh of satisfying quality. While minimal orthogonal quality assumes good number of 0.19, maximal cell skewness equals to 0.9, which is borderline satisfactory result for computable mesh. The improved mesh is shown in the Fig. 8.

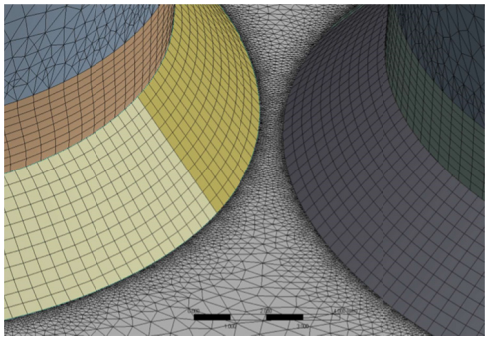

Fig. 8. High refinement of combustion chamber mesh cells adjacent to valve seals

4.2. Boundary conditions

For the simulation to run properly, a group of initial conditions must be set [14]. Those conditions not only regulate the cycle of the engine, but also directly influence the flow and behavior of the air/fuel mixture. Technical data of the researched engine provides information about values of these conditions. Following boundary conditions are being set:

- Intake pressure – value of underpressure created in the intake manifold due to continuous suction of fresh air into the combustion chamber. In the discussed engine, the intake pressure is 10 kPa lower than ambient pressure, equaling 91 kPa, that mean the engine full load work condition (Throttle Wide Open).
- Exhaust pressure value of elevated pressure existing in the exhaust manifold due to continuous expulsion of exhaust gases to the restricted system. In the discussed engine, the exhaust pressure is 14 kPa higher than ambient pressure, equaling 115 kPa.
- Revolutions per minute – simulated cycle is taking place at 1800 rpm.
- Combustion chamber temperature – as previously assumed, all combustion chamber boundaries have ambient temperature of 300 K.

The k-omega SST model was chosen for flow simulation, since k-epsilon is not able to capture the appropriate turbulent behavior of the boundary layer until it is detached [5]. The SST turbulence model k-ω is a two-equation model hybrid. It is a smooth transition from the k-omega standard model, used in the boundary layer, for the model k-ε as far as moving away from the surface that limits flow. Contains modified formulation of turbulent viscosity for the purpose taking into account the effect of transport of main shear stresses.

5. Result analysis

5.1. Analysis methodology

For the simulation the simulated data will be presented in form of charts placed on the plane sectioning both valves. This method will provide essential and concise depiction of flow characteristics. Five separate stage samples will be presented – two describing different valve displacement for each intake and exhaust stroke and one depicting overlap phenomenon.

Each stage sample will be analyzed with regard to two best suited parameters describing flow of the gas – it's magnitude velocity, portrayed by contour charts and turbulence kinetic energy (TKE) which will be presented as contour charts as well.

The TKE is defined to be half the sum of the variances of the velocity components and can be description [24]:

$$\mathrm{TKE} = \frac{1}{2}\left(\overline{(u')^2} + \overline{(v')^2} + \overline{(w')^2}\right) \tag{1}$$

where the turbulent velocity component is the difference between the instantaneous and the average velocity $u' = u - \bar{u}$, whose mean and variance are:

$$\bar{u'} = \frac{1}{T}\int_0^T (u(t) - \bar{u})\,dt = 0 \text{ and}$$

$$\overline{(u')^2} = \frac{1}{T}\int_0^T (u(t) - \bar{u})^2 \, dt \geq 0.$$

This will give us precise information about the type and dynamic parameters of the flow taking place in every spot of the combustion chamber and intake/exhaust porting.

5.2. Exhaust stroke with 3.75 mm exhaust valve displacement

With the valve opened halfway through, the flow characteristic becomes discernible. Gases are being expulsed through the crevice created between valve and the seating face of the cylinder head, and pushed onto the valve stem. They are forced around the valve stem, then proceed along the upper wall of the exhaust channel and the valve guide. As the gas velocity in the reducer reaches speed of about 200 m/s, it carries significant portion of kinetic energy. There are few significant technological flaws in the exhaust porting itself. Firstly, due to incorrect curvature of the exhaust channel wall, localized, highly turbulent flow occurs in the upper section of the channel, directly next the valve stem. This results in high local flow resistance, negatively impacting engine's capability to expulse exhaust gases. Parameters were tested during the simulation of velocity (Fig. 9) and turbulence (Fig. 10) [15].

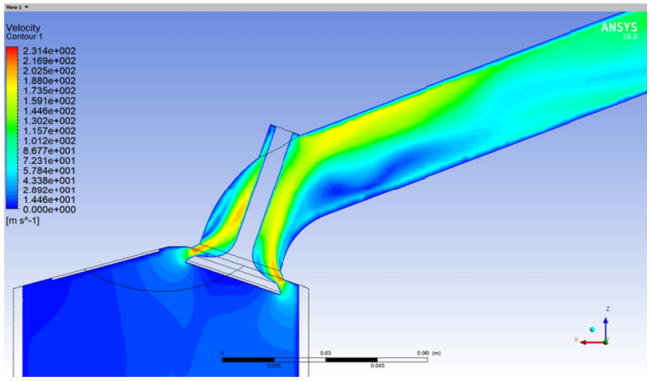

Fig. 9. Contour chart of the velocity of flow during exhaust stroke with 3.75 mm exhaust valve displacement

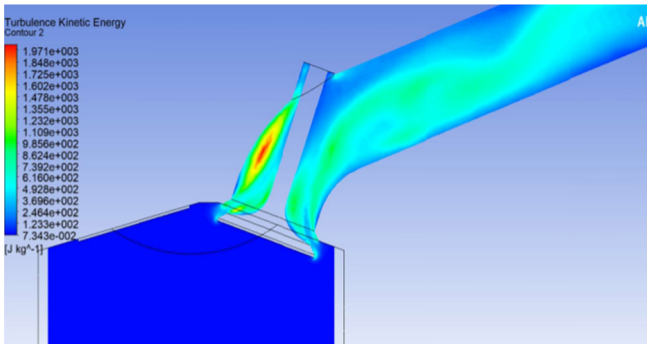

Fig. 10. Contour chart of the turbulence kinetic energy of flow during exhaust stroke with 3.75 mm exhaust valve displacement

5.3. Exhaust stroke with 7.5 mm exhaust valve displacement

As the exhaust valve reaches maximal displacement, highest volumetric flow is achieved. The maximal velocity of gases is further increased, reaching about 240 m/s in the reducer, and spans on much higher volume. Therefore, flow issues become more dominant, resulting in three localized turbulence zones. Parameters were tested during the simulation of velocity (Fig. 11) and turbulence (Fig. 12). First one possesses same characteristics as in previous stage sample. Second one, is a direct effect of exhaust gasses hitting the valve stem at high speed, and is a design flaw of this particular combustion chamber sealing solution.

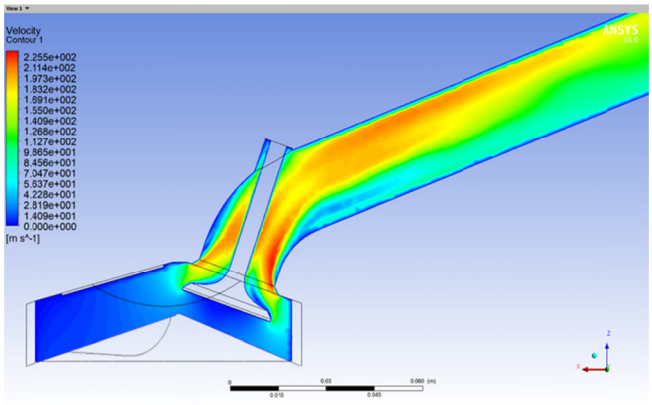

Fig. 11. Contour chart of the velocity of flow during exhaust stroke with 7.5 mm exhaust valve displacement

Third turbulence zone is located next to the lower wall of the exhaust channel, and is a result of gasses being peeled off the main flow streamline, and having tendency to eddy against the main flow. The valve guide cutout also poses a significant problem, as it breaks the smoothness of the channel wall, resulting in gasses being trapped inside it and inducing further turbulences [15].

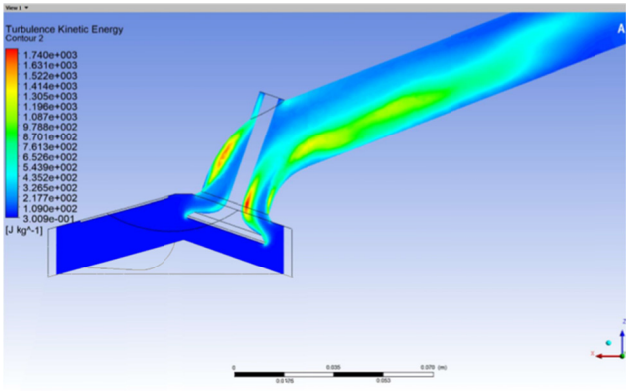

Fig. 12. Contour chart of the turbulence kinetic energy of flow during exhaust stroke with 7.5 mm exhaust valve displacement

5.4. Overlap phase with 2 mm exhaust and intake valve displacement

On most engines, during a short angle span of the crankshaft rotation, both valves are simultaneously opened with a certain displacement. In theory, this allows for inflow of fresh air/fuel mixture into the combustion chamber, and further ventilation of the post-combustion gases. This process generally increases the cleanliness and efficiency of the combustion itself. Simulation has shown that while the actual ventilation does take please, resulting in a flow of the gases from intake to the exhaust channel, this flow seems almost completely separated from the combustion chamber volume. Parameters were tested during the simulation of velocity (Fig. 13) and turbulence (Fig. 14).

Assumption was made, that the coldflow type of the simulation affect this process. Lack of the post-combustion gases results in different, unrealistic pressure in the combustion chamber, introducing the deviations in the simulation model. It is important to note, that while combustion chamber is not involved in the gas exchange, the flow from the intake valve actually moves the masses of gas which are located in the corner of the cylinder head. These masses were virtually trapped in that corner during both stage samples of exhaust stroke (it's velocities were close to 0), resulting in poor ventilation of these areas.

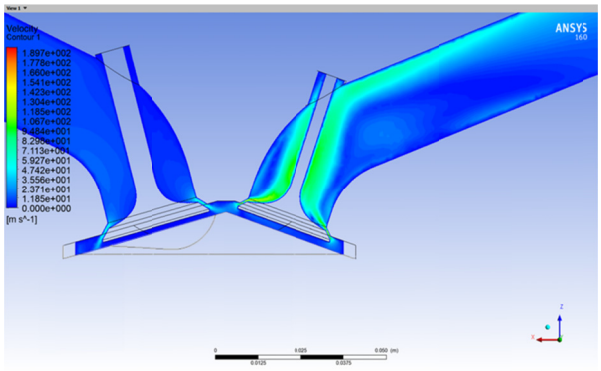

Fig. 13. Contour chart of the velocity of flow during overlap phase with 2 mm exhaust and intake valve displacement

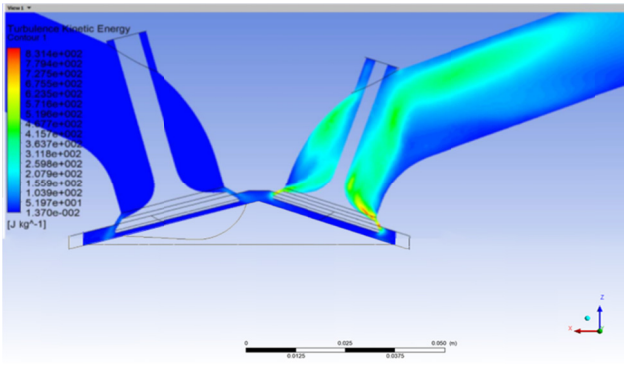

Fig. 14. Contour chart of the turbulence kinetic energy of flow during overlap phase with 2 mm exhaust and intake valve displacement

It means that the overlap, while not providing noticeable impact on the gas exchange, does improve gas circulation in the combustion chamber. Another theory implies that design of the combustion chamber is flawed, with the valves being too close to each other [15].

5.5. Intake stroke with 4.25 mm intake valve displacement

During the intake stroke, intake valve is opened for a fresh air/fuel mixture to enter the combustion chamber. The shape and curvature of streamlines formed by the gas entering the combustion chamber is extremely important – proper mixing of the gas inside the chamber will positively impact the combustion process, eliminating hot spots, lowering the emission of toxic fumes and limiting knocking. The flow of the gas is much more ordered, compared to the exhaust stroke. Throughout the intake channel, turbulence kinetic energy of the gas is very low, and the flow can be described as laminar. This is not surprising, as the shape of crevice and intake channel directs the air flow in much more orderly fashion. Due to that fact, velocities of the gas reach the maximal value of 60 m/s, but typically are oscillating around 40 m/s. It is worth noticing how the flow is directed by the cylinder walls, and further by the piston. This leads to the formation of swirls inside the combustion chamber, resulting in throughout mixing. Parameters were tested during the simulation of velocity (Fig. 15) and turbulence (Fig. 16).

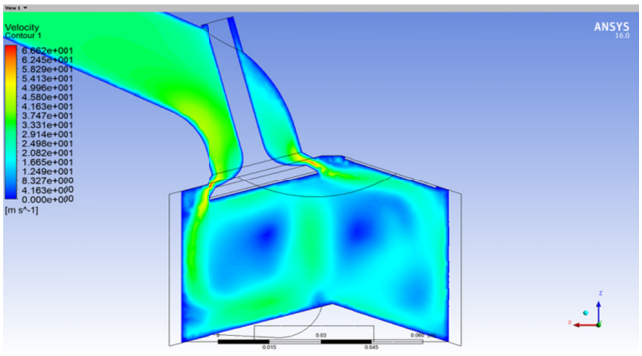

Fig. 15. Contour chart of the velocity of flow during intake stroke with 4.25 mm intake valve displacement

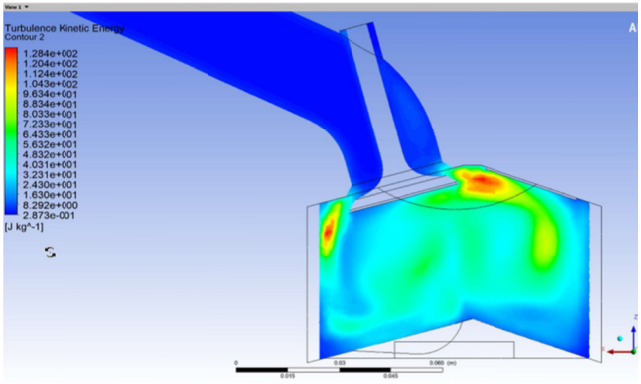

Fig. 16. Contour chart of the turbulence kinetic energy of flow during intake stroke with 4.25 mm intake valve displacement

Two noticeable turbulence zones occur – both are positioned in the combustion chamber, in closed proximity to the intake valve. They are created by the inflowing gas bouncing of the edge of the valve's seating face [15].

5.6. Intake stroke with 8.5 mm intake valve displacement

With the intake valve fully open, the maximal volumetric flow occurs. All described phenomena in the previous stage sample are gaining on intensity. Parameters were tested during the simulation of velocity (Fig. 17) and turbulence (Fig. 18).

Mixing of the gas inside the combustion chamber is much more erratic, with the swirls noticeable, but much less visible than in previous stage sample. The velocity of the gas does not change, and ranges from the maximum of 60 m/s, to the average of 40 m/s. It should be pointed out that the turbulences occurring in close proximity to valve, during early stages of intake valve opening, are decreasing, and even disappearing with the increase of intake valve displacement [15].

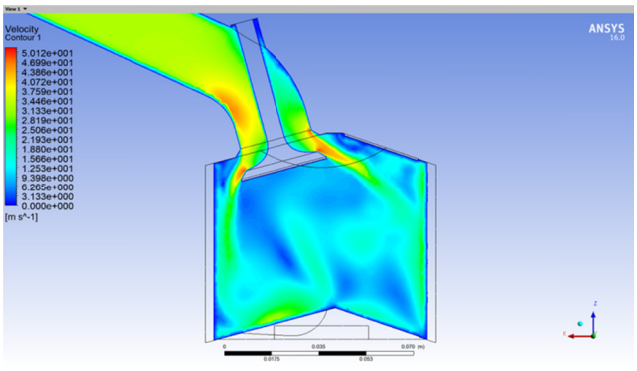

Fig. 17. Contour chart of the velocity of flow during intake stroke with 4.25 mm intake valve displacement

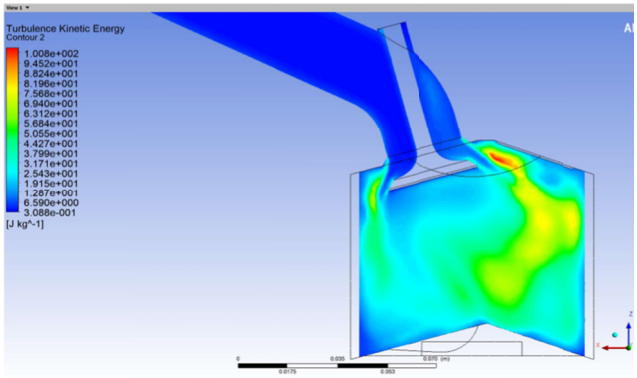

Fig. 18. Contour chart of the turbulence kinetic energy of flow during intake stroke with 8.5 mm intake valve displacement

6. Thermodynamic analysis

Due to high complexity of flow occurring throughout the combustion chamber volume, thermodynamic parameters are ought to change. As the pressure and temperature are strictly bound to the type of flow and it's velocity, it already can be concluded that evident pressure and temperature gradient will arise. While simulation model does not include temperature convection, it does feature ideal, compressible gas, meaning the temperature of the gas will fluctuate depending from the pressure and flow it experiences. All pressure values are relative to the ambient pressure, which means, that absolute pressure value is sum of gauge pressure and ambient pressure.

- Exhaust stroke with 3.75 mm exhaust valve displacement. The exhaust stroke is happening with stable pressure of 77 kPa inside the combustion chamber. As the flow of the gas is accelerated inside the exhaust channel, it's pressure drops to average of 20 kPa. Local discontinuities in exhaust channel surface, like valve guide cutout restrict the flow, locally increasing the pressure up to 25 kPa. Temperature of the gas in the main streamlines is significantly lower compared to the surroundings, and ranges from 250 to 275 K. As the highest flow is achieved in the valve crevice, it is also the point of highest decompression and lowest temperature.
- Exhaust stroke with 7.5 mm exhaust valve displacement. The value of exhaust stroke pressure inside the combustion chamber changes slightly to 76 kPa. The flow is significantly stronger, leading to the further drops of pressure and temperature. In the main streamlines temperature drops down to 250 K while the absolute pressure value oscillates around the ambient pressure value. Pressure inside the exhaust channel averages around 6 kPa.
- Intake stroke with 4.25 mm intake valve displacement. In the early stage of intake valve opening, the flow is low and ordered enough to not cause high temperature and pressure changes. With the exception of valve crevice where temperature drops about 6 K, it is uniform across the volume of the combustion chamber and oscillates around 300 K.
- Intake stroke with 8.5 mm intake valve displacement. With the valve fully extended, intake flow is much higher. This results in small temperature gradient forming in the combustion chamber, with the maximum gradient (of about 2 K) located similarly to previous stage samples, in the valve crevice.

7. Conclusions

In CFD methods, the problem is the interpretation of results, because the computer "counts everything", unfortunately not always in accordance with the physical characteristics of the phenomenon. This requires a skillful interpretation of the results [4, 16, 23].

While this engine project in theory fulfilled every design criterion, analytical calculations never actually included the gas exchange occurring inside the intake/exhaust ports and combustion chamber. CFD analysis proved useful in defining parameters of simulated flow, and it's visualization inside the combustion chamber. It also pointed out several design features that can be altered in order to achieve smoother, less disturbed and what's more, less resistive flow. Following features seem to negatively impact the flow of the gas:

- Exhaust channel curvature – wrong curvature induces reverse flow in the proximity of valve stem (Figs 9, 11). Introduction of lower curvature channel would unify the flow around the stem, but what's more important, it would minimalize the turbulence.
- Exhaust channel cross sectional area – an alteration of exhaust channel cross section into the oval instead of circle seems to unify the flow throughout the whole width of the exhaust channel, eliminating elongated turbulence zone (Figs 9, 11).
- Intake and exhaust valve position in combustion chamber – as the gas exchange during the valve overlap seems poor, increased distance between intake and exhaust valve would theoretically force the inert combustion chamber gases to participation in this exchange.
- Exhaust valve guide cutout – as the valve guide cutout poses a significant flow obstacle, decreases in this size or shape would bring positive effect on. When the mechanical construction of poppet valve does not allow us to do so, cast radiuses are the alternative.

As the simulated values of flow's velocity differ significantly from the theoretical values, it is important to analyze the factors that could somehow affect the flow to such extent. In theoretical calculations, this values are selected based on statistic data regarding flow in intake/exhaust port of the industrial engines [22]. That data is extremely impre-

cise, and provides only an estimation of the real-life values. The CFD analysis takes into account not only the cross sectional area of the intake/exhaust channels, but also examines their curvature and every obstruction which can lead to separation and turbulences of the flow. Those obstacles might be of any kind, like the valve stem, valve guide cut out, seating face of the cylinder head and so on. Therefore, while theoretical calculations are based on the extract data from statistics, real-life parameters might have completely different value.

In the CFD calculation methods, the interpretation of results is an important aspect. These methods give results that in many cases are demonstrative and not always consistent with the physical characteristics of the phenomenon. They can be used as preliminary tests for real-world tests, initial selection of structural parameters and designing changes. By extending knowledge in the field of frequency analysis of pulsation of pressure with the influence of work, design and thermodynamic parameters on the spectrum of the signal, a tool can be created for effective and quick assessment of changes in the system [19, 21].

Nomenclature

CFD	computational fluid dynamics
DOHC	double overhead camshaft
ICE	internal combustion engine
SI	spark ignition
TDC	Top Dead Center

Bibliography

[1] KALGHATGI, G.T. Developments in internal combustion engines and implications for combustion science and future transport fuels. *Proceedings of the Combustion Institute*. 2015, **35**(1), 101-115. https://doi.org/10.1016/j.proci.2014.10.002

[2] NABER, J.D., JOHNSON, J.E. Alternative fuels and advanced vehicle technologies for improved environmental performance. *Woodhead Publishing*. 2014, 197-224. https://doi.org/10.1533/9780857097422.1.197

[3] HONG, H., PARVATE-PATIL, G.B., GORDON, B. Review and analysis of variable valve timing strategies – eight ways to approach. *Proceedings of the Institution of Mechanical Engineers, Part D: Journal of Automobile Engineering*. 2004, **218**(10), 1179-1200. https://doi.org/10.1177/095440700421801013

[4] GÓRNIAK, A., MICHAŁOWSKI, R., TKACZYK, M. Symulacje układu dolotowego silnika zasilanego CNG. *Autobusy*. 2011, **12**.

[5] ANSYS Meshing User's Guide_r130.pdf. ANSYS 2013.

[6] MERKISZ, J., PIELECHA, J., RADZIMIRSKI, S. Emisja zanieczyszczeń motoryzacyjnych. *Wydawnictwa Komunikacji i Łączności*. Warszawa 2012.

[7] WILCOX, D. Turbulence modeling for CFD. *KNI*, Inc., Anaheim, 2002.

[8] THOMPSON, J., WARSI, Z., MASTIN, C. Numerical grid generation. Foundations and applications. *Elsevier Science Publishing Co., Inc.,* New York 1985.

[9] SHARCNET https://www.sharcnet.ca/Software/Ansys/17.0/enus/help/wb_icom_decomp_part_bods_pis3 .html [Accessed 15.5.2019]

[10] CIEŚLIK, W. Silnik spalinowy ZI. Projekt. *Politechnika Poznańska*. Poznań 2011.

[11] WAJAND, J.A., WAJAND, J.T. Tłokowe silniki spalinowe średnio- i szybkoobrotowe. *Wydawnictwa Naukowo-Techniczne*. Warszawa 2003.

[12] ANSYS-Fluent-Tutorial-Guide_r170.pdf

[13] http://zss.lublin.eu/wp-content/uploads/2016/09/2.5-Proces-spalania.pdf, 12.01.2019.

[14] FORTUNA, Z., MACUKOW, B., WĄSOWSKI, J. Metody numeryczne. *Wydawnictwa Naukowo-Techniczne*. Warszawa 1982.

[15] KAWECKI, J. Evaluation of selected thermodynamic parameters in simulation tests of an internal combustion engine. *Master's thesis*. Wroclaw 2019.

[16] TUTAK, A., JAMROZIK, A. Modelling of the thermal cycle of a gas engine using AVL FIRE Software. *Combustion Engines*. 2010, **141**(2).

[17] TUTAK, W. Modelowanie i analiza wybranych parametrów obiegu cieplnego silnika tłokowego z EGR. *Combustion Engines*. 2011, **147**(4).

[18] HEYWOOD, J.B. Internal combustion engines fundamentals. *McGraw-Hill*, New York 1988.

[19] TUTAK, W. Interpretacja wyników pomiarów prędkości przepływu ładunku w komorze spalania tłokowego silnika spalinowego. *Pomiary Automatyka Kontrola*. 2008, **54**(2).

[20] ANDRYCH-ZALEWSKA, M., CHŁOPEK, Z., MERKISZ, J. et al. Evaluation of the test drive cycle conditions impact on exhaust emissions from an internal combustion engine. *Combustion Engines*. 2018, **175**(4), 3-9. https://doi.org/10.19206/CE-2018-401

[21] PYSZCZEK, R., SCHMALHORST, C., TEODORCZYK, A. Numerical investigation on diesel combustion and emissions with a standard combustion model and detailed chemistry. *Combustion Engines*. 2015, **162**(3), 19-33.

[22] GĘCA, M., HUNICZ, J., JAWORSKI, P. Numerical investigation into the effect of direct fuel injection on thermal stratification in HCCI engine. *Combustion Engines*. 2017, **169**(2), 137-140. https://doi.org/10.19206/CE-2017-224

[23] KOWALSKI, J. The CFD analysis of influence the start of fuel injection (SOI) on combustion parameters and exhaust gas composition of the marine 4-stroke engine. *Combustion Engines*. 2019, **177**(2), 40-45. https://doi.org/10.19206/CE-2019-207

[24] POPE, S.B. Turbulent flows. *Cambridge University Press*. 2000, 122-134.

Monika Andrych-Zalewska, DEng. – Faculty of Mechanical Engineering, Wroclaw University of Science and Technology.
e-mail: *monika.andrych@pwr.edu.pl*

Article citation info:
ENGELMANN, D., COMTE, P., CZERWINSKI, J. et al. Non-regulated emissions and particle number emissions of two passenger cars with diesel-butanol blends. *Combustion Engines*. 2020, **183**(4), 29-38. https://doi.org/10.19206/CE-2020-405

Danilo ENGELMANN
Pierre COMTE
Jan CZERWINSKI
Stephan RENZ
Peter BONSACK

CE-2020-405

Non-regulated emissions and particle number emissions of two passenger cars with diesel-butanol blends

Biofuels represent one of the alternatives to obtain the CO_2-neutral propulsion of IC-engines. Butanol, which can be produced from biomass, is considered and was investigated in the last years due to the very advantageous characteristics of this alternative fuel. Butanol can be easily and irreversibly blended both with light (gasoline) and heavier (diesel) fuels. Comparing with ethanol it has the advantages of: higher calorific value, lower hygroscopicity and lower corrosivity. It can replace the aviation fuels.

This paper presents the emission results obtained on two diesel passenger cars with different technology (Euro 2 and Euro 6c) and with addition of butanol to diesel fuel, as a part of the research project DiBut (diesel and butanol). Interesting results are given about some non-legislated (non-regulated) components, acetaldehyde (MeCHO) and formaldehyde (HCHO) and about the PN-emissions with/without DPF.

Key words: *alternative fuels, non-legislated emissions, ultrafine particles, diesel particle filter, cold start emissions*

1. Introduction

Butanol with chemical formula ($CH_3(CH_2)_3OH$) is a higher-chain alcohol, comparing to methanol or ethanol. There are different isomers of butanol, which have various positions of the hydroxyl group (-OH) in the molecule.

The most common and important is n-butanol with a straight-chain structure and with the OH-group at the terminal carbon [1, 2]. The known research in diesel application, and also in the present project, was performed with n-butanol.

Some data of diesel-butanol blend fuels, according to [3, 4], are given in the following Table 1.

Table 1. Data of diesel fuel, n-butanol and their blends

	Ref. Diesel	**Bu05**	**Bu15**	**Bu30**	**Bu50**	**n-Bu**
Density at 15°C in kg/m^3	833–837	833	832	828	822	806
Net calorific value in MJ/dm^3	35.3	34.9	34.0	32.8	31.4	26.7
Stoichiometric air/fuel ratio	14.6	14.4	14.0	13.5	12.9	11.2
Oxygen content in wt.-%	< 0.03	1.1	3.1	6.4	10.7	21.6
H:C ratio (molar)	0.157	0.160	0.165	0.170	0.179	0.208
Cetane number	52–54	≈51	≈48	≈43	≈35	≈19

The higher oxygen content of butanol and butanol blend fuels (BuXX) has similar advantages for engine-out (EO) emissions, like other alcohols or oxygenated fuels. The general tendency is lowering of CO and HC (especially for SI-engines, EO) and lowering of PM (for diesel engines, EO) [5–17].

The importance of alternative, sustainable, CO_2-neutral fuels for IC-engines cannot be too strongly emphasized. There is a lot of world-wide research on many variants of potentials fuels, substitutes or derivatives both: for SI- and CI-applications. Examples of interesting variety of research topics can be found in the CO-OPTIMA Publications Library of the US Department of Energy [18].

With the present research activities, the authors tried to complete the knowledge concerning nanoaerosol particle number (PN) and non-legislated gaseous emission components with the butanol blend fuels in diesel application. The project "Diesel-Butanol" (DiBut) consisted of two parts, which were performed on engine dynamometers and on passenger cars.

The first part of the results on engine dynamometers was presented in [19] and it confirmed the lowering of PN engine-out emissions with butanol blends (BuXX). For the combustion it results that, with rising butanol shares of fuel blends, their characteristics are changing, causing aptitudes of quicker evaporation and of slower self-ignition. The last one is due to the significantly lower cetane number of butanol. The operating limit blend ratio concerning cold start, warm-up and low load operation is at approximately Bu30.

The modern exhaust aftertreatment of a Euro 6 engine consisting of DOC/DPF/SCR contributes to the elimination of PN and shows excellent deNO_x-performances with butanol blends.

In the second part of DiBut-project butanol mixed fuels were applied on two diesel passenger cars with different engine technologies. These results of testing cars on chassis dynamometer, included cold starts and non-legislated gaseous emissions and they are subject of the present paper.

An important problem by application of alternative, and biogene fuels in diesel engines, is the lubricity (concerning the injection system) and the long-term impact on lube oil [20–23]. For butanol special lubricating additives can be

Received 1 September 2020; Received in revised form 27 October 2020; Accepted 27 October 2020
Available online 15 December 2020

applied. Nevertheless, this problem was not investigated in the present project.

2. Test vehicles, fuels and lubricants

Two vehicles were used for the present tests. An older car (Euro 2), with traditional concept of injection (distributor pump) and exhaust after-treatment (DOC) and a newer one (Euro 6c), with common rail injection and exhaust aftertreatment (DPF + deNO_x).

The most important data of the test vehicles are given in the Table 2.

Table 2. Data of test vehicles

Vehicle	**Opel Astra DI16V V1**	**VW Passat Variant V 2.0TDI V2**
Cylinder	4	4
Overall displacement [cm^3]	1994	1968
Power [kW]	60	110
Injection type	DI distr. pump	DI/CR
Fuel	diesel	diesel
Weight empty [kg]	1390	1621
Transmission	M5/Front	M7/Front
Matriculation	20.01.1998	9.02.2018
Turbocharging	yes	yes
Exhaust aftertreatment	DOC	DOC, DPF, SCR
Emission level	Euro 2	Euro 6c

Fuels: the diesel fuel used was from the Swiss market, according to SN EN590. The used blend fuels were: Bu15 (15% v butanol in diesel fuel) and Bu30 (30% v butanol in diesel fuel). Some data of diesel-butanol blend fuels are given in the Table 1.

Lubricants: the lubricants were used according to the recommendations of the manufacturers, they were not specially changed or analyzed.

3. Instrumentation

Following instrumentation and equipment have been used.

Chassis dynamometer: Schenk 500 GS 60 with driver conductor system: Tornado, version 3.3 and CVS dilution system: Horiba CVS-9500T with Roots blower. There is an automatic air conditioning in the hall (for intake- and dilution air).

Test equipment for regulated exhaust gas emissions fulfils the requirements of the Swiss and European exhaust gas legislation. It consists of exhaust gas measuring system Horiba MEXA-9400H: CO, CO_2 – infrared analyzers (IR), HCIR, HCFID, NO/NO_X, CLA. The accuracy of these analyzers is ±1% of full scale. The dilution ratio DF in the CVS-dilution tunnel is variable and can be controlled by means of the CO_2-analysis. The accuracy of the entire exhaust gas measuring system, including analyzers, CVS-system and chassis dynamometer is ±4%.

FTIR for non-legislated gaseous emissions: FTIR (Fourier Transform Infrared) Spectrometer (AVL SESAM) offers the possibility of simultaneous, time-resolved measurement of approx. 30 emission components – among others: NO, NO_2, NO_x, NH_3, N_2O, HCN, HNCO, HCHO and MeCHO.

The sampling for measurements with FTIR was carried out at tailpipe. The sensitivity of this system is in the range of 1 ppm.

3.1. Nanoparticle analysis

The measurements of particle size distributions were conducted with different SMPS-systems, which enabled different ranges of size analysis (SMPS – scanning mobility particle sizer):

SMPS: DMA TSI 3081 & CPC TSI 3772 (9.8–429 nm).

nSMPS: nDMA TSI 3085 and CPC TSI 3776 (2–66 nm).

For measuring of the summary particle counts according to the legal guidelines (PMP) a CPC TSI 3790 was used. The accuracy of this device is given by the manufacturer with ±10%.

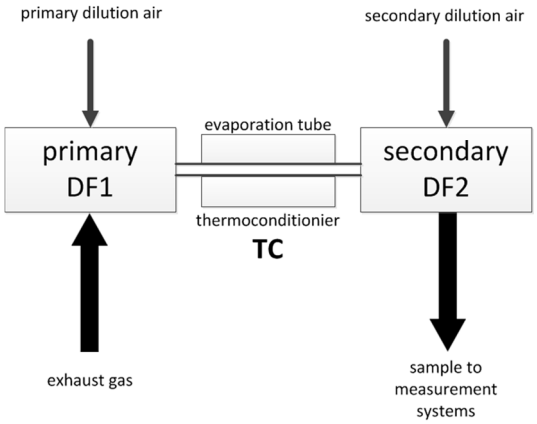

Fig. 1. Set-up of dilution stages and sample preparation for nanoparticle measurements

The Figure 1 shows the scheme of the used sample preparation for PN-measurements (ASET), which consists of 2-stage dilution and thermo-conditioning (TC) with sample heating at 300°C.

The measuring set-up on chassis dynamometer and the possible sampling positions for particle analytics are represented in the Fig. 2. In the present tests, the sampling with both systems SMPS and CPC was carried out at tailpipe.

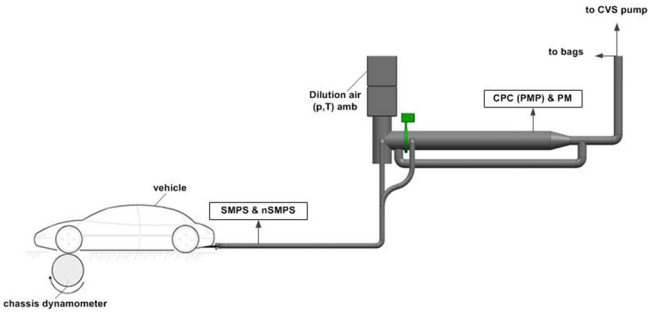

Fig. 2. Sampling of exhaust gas for analysis of particles

4. Test procedures

The tests were performed with both vehicles on a chassis dynamometer in the dynamic driving cycles WLTC and at constant speeds in the steady state cycle (SSC).

WLTC represents different driving situations, like city, over-land and speedway, in the Fig. 3.

SSC consists of 20 min steps at constant vehicle speeds 95, 45 km/h and idling, which are driven from the highest to the lowest speed. These vehicle speeds respond to the average speeds in parts of the WLTC.

The test sequences with all fuels were identical: WLTC with cold start (20–25°C), 10 min idling for bag evaluation, acceleration to 95 km/h and continuation of the SSC.

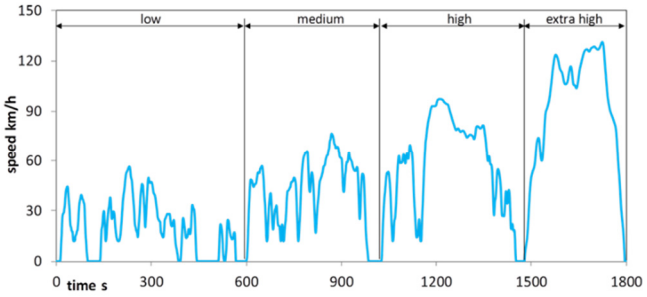

Fig. 3. WLTC driving cycle

5. Cold start

Repetitive cold start tests were performed with Bu0/Bu15/Bu30, in two temperature domains: 20 to 25°C, which is obtained by conditioning the vehicle in the laboratory hall and –2°C to 4°C, which could be obtained by conditioning the vehicle outside during the winter period. The cold start (CS) in the higher temperature range can be considered as a summer cold start and it is described for simplification as CS@20°C. The lower temperature represents the mild winter cold start and is designed in the further tests as CS@0°C. The vehicles were started and operated at idling with on-line measurement of all emission components. After the measuring period at idling a WLTC was performed as conditioning for the next CS.

For the CS@0°C, the vehicle was pushed from outside into the test hall. For the start and for the following operation the intake air from the hall (20–25°C) was available.

6. Results

6.1. Comparisons of emissions of vehicles with older and with newer technology

The Figure 4 shows the cumulated emissions of both vehicles in $WLTC_{cold}$. The cumulated concentrations of respective components in the CVS-diluted exhaust gas are equivalent to the emitted mass of these components but enable the representation of relationships over the cycle time. It can be remarked, that with increasing Butanol content in the fuel (BuXX), the cumulated emissions of CO, HC and NO_x in the $WLTC_{cold}$ increase and PN decrease. Similar tendency, but less pronounced is also given in $WLTC_{warm}$ (not presented here).

Vehicle V2 (with newer technology) has much lower emission level and the differences between Bu00 and Bu30 are less significant.

The Figure 5 compares the SMPS particle size distributions (PSD) of both vehicles at two constant OP's (idling and 95 km/h). For better representation linear and logarithmic scales are used. In the linear scale, the Euro 6c (V2) particle numbers are not visible. In the logarithmic scale single counts (no distributions) are possible to remark for Euro 6c.

Without DPF (V1) the same tendency, like in previous research of this project, was found. With increasing BuXX there are: higher PN in nuclei mode and lower PN in accumulation mode, so that the summary PN is lower.

Similar results were found in other projects with alternative fuels, like RME, crude rapeseed oil, or ethanol [20, 21, 24]. The reasons of modified PSD-shapes with those fuels at engine-out are first of all: the higher oxygen content of the fuels and the modified chemistry of the nanoaerosol (especially the heaviest HC-fraction/SOF). For this modified chemistry the interaction of fuel with the lube oil layer in the combustion chambers plays a very important role [22, 23].

With DPF (V2) the particle count concentrations are strongly reduced (by 2 to 5 orders of magnitude), but they are higher with Bu30, than with Bu00. This also confirms the tendency found previously on engine with DPF and it is explained with another composition of the aerosol SOF and consequently modified behavior (nucleation, diffusion loses) in the exhaust and in the sampling systems.

More detailed explanation of this artefact is: the presence of Butanol in the blend fuel causes among others a modified structure of heavy SOF in exhaust. Part of these SOF, which pass the DPF in gaseous state of aggregation produce spontaneous condensates, which become semi-solids in the sampling (analyzing) line and cannot be entirely eliminated by the sample treatment of the PN measuring system. These effects are only visible with a very low (near to ambient) PN emission level with DPF. Without DPF (Euro 2) the PN emission level is up to 5 ranges of magnitude higher and the effects from engine-out emissions are predominant. Despite that the DPF reduces or eliminates the nanoparticles down to the ambient count concentration level or below it.

The Figure 6 gives a sample of PSD results with SMPS (10–400 nm) and with nSMPS (2–66 nm). The results of both measuring systems correlate very well in the common measured size range (10–66 nm). Without DPF (V1) there are sporadic counts down to 5 nm, with DPF (V2) there are no counts below 10 nm. It can be stated that the filtration efficiency of a right-quality DPF is valid or even improved in the sub 23 nm size range. There are no differences of count concentrations with different investigated fuels.

The Figure 7 summarizes the comparisons of NO_x and PN with both vehicles and with different fuels in $WLTC_{warm}$. The lower PN-emissions of vehicle V2 (with DOC/DPF/SCR) are clearly visible. With increasing BuXX for vehicle V1 NO_x increases and PN decreases very slightly, while for vehicle V2 there is no effect on NO_x and there is a reduction of PN.

Vehicle 1

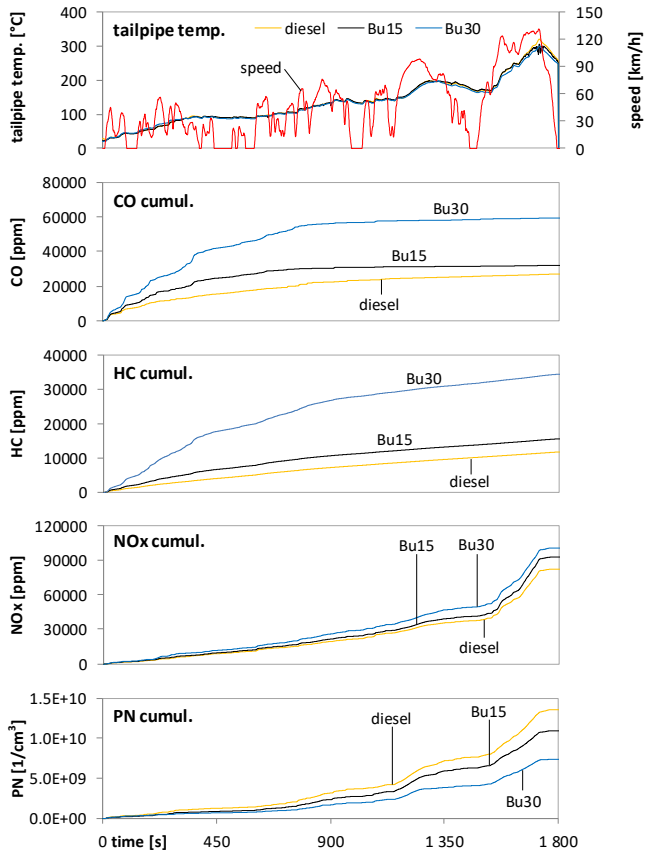

Fig. 4a. Cumulated diluted exhaust emissions and tailpipe temperatures in WLTC cold with different fuels, V1

Vehicle 2

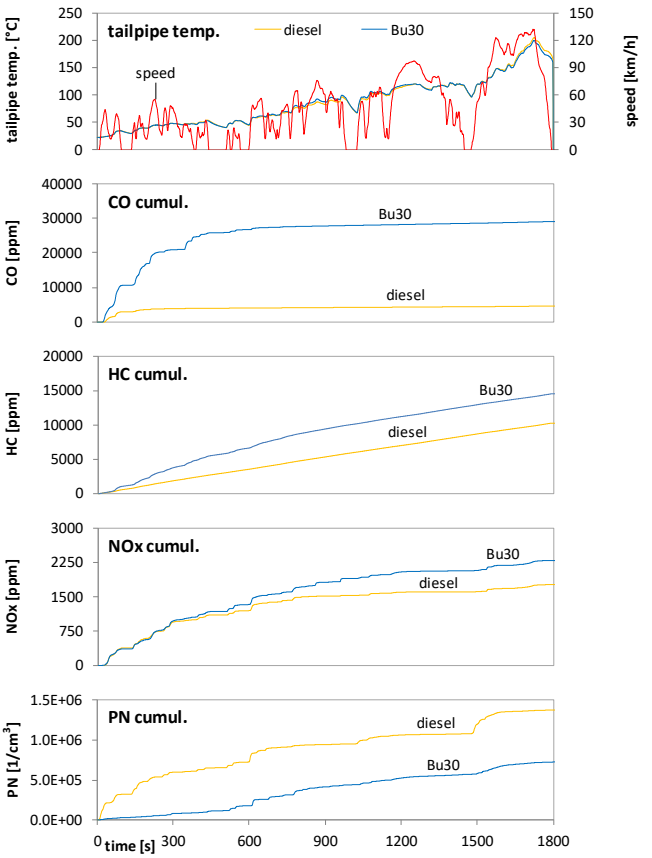

Fig. 4b. Cumulated diluted exhaust emissions and tailpipe temperatures in WLTC cold with different fuels, V2

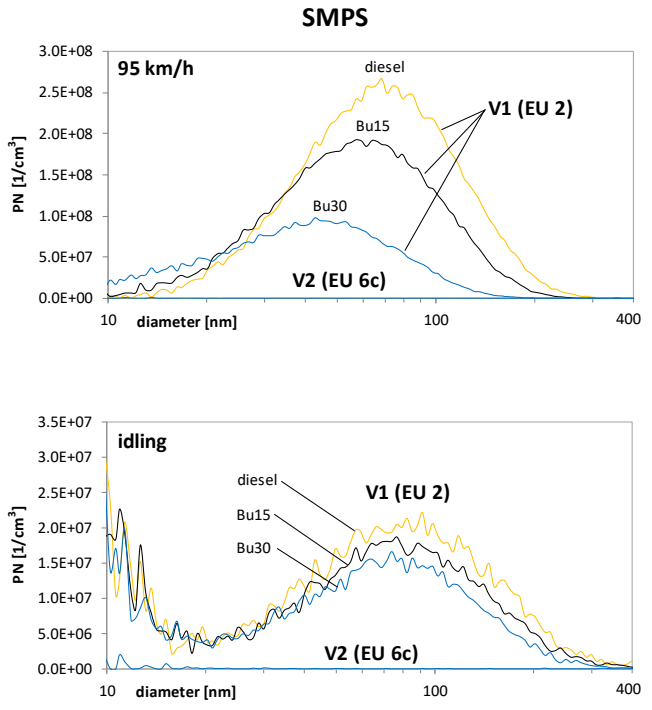

Fig. 5a. Comparison of the Particle Size Distribution (PSD) during the driving cycle SSC with different fuels and with vehicles V1 & V2, (linear scale)

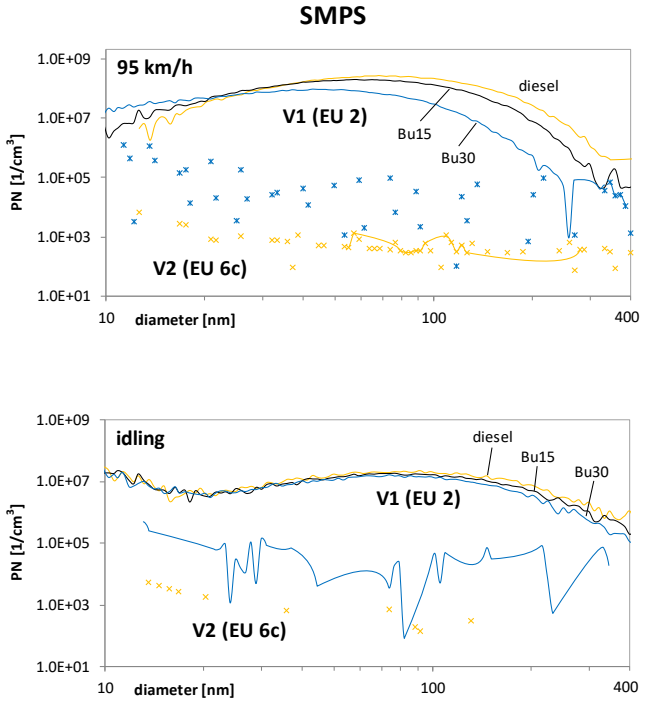

Fig. 5b. Comparison of the Particle Size Distribution (PSD) during the driving cycle SSC with different fuels and with vehicles V1 & V2, (logarithmic scale)

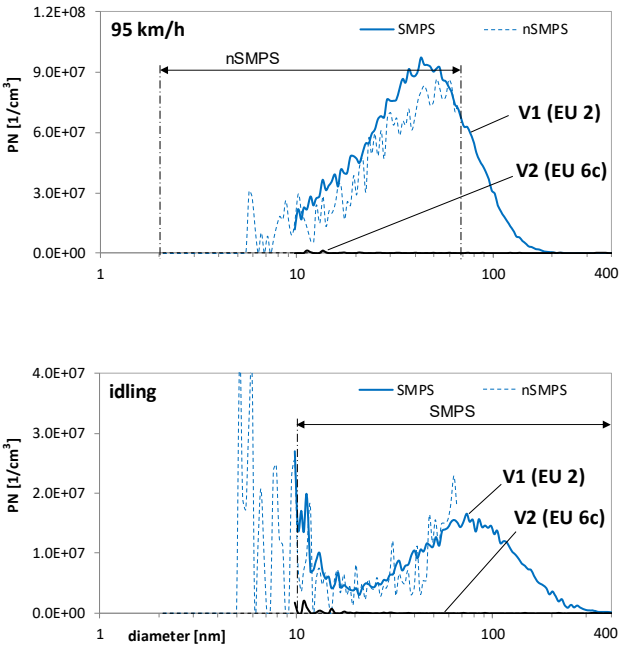

Fig. 6. Particle Size Distribution (PSD) during the SSC cycle in different ranges of size spectrum, Comparisons SMPS – nSMPS, Bu30, V1 & V2

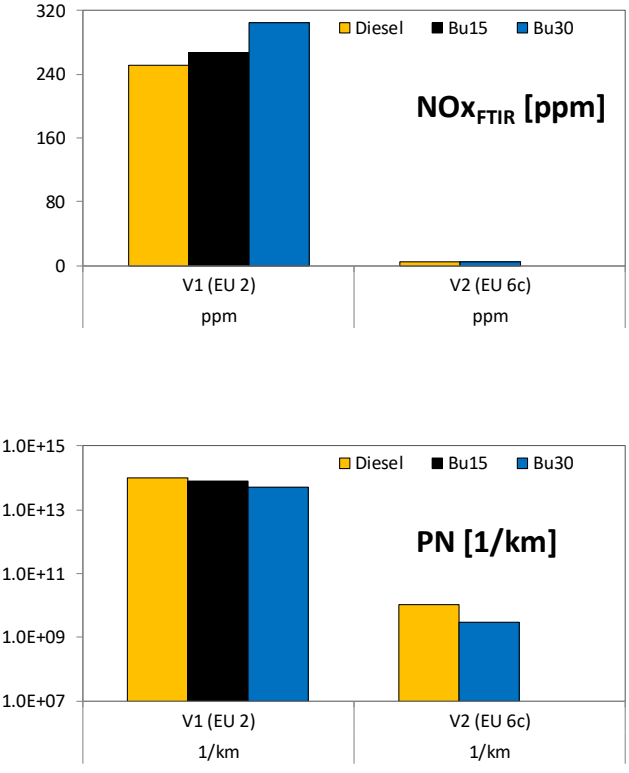

Fig. 7. Comparison of NO_x- and PN-emissions in WLTC warm with different fuels and with both vehicles V1 & V2

6.2. Non-legislated emissions of both vehicles

Comparisons of non-legislated (legally not regulated) gaseous emissions, as average values in $WLTC_{warm}$ are represented in the Fig. 8 for both vehicles and for all investigated fuel variants. With higher Bu-content, especially with Bu30 the emissions of Formaldehyde (HCHO) and of Acetaldehyde (MeCHO) are clearly increased with V1 (older technology) while with V2 (new technology) these emissions are near to zero and there is no influence of Bu-rate.

With the vehicle V2, the emission of NO_2 is nearly eliminated and the emission of N_2O is increased staying nevertheless at a very low absolute level < 4 ppm.

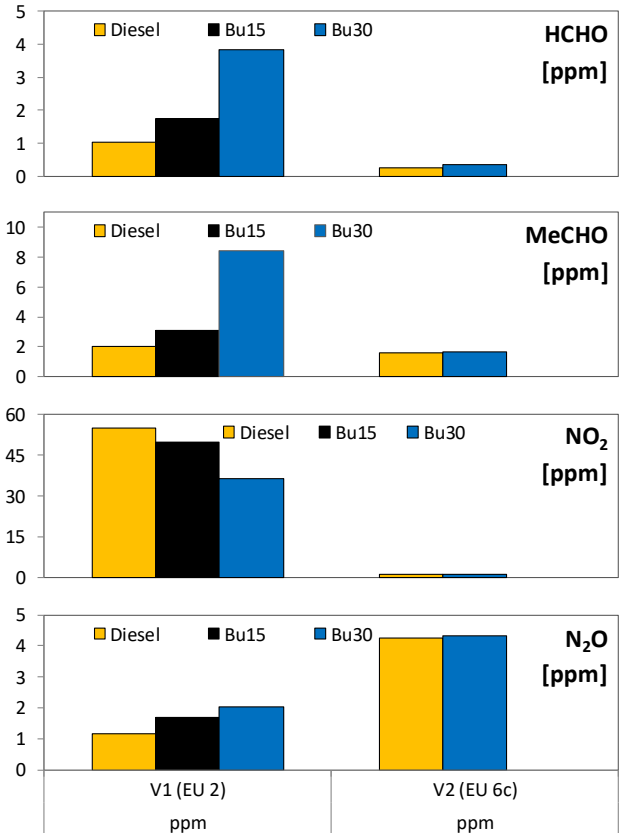

Fig. 8. Comparison of average non-legislated gaseous emissions in WLTC warm with different fuels and with both vehicles V1 & V2, measured with FTIR at tailpipe

6.3. Cold start

The Figure 9 shows some non-legislated gaseous components, emitted by vehicle V1, comparing Bu00/Bu15/Bu30 in two temperature domains of the CS: 0°C and 20°C. All measurements at cold starts (CS) were performed with FTIR at tailpipe i.e. sampling position SP1.

With higher Bu-content the peaks of Formaldehyde HCHO and of Acetaldehyde MeCHO after CS increase. Starting with a lower temperature, these peak-values are higher and can attain for MeCHO 250 ppm.

During the warm-up of the exhaust system, between 180 s and 900 s idling time, there is a clear influence of BuXX on the production of formic acid HCOOH. Nevertheless, it appears in insignificant concentrations (up to 7 ppm at 0°C). The ammonia NH_3 concentrations in all CS-attempts were zero and are not further represented.

The Figure 10 compares the nanoparticle emissions with the fuels Bu0/Bu15/Bu30 at CS in both temperature ranges 0°C & 20°C.

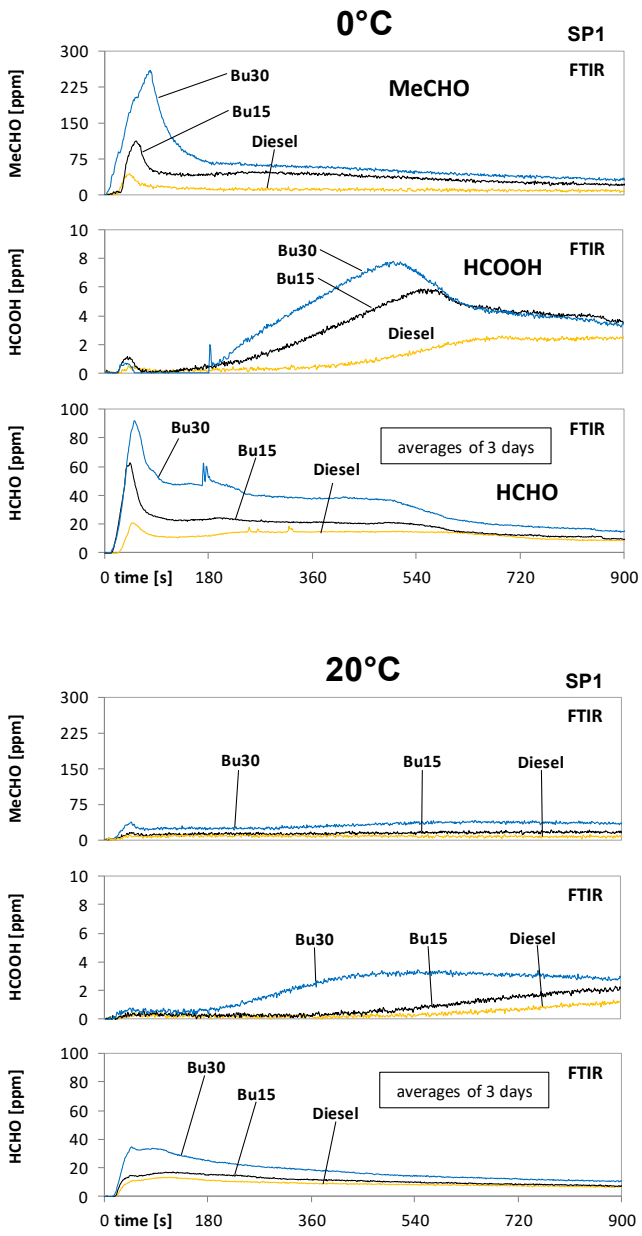

Fig. 9. Comparison of the non-legislated gaseous emissions during cold start (CS) at idling, with Bu 00/15/30, measured with FTIR at tailpipe, vehicle V1

Let us remember that the condensation particle counter (CPC) analyzes simultaneously all particle sizes. It can perform dynamic measurements and according to PMP-guidelines it has a cut-down at 23 nm. The SMPS (scanning mobility particle sizer) in contrary needs a certain time (2–3 min) in order to carry out a scan and to indicate a particle size distribution (PSD) i.e. distribution of particle counts in function of their equivalent size.

During each CS & warm-up in the present tests three successive SMPS-scans were performed (each one 5 minutes for scanning & purging). With the progressing time and progressing warm-up the PN-level of the results was decreasing, showing the lowest values for the latest sample (this is not represented here). The 1st sample was well repeatable and the PSD's in Fig. 10 are averages from three cold starts of the 1st scan.

The most important information of Fig. 10 is, that during the CS Bu15 emits similar or slightly higher level of particle counts concentration, like Bu0, while B30 increases clearly the PN emissions. This increase is produced in the first 1.5 min after CS and originates mainly from the higher nuclei mode (with higher BuXX).

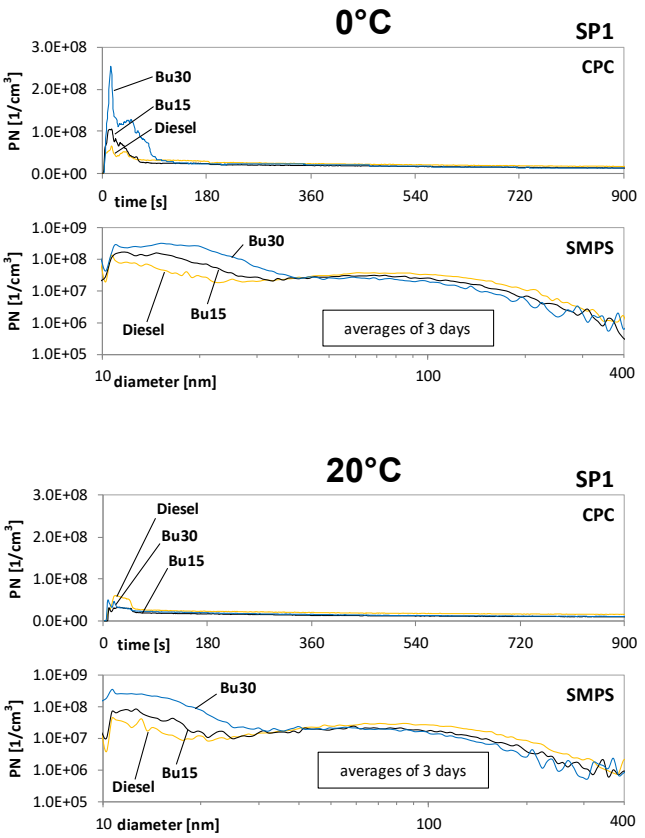

Fig. 10. Comparison of the particle counts during cold start (CS) at idling, with Bu 00/15/30, measured with CPC and with SMPS at tailpipe, vehicle V1

The PN concentrations in accumulation mode nevertheless are lower with higher BuXX – this is similar finding like observed on engines.

Similar representations of emissions during the cold start tests in both temperature ranges (0°C and 20°C) are given for vehicle V2 in the Figs 11 and 12. The most important observations are:

– with cold start (WLTC cold), the concentrations of Formaldehyde HCHO and Acetaldehyde MeCHO are with Bu30 higher than with Bu00; the absolute average values of those components are, nevertheless, insignificant (0.5–8 ppm),
– the particle counts (PC) concentrations (after DPF) are very low, there are no particle size distributions, but occasional, scattered counts; in sub 23 nm size range, there are no counts at all; the PC's with Bu30 are higher than with Bu00 – this is the effect of modified chemistry of the fuel and consequently modified interaction of fuel and of combustion with the lube oil,

– at cold start, there are higher values of CO, HC (not represented in these figures), HCHO and MeCHO with Bu30,
– the emissions of formic acid HCOOH are for this vehicle with newest technology not present; the Fig. 11 shows for HCOOH a noise below the resolution level of the analyzer (this in the sense of comparison with the older technology in the Fig. 9).

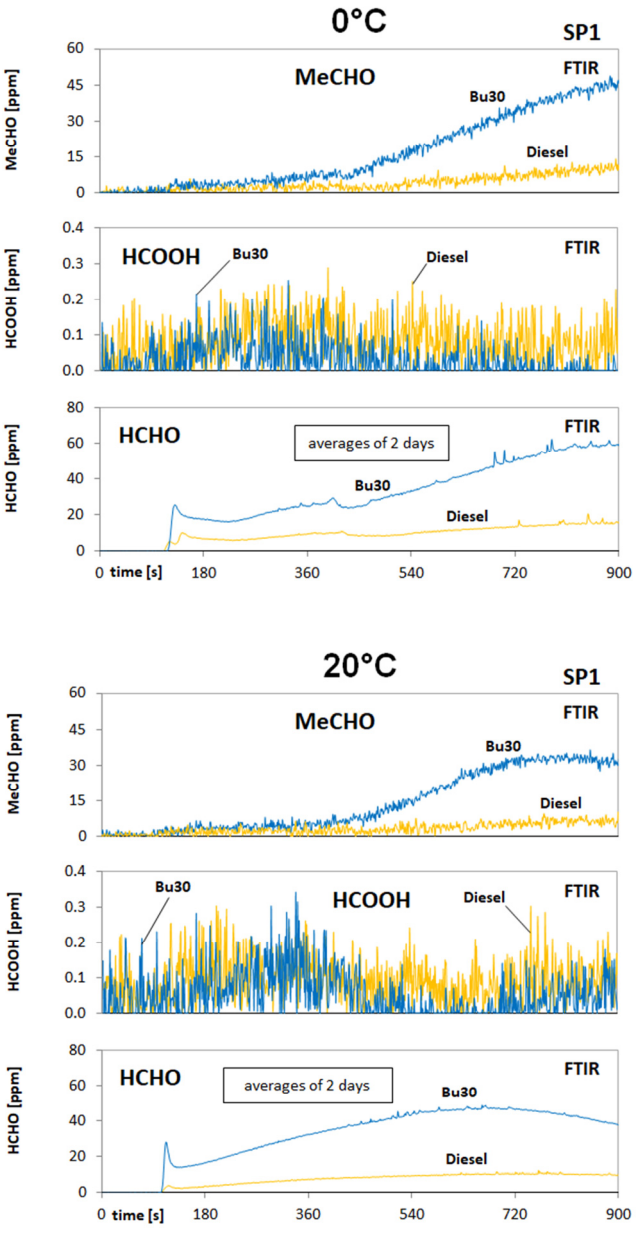

Fig. 11. Comparison of the non-legislated gaseous emissions during cold start (CS) at idling, with Bu00/Bu30, measured with FTIR at tailpipe, vehicle V2

Direct comparisons of emissions of both investigated vehicles, at 0°C cold start, are given in the following figures:

The Figure 13 shows the plots of the most prominent non-legislated components at cold start 0°C. With an older technology, the higher Bu-content in fuel increases significantly the emission peaks of acetaldehyde (MeCHO) and formaldehyde (HCHO) at cold start. With a newer technology, this tendency is also present but at a very low and insignificant absolute emission level.

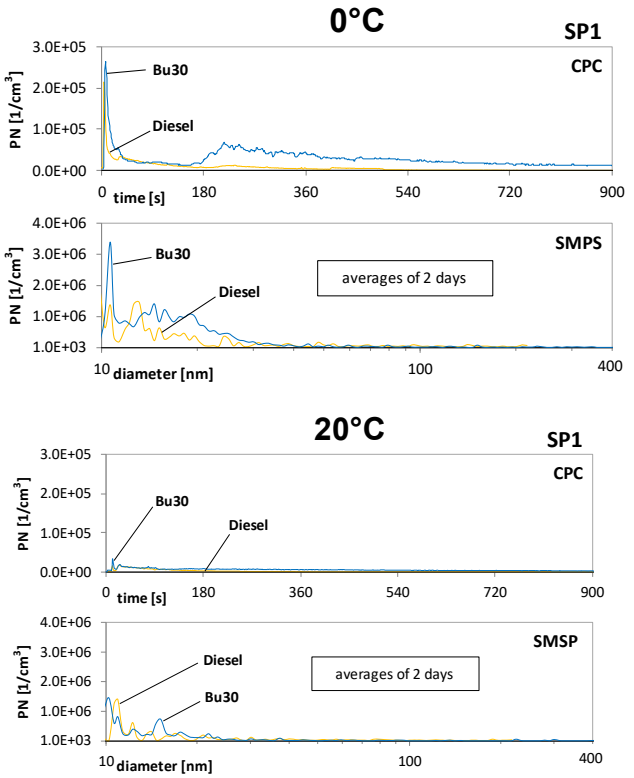

Fig. 12. Comparison of the particle counts during cold start (CS) at idling, with Bu00/Bu30, measured with CPC and with SMPS at tailpipe, vehicle V2

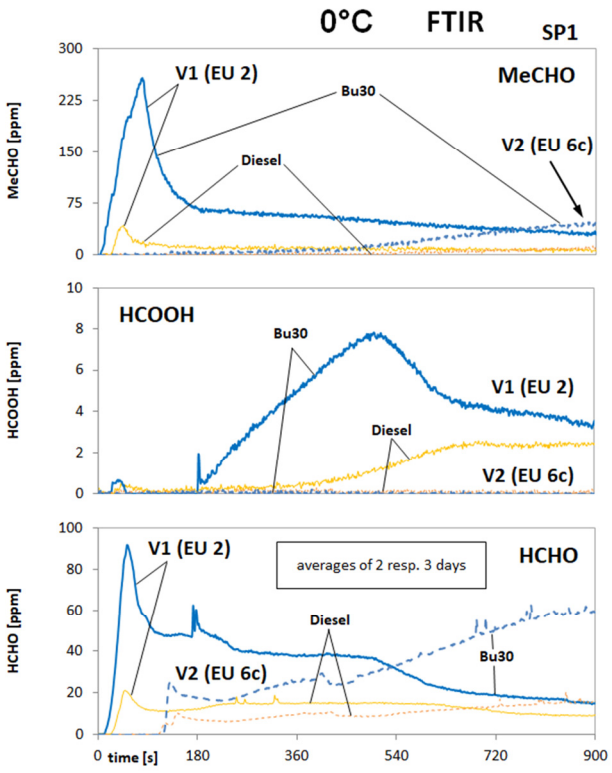

Fig. 13. Comparison of non-legislated gaseous exhaust emissions during cold start at 0°C and idling with different fuels, V1 & V2

The Figure 14 shows PN-emissions during and after the cold start at 0°C with both vehicles. The significantly lower PN-emission with DPF is confirmed.

The representation of summary particle counts indicated by CPC over time in the upper part of this figure shows for vehicle V2 (with DPF) higher PN with Bu30 (comparing to diesel). The major reason of that is the artefact, which is described by the Fig. 5. The resulting PN-concentrations after DPF at 900 [s] are for Bu30 in the range of 10^4 which is still in the upper level of the possible ambient concentrations. The lower part of this figure confirms the findings of the Fig. 5.

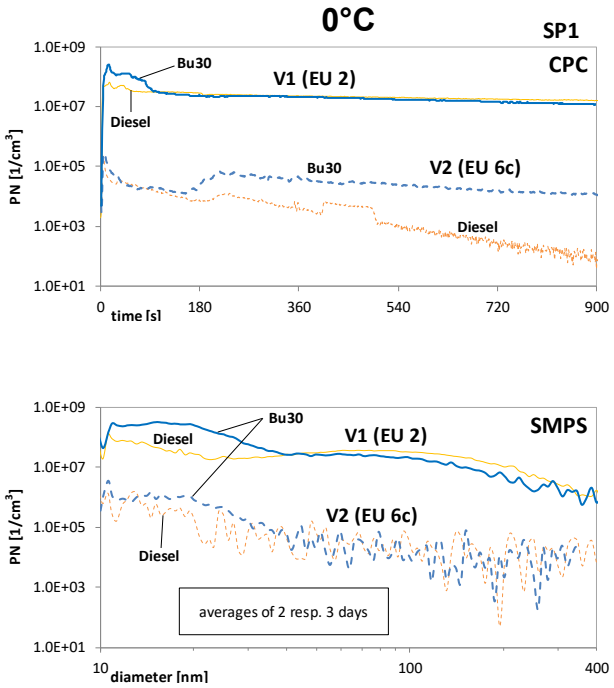

Fig. 14. Comparisons of the particles counts during cold start at 0°C and idling with different fuels, V1 & V2

7. Conclusions

Using two vehicles with older (V1, Euro 2) and with actual (V2, Euro 6c) technical state of the art allowed to make some supplementary findings. The emissions of CO, HC and NO_x for both vehicles are with Bu30 in WLTC and at engine part load higher than with Bu00. With the modern exhaust aftertreatment technology (DOC/DPF/SCR/EGR), with a significantly lower emission level, these differences are smaller or not existing.

The non-regulated emissions in warm operation (WLTC) are for the modern car (V2) near to zero (Fig. 8). At cold start with an older technology (Euro 2), the higher Bu-content in fuel increases significantly the emission peaks of acetaldehyde (MeCHO) and formaldehyde (HCHO). With a newer technology (Euro 6c), this tendency is also present but at a very low and insignificant absolute emission level.

Interesting facts about DPF-effects and nanoparticle emissions with/without DPF were confirmed: with the newest technology (Euro 6c), the particle counts concentrations (after DPF) are very low. There are no particle size distributions, but occasional, scattered counts. In sub 23 nm size range, there are no counts at all. This confirms the excellent filtration quality of solid particles of the right DPF's in good condition. The slightly increased particle counts with Bu30, which were observed in this research after DPF, are an effect of artefact due to the modified SOF-matrix of the nanoaerosol (in the Fig. 5).

Butanol, like several other biofuels modifies the interference with the lube oil. As a result, there are the tendencies of increasing the particle number concentrations in nuclei mode and of reducing them in accumulation mode, with the effect of reducing the total PN (summary of all sizes). This can be observed without DPF (V1). After DPF (V2) the PN-values are very low and such tendencies cannot be visible. Therefore, the higher Bu-content lowers the summary engine-out PN-emissions. With DPF, the PN-level is so much reduced that the influence of fuel on PN is insignificant.

In summary, we can state that the butanol blends have some influences on engine-out emissions, but with the application of modern exhaust aftertreatment systems these influences are at tailpipe insignificant.

Another important result of the investigations is the assessment of the blend ratio limit. Due to the very low cetane number of butanol, this limit is approximately at 30% vol. butanol content. The cold startability at 0°C with Bu30 is already bad. Further improvements of CN by means of additives or other blended fuels were not the subject of this project.

For practical implementation of the butanol blend fuels in diesel engines it is important to mention that the questions of durability of the injection system due to lower lubricity of butanol blend fuels and durability of the lube oil were not investigated in the present project.

Acknowledgements

The institutions, which financially supported these research activities: Swiss Federal Office of Energy (BfE) and Swiss Federal Office of Environment (BAFU) are gratefully acknowledged.

Nomenclature

AFHB	Abgasprüfstelle FH Biel, CH
ASET	Aerosol Sampling and Evaporation Tube
ATS	aftertreatment system
BAFU	Bundesamt für Umwelt, (Swiss EPA)
BfE	Bundesamt für Energie
Bu	butanol
Bu30	30% vol butanol in diesel
BuXX	butanol portion in fuel XX vol %
CI	compression ignition (diesel)
CLD	chemoluminescence detector
CN	cetan number
CO	carbon monoxide
CO_2	carbon dioxide
CPC	condensation particle counter
CR	common rail
CS	cold start

CVS	constant volume sampling
DF	dilution factor
DI	direct injection
DiBut	Diesel–Butanol project
DOC	diesel oxidation catalyst
DPF	Diesel Particle Filter
DMA	differential mobility analyser
EGR	exhaust gas recirculation
FE	filtration efficiency
FID	flame ionization detector
FL	full load
FOEN	Federal Office of Environment (BAFU), CH
FTIR	Fourier Transformation Infra-Red Analyzer
HC	unburned hydrocarbons
HCHO	formaldehyde
HCOOH	formic acid
HNCO	isocyanic acid
Hu	lower heat value
ICE	internal combustion engines
MeCHO	acetaldehyde
NDIR	non-dispersive infrared
N_2	nitrogen
N_2O	nitrous oxide
NH_3	ammonia
NO	nitrogen monoxide
NO_2	nitrogen dioxide
NO_x	nitric oxides
NP	nanoparticles < 999 nm (SMPS – range)
nSMPS	nano SMPS
PCFE	particle count filtration efficiency
PM	particle mass
PMFE	particle mass filtration efficiency
PMP	Particle Measuring Program (ECE)
PN	particle number
PSD	particle size distribution
RAI	reduction agent injection
RR	reduction rate
SCR	selective catalytic reduction
SI	spark ignition
SOF	soluble organic fraction
SMPS	Scanning Mobility Particle Sizer
SP1	sampling position 1 (tailpipe)
SSC	steady state cycle
TC	thermo conditioner
T_{exh}	exhaust temperature
TP	tailpipe
V1, V2	vehicle 1, vehicle 2
WLTC	World Harmonized Light Duty Test Cycle

Bibliography

[1] GIAKOUMIS, E.G., RAKOPOULOS, C.D., DIMARATOS, A.M. et al. Exhaust emissions with ethanol or n-butanol diesel fuel blends during transient operation: A review. *Renewable and Sustainable Energy Reviews.* 2013, **17**, 170-190.

[2] RARBACH, M., SÖLTL, Y. Cellulosic ethanol from agricultural residues. *MTZ,* 2013, **4**(74**)**, 4-8. https://doi.org/10.1007/s38313-013-0034-3

[3] KAACK, M., WEISKIRCH, CH., EILTS, P. Alcoholic biofuels as an admixture component for conventional and alternative diesel combustion processes. *MTZ.* 2009, **7-8**(70**)**, 58-65. https://doi.org/10.1007/BF03226971

[4] BRASSAT, A., THEWES, M., MÜTHER, M. et al. Massgeschneiderte Kraftstoffe aus Biomasse für Ottomotoren. *MTZ.* 2011, **12**(72**)**, 988-995. https://doi.org/10.1365/s35146-011-0212-2

[5] SIWALE, L., KRISTOF, L., ADAM, T. et al. n-butanol-diesel (D2) blend fired in a turbo-charged compression ignition engine. *Performance and Combustion Characteristic*. 2018, March. http://dx.doi.org/10.5772/intechopen.72879

[6] LAPUERTA, M., HERNÁNDEZ, J.J., RODRIGUEZ-FERNÁNDEZ, J. et al. Emission benefits from the use of n-butanol blends in a Euro 6 diesel engine. *International Journal of Engine Research*. 2018, **19**(10).

[7] SHUKLA, M.K., THARKE, G.D., SAXENA, R.C. et al. Butanol/diesel blends as a CI engine fuel: physicochemical and engine performance characteristics evaluation. *TAE Technische Akademie Esslingen. 9th International Colloquium "Fuels"*. 2013, January 15-17.

[8] HAN, X., YANG, Z., WANG, M. et al. Clean combustion of n-butanol as a next generation biofuel for diesel engines. *Applied Energy*. 2017, **198**, 347-359. https://doi.org/10.1016/j.apenergy.2016.12.059

[9] SOLOIU, V., DUGGAN, M., HARP, S. et al. PFI (port fuel injection) of n-butanol and direct injection of biodiesel to attain LTC (low-temperature combustion) for low-emissions idling in a compression engine. *Elsevier Energy*. 2013, **52**, 143-154.

[10] WALLNER, T., ICKES, A., LAWYER, K. et al. Higher alcohols in multi-component blends with gasoline – experimental and analytical assessment. *14. Tagung "Der Arbeitsprozess des Verbrennungsmotors", TU Graz*. 2013, September.

[11] TORNATORE, C., MARCHITTO, L., VALENTINO, G. et al. Optical diagnostics of the combustion process in a PFI SI boosted engine fueled with butanol-gasoline blend. *Energy*. 2012, **45**(1), 277-287. https://doi.org/10.1016/j.energy.2012.03.006

[12] MEROLA, S., TORNATORE, C., MARCHITTO, L. et al. Experimental investigations of butanol-gasoline blends effects on the combustion process in a SI engine. *International Journal of Energy and Environmental Engineering.* 2012, **11**(3). https://doi.org/10.1186/2251-6832-3-6

[13] MARCHITTO, L., MAZZEI, A., MEROLA, S.S. et al. Optical investigations of combustion process in SI and CI engines fuelled with butanol blends. *TAE Technische Akademie Esslingen. 9th International Colloquium "Fuels"*. 2013, January 15-17.

[14] IRIMESCU, A., TORNATORE, C., MEROLA, S.S. et al. Integrated diagnostics for combustion investigation in a DISI engine fueled with butanol and gasoline at different load settings. *TAE Technische Akademie Esslingen. 10th International Colloquium „Fuels", Stuttgart/Ostfildern*. 2015, January 20-22.

[15] GU, X., HUANG, Z., CAI, J. et al. Emission characteristics of a spark-ignition engine fuelled with gasoline-n-butanol blends in combination with EGR. *Fuel*. 2012, **93**, 611-617. https://doi.org/10.1016/j.fuel.2011.11.040

[16] LIU, H., WANG, X., ZHANG, D. et al. Investigation on blending effects of gasoline fuel with n-butanol, DMF, and ethanol on the fuel consumption and harmful emissions in a GDI vehicle. *Energies.* 2019, **12**(10), 1845. https://doi.org/10.3390/en12101845

[17] VOJTISEK-LOM, M., PECHOUT, M., MAZAC, M. Real-word on-road exhaust emissions from an ordinary gasoline car operated on E85 and on butanol-gasoline blend. *SAE Technical Paper* 2013-24-0102. 2013. https://doi.org/10.4271/2013-24-0102
[18] US DOE CO-OPTIMA Publications Library: https://www.energy.gov/eere/bioenergy/co-optima-publications-library-0
[19] ENGELMANN, D., CZERWINSKI, J., NAUROY, H. et al. Use of butanol blend fuels on diesel engines – effects on combustion and emissions. *SAE Technical Paper* 2020-01-0333. 2020. https://doi.org/10.4271/2020-01-0333
[20] STEPIEN, Z., CZERWINSKI, J., URZEDOWSKA, W. et al. Research on emissions and engine lube oil deterioration of diesel engines with biofuels (RME). *SAE Technical Paper* 2011-01-1302. 2011. https://doi.org/10.4271/2011-01-1302
[21] CZERWINSKI, J., COMTE, P., STEPIEN, Z. et al. Effects of ethanol blend fuels E10 & E85 on the non-legislated emissions of a flex fuel passenger car. *SAE Technical Paper* 2016-01-0977. 2016. https://doi.org/10.4271/2016-01-0977
[22] HADLER, J., LENSCH-FRANZEN, CH., GOHL, M. et al. Concept for analysing and optimising oil emission. *MTZ Worldwide*. 2014, **1**(75)**,** 24-29. https://doi.org/10.1007/s38313-014-0006-2
[23] HADLER, J., LENSCH-FRANZEN, CH., GOHL, M. et al. Emission reduction a solution of lubricant composition, calibration and mechanical development. *MTZ Worldwide*. 2015, **9**(76)**,** 30-33. https://doi.org/10.1007/s38313-015-0040-8
[24] CZERWINSKI, J., ZIMMERLI, Y., NEUBERT, T. et al. Injection, combustion and (nano) particle emissions of a modern HD-diesel engine with GTL, RME & ROR. *SAE Technical Paper* 2007-01-2015. 2007. https://doi.org/10.4271/2007-01-2015

Danilo Engelmann, DEng. – Professor at the University of Applied Sciences, Biel-Bienne, Switzerland.
e-mail: *danilo.engelmann@bfh.ch*

Pierre Comte, Dipl.-Ing. HTL – University of Applied Sciences, Biel-Bienne, Switzerland.
e-mail: *pierre.comte@bfh.ch*

Prof. Jan Czerwinski, DEng. – Professor Emeritus at the University of Applied Sciences, Biel-Bienne, Switzerland, CJ Consulting.
e-mail: *cjcons19@gmail.com*

Stephan Renz, CEO – Renz Consulting, Basel, Switzerland.
e-mail: *renz.btr@swissonline.ch*

Peter Bonsack, MSc ME – Federal Office for the Environment FOEN, Bern, Switzerland.
e-mail: *peter.bonsack@bafu.admin.ch*

Article citation info:
TIKHONENKOV, S. An internal combustion engine without a crankshaft. Perspectives. *Combustion Engines*. 2020, **183**(4), 39-44. https://doi.org/10.19206/CE-2020-406

Serguei TIKHONENKOV

CE-2020-406

An internal combustion engine without a crankshaft. Perspectives

The article examines the level of perfection of the modern internal combustion engine design, their impact on the environment and population. A new engine concept has been developed. As a result a decrease in fuel consumption by 80% has been discovered as well as the effects of the new engine in the field of ecology such as a decrease in the number of diseases caused by poor environmental conditions, a lower risk of global warming, lower health care costs, an increase in life expectancy, etc. Also, for countries with fossil fuel deposits, can be anticipated dropping treasury income, factory closures, high unemployment, the likelihood of protests and uprisings.

Key words: *engine, fuel efficiency, global warming, pollution*

1. Global warming and pollution

The growing population of the world is an objective phenomenon and it has a strong relationship with such phenomena as, on the one hand, pollution of the air, water and land, starvation, spread of diseases, etc., and, on the other hand, the demand for energy from different sources to prevent the above-mentioned pollution, starvation, spread of diseases, etc. This means that the more goods and food are produced and services provided, the more pollution, including CO_2, will be thrown into the environment and the faster the temperature will increase.

This issue is alarming and attracts the attention of national governments and international organizations.

NASA has published the latest measurements on July 2020 – 414 ppm and chart "Direct measurement: 2005-present" [1].

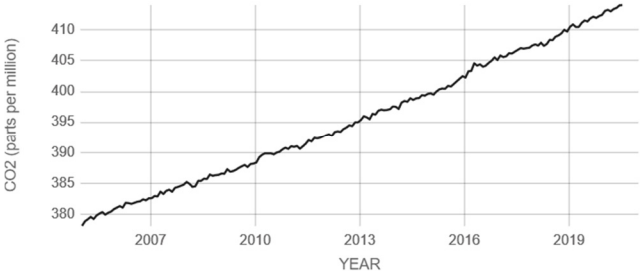

Fig. 1. Direct measurement: 2005-present [1]

It is easy to see that global warming is getting worse and could be described by an equation. It means that using this equation we can anticipate the levels of global temperature and carbon dioxide in the near future and beyond. It is well known that the burning of 1 liter of gas produces about 2 kilos of CO_2 [2]. It is easy to count, but, honestly, scary.

So far, a huge amount of work has been done with noticeable results in reducing the level of CO_2 and pollution. For example, new sources of biofuels such as wood, soybeans, algae, sugar cane, palm oil and rape oil seeds have demonstrated that they are applicable, but actually didn't solve the problem.

An idea to replace ICE by an electric vehicle powered by batteries looks like an attempt to mislead. EV advocates claim that EV will be fuelled by renewables sources, such as wind and solar but they always forget to say that according to research of BP a part of they are only 3–5% world's energy supply [3].

A research of BP also shown, that the total part of the fossil fuels like oil and gas in all primary sources of power is about 60% and coal 20% [3].

At the same time the UN has made step to limit GHG. The United Nations Framework Convention on Climate Change (UNFCCC) entered into force on 21 March 1994 and set a goal "to stabilize greenhouse gas concentrations "at a level that would prevent dangerous anthropogenic (human induced) interference with the climate system" and "such a level should be achieved within a time-frame sufficient to allow ecosystems to adapt naturally to climate change, to ensure that food production is not threatened, and to enable economic development to proceed in a sustainable manner [4]".

It means that in the foreseeable future the main roles in the development and prosperity of the whole world will be played by the internal combustion engine and fossil fuels. Moreover "IJER editorial: The future of the internal combustion engine" defined the problem clearly –"The CO_2 emitted from an engine is directly proportional to the hydrocarbon fuel consumed" [5]. Therefore, there is the vital requirement to find a new approach in reducing fuel consumption and, therefore, carbon dioxide emissions.

2. An internal combustion engine without a crankshaft

The research shown that the main directions to reduce emission are "advanced combustion modes and innovative after-treatment systems, including extensive use of catalysts and high-filtration-efficiency diesel and gasoline particulate filters (D/GPF) in the aftertreatment system, while the use of urea injections and selective catalytic reduction (SCR)" [5]. However, another path and a critical look at traditional internal combustion engines also deserve an attention.

Modern internal combustion engines are built using the classical design: cylinder, piston, connecting rod and crankshaft, and we should note a number of known flaws in traditional engines:

Inefficient combination of pressure within the cylinder and tangential force on the crankshaft.

Two points need to be looked at closely here:

a) With the pressure increasing to a maximum and combustion of a significant part of the mixture, the crankshaft rotates 180 degrees, and the ratio of the tangential force on

Received 14 July 2020; Received in revised form 28 October 2020; Accepted 29 October 2020
Available online 15 December 2020

the crankshaft to the force acting on the piston varies from 0 to 1 and from 1 to 0.

Thus, two phenomena are observed when the crankshaft rotates 180 degrees:

– the pressure changes from a maximum to a minimum value (Fig. 2), which coincides with an isothermal part (combustion stroke) of the Carnot cycle [6].

A polytropic process is [7]:

$$P \cdot V^n = \text{const} \quad (1)$$

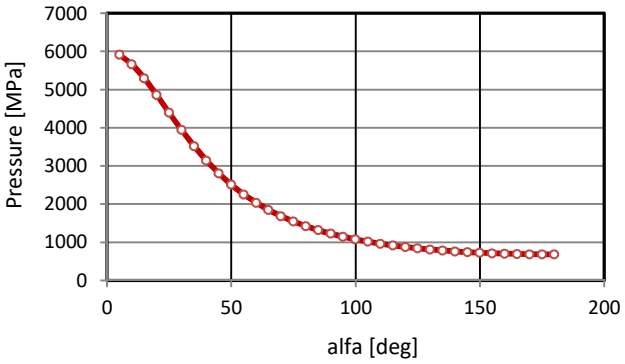

Fig. 2. A change in pressure when a shaft turns from 0 to 180 degrees

– the tangential force on the crankshaft changes from 0 to 1 and from 1 to 0 (Fig. 4) [8]:

$$T = P \cdot \sin(a + B)/\cos B \text{ (Fig. 3)} \quad (2)$$

P = 1 – force acting on the piston (conventionally assumed equal to 1), T – tangential force.

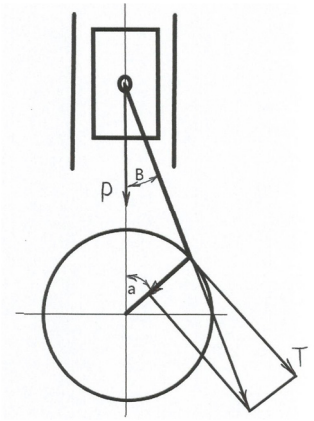

Fig. 3. A crank mechanism

b) The compressed mixture is ignited when the piston is at TDC. It is known that high temperature and high pressure are necessary for the complete and effective combustion of the air-fuel mixture. This condition is violated in traditional engines. After passing the TDC, the piston goes down. The space above the piston increases, and the pressure and temperature decrease, and the fuel-air mixture does not burn up completely.

"Ideally, if the combustion process is complete, the exhaust gases should only be carbon dioxide (CO_2) and water vapour (H_2O). In reality, mainly due to incomplete combustion, the exhaust gases also contain pollutant emissions: oxides of nitrogen (NO_x), unburnt hydrocarbons (HC), carbon monoxide (CO), soot's/particles (PM), polyaromatics, aldehydes ketones and nitro-olefins" [9].

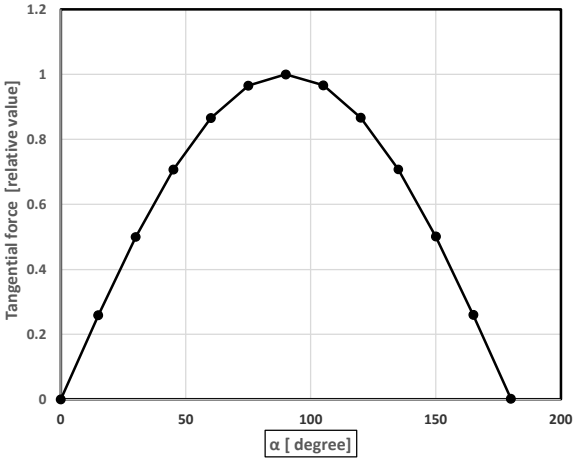

Fig. 4. Changes of a tangential force when crankshaft turns 180 degrees

Therefore, we need to define a goal to overcome the above-mentioned flaws, namely, to create a new concept of an internal combustion engine.

Three tasks need to be solved.

1. The lever of tangential force on the drive shaft must be constant along the piston's entire travel path.

2. At the TDC the piston has to be stationary for a short time to ensure an increase of the pressure and temperature till the optimal values and also at the BDC to ensure the exhaust of the entire amount of burned gas.

3. The fresh fuel-air mixture should not mix with the remnants of the combusted mixture.

The idea of the new engine concept is to replace the crankshaft by gear racks that move linearly and drive the gear wheels (sprockets) creating torque.

Two videos show the new engine (*YouTube. Serguei Tikhonenkov – "Engine of an internal combustion without a crankshaft", "2-strokes engine without a crankshaft. Every stroke is combustion*").

The engine (Figs 5–7) can contain from 1 (*YouTube. Serguei Tikhonenkov "Engine of an internal combustion without a crankshaft"*) to 2 or 4 units; optimally – 4 (*YouTube. Serguei Tikhonenkov "2-stroke engine without a crankshaft. Every stroke is combustion"*).

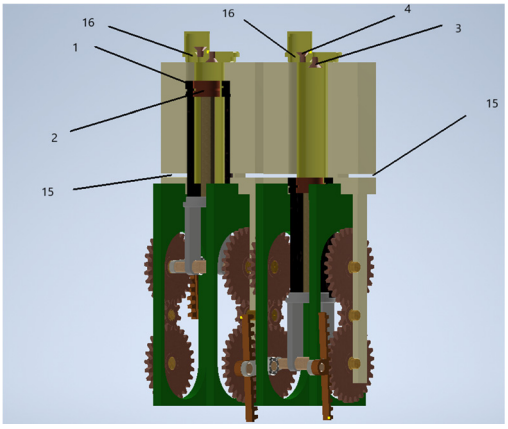

Fig. 5. 2-stroke engines without crankshaft

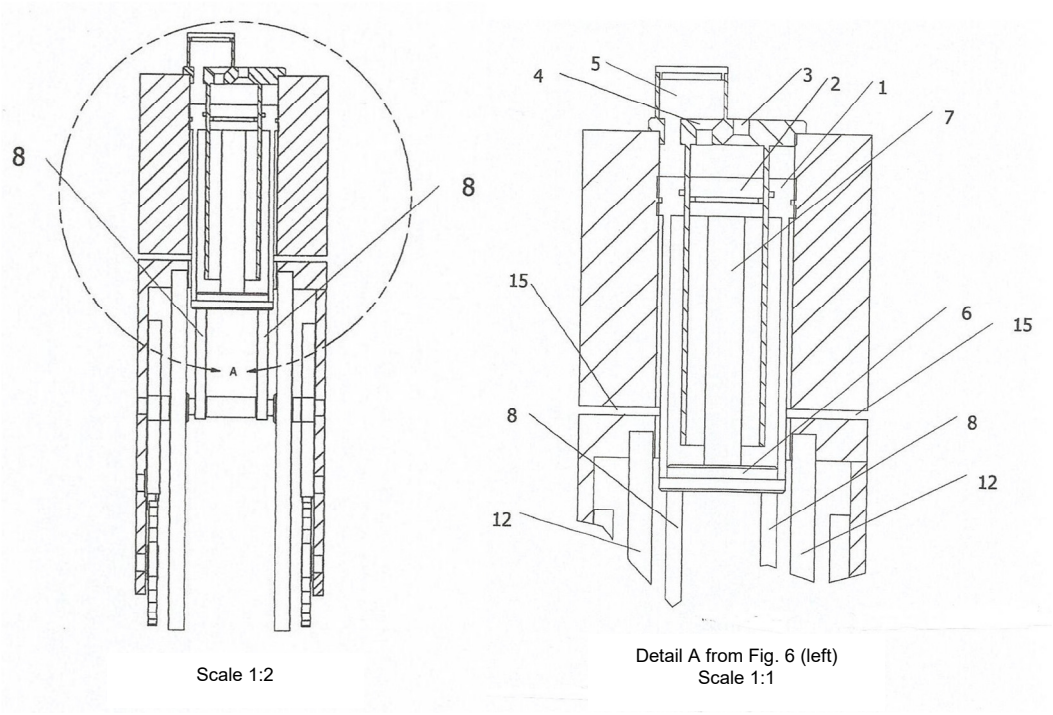

Fig. 6. Engine details of an internal combustion without a crankshaft

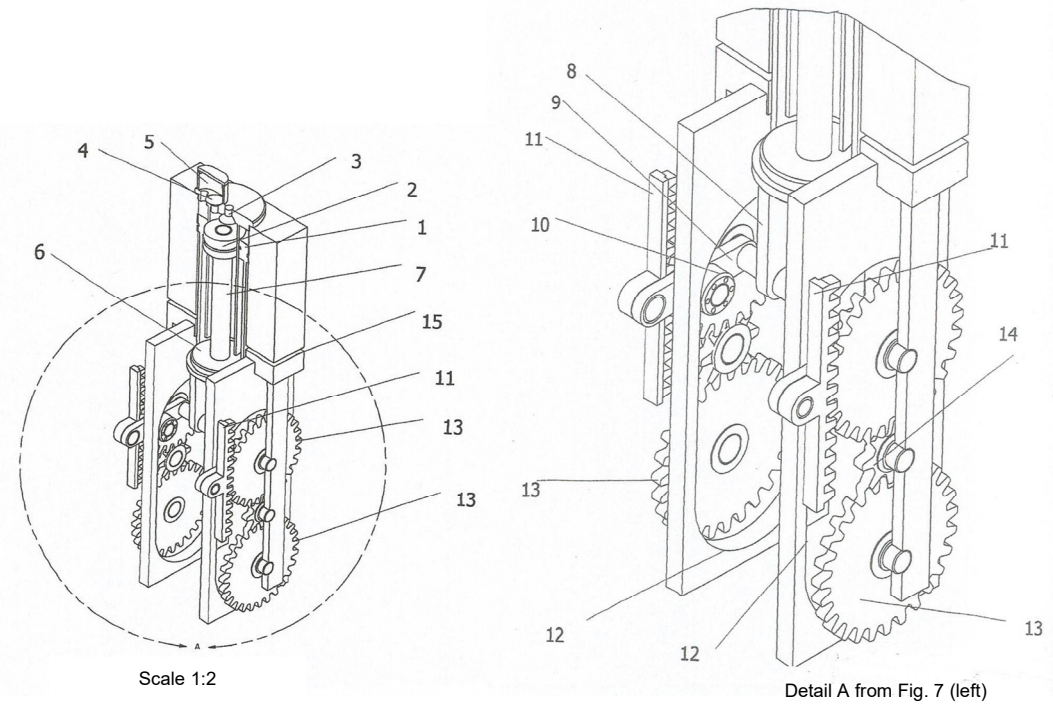

Fig. 7. View of engine (left) and details of an engine (right)

Each unit consists of a main 1 and additional 2 cylinders, an intake valve 3 and a valve 4 connecting the cavities above piston of the main 1 and piston of the additional 2 cylinders, a common chamber 5, a base 6, on which piston of cylinder 1 and rod 7 of piston of cylinder 2 are mounted, and on the lower part of the base 6 there are two struts 8. On each strut 8 there are pivotally mounted levers 9 with rollers 10 and gear racks 11 fixed onto them. The rollers 10 roll along the guides 12 and the gear racks 11 interact with the gear wheels 13 (sprockets) connected by a pinion 14. In the bottom part of the block apertures 15 for exhaust gases are located. The common chamber 5 and the cavity above the piston of the main cylinder 1 are connected by a channel 16.

The engine operates as follows. When the working mixture is ignited above piston of the main cylinder 1, valve 4 is closed by pressure. The pressure makes the piston of the main cylinder 1 and the base 6 move down. At the same

time, the rod 7 and the piston of the additional cylinder 2 move downward, while the valve 3 is opened by vacuum and ensures the intake of the combustible mixture. The levers 9 mounted on the struts 8 also move down. At the same time, the rollers 10 run along the guides 12, and the gear racks 11 drive the gears wheels (sprockets) 13, creating torque. When piston of the cylinder 1 reaches its extreme low point, the exhaust gases are discharged through openings 15. At this point the sprockets make the gear racks to rotate a 180-degree arc around the sprockets due to their inertial forces and interaction with the attached units. After that the base 6 and the pistons of the cylinders 1 and 2 installed on it are moved upward also due to inertial forces and interaction with the attached units. When moving upward, the mixture entering the cavity above piston of the additional cylinder 2 moves through the valve 4 which is opened by pressure, the common chamber 5 and the channel 16 into the cavity above piston of the main cylinder 1. Now valve 3 is closed by pressure above the piston of the additional cylinder 2. Thus, compressed combustible mixture is created in the cavity above the piston of the main cylinder 1. When the mixture is ignited, the cycle repeats.

3. Differences between the new engine and the traditional one

At the TDC, the piston is stationary while the gear racks run around a 180-degree arc on a sprocket. At this moment, the fuel-air mixture in the space above the main piston ignites. The volume in this case will be kept constant, which will lead to a many-fold increase in pressure and temperature. These parameters can reach values at which engine failure will occur. This means that the moment of ignition of the fuel-air mixture must be optimized. Optimization will allow us to avoid the destruction of the engine and, at the same time, create a significantly increased pressure above the piston.

Engine power (HP) is defined by an equation [10]

$$HP = n \cdot M \tag{1}$$

where: M – torque on the shaft, n – revolutions per minute,

$$M = T \cdot L \tag{2}$$

where: L – a size of the lever on the shaft, T – tangential force.

Force acting on the piston:

$$P = S \cdot F \tag{3}$$

where: S – area of the piston, F – value of pressure in the cylinder.

Therefore, in the new concept of the engine the temperature and pressure will be increased because piston is stationary during the calculated short time at the TDC.

It means that the pressure and temperature in the engine and as well the power depend on the time of the pistons delay at the TDC. This is a functional relationship.

$$HP, P, T = f(t) \tag{4}$$

where: t – time of the delay.

The advantage of the new engine compared with the traditional one is demonstrated in Fig. 8. Figures 8a and 8b clearly show that equal amounts of fuel for both engines are used more efficiently in the new one (Fig. 8b, red). In the new engine, due to the time delay, the pressure and temperature are significantly higher than in the traditional one. It means, that the HP of the new engine with the same n will be more in the same scale.

At the same time as we know the efficiency of any machine is defined by the coefficient efficiency [11]:

$$\eta = (T_h - T_c)/T_h \tag{5}$$

where: T_h – heater temperature, T_c – cooler temperature.

It means, that an efficiency of the new engine will be higher than in the traditional one.

At the bottom dead center (BDC), the piston is stationary, same as at TDC, while the gear racks run around a 180-degree arc on sprockets providing a high level of exhaust. As a result, this means that fresh fuel-air mixture will not mix with the remnants of the combusted mixture. In the proposed engine, the working stroke and the injection stroke are performed simultaneously, both strokes being isolated. While the pistons of the main 1 and additional 2 cylinders are moving up, the fresh fuel-air mixture is pumped by the piston of the additional cylinder 2 into the space above the piston of the main cylinder 1 through the valve 4 which is opened by pressure, the common chamber 5 and the channel 16.

In the proposed engine the lever of tangential force on the drive shaft remains constant along the piston's entire travel path (Fig. 9).

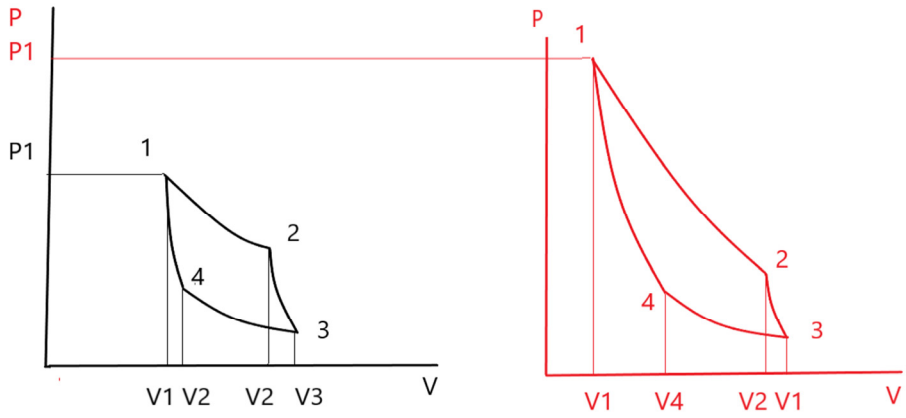

Fig. 8. Cycle: a) in the traditional engine, b) in the new engine

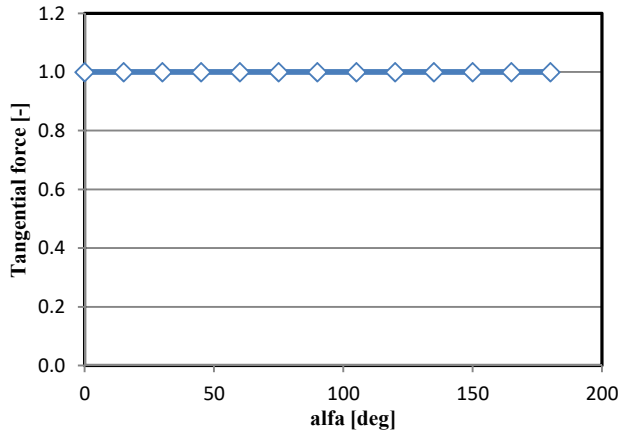

Fig. 9. A tangential force when a shaft turns from 0 to 180 degrees

T = P;
P = 1 – force acting on the piston (conventionally assumed equal to 1).

The change in torque values in the proposed engine is determined only by the change of pressure in the cylinder. Statistical values of moment variations in the proposed engine and in an engine with a crankshaft are characterized by arithmetic averages. The arithmetic average of the moment in the proposed engine is 1.83 times the arithmetic average of the moment in the traditional engine (Fig. 10).

So, it is possible to say, that the proposed engine provides the significantly reduced fuel consumption and a perfection of the fuel process's burn.

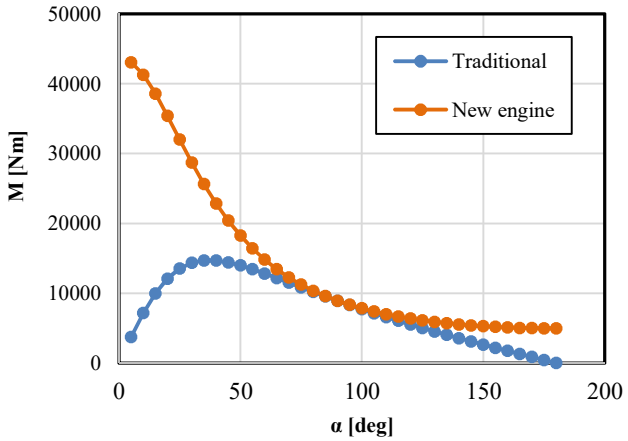

Fig. 10. Variation of the moments in the new engine and traditional one

The new engine must be equipped with efficient flywheels to compensate for the uneven rotation.

We should also note that there are no camshafts and the gas distribution mechanism.

”Valve mechanism system is one of more system which influence of characteristic and performance an engine. To changes or other word is modification a working cycle, it’s means changes control system in the work cycle. Control system in an engine is valve mechanism system. To be changes a mechanism it’s means to be changes control component design of that mechanism. Control component in a valve mechanism system is camshaft” [12].

The gas distribution mechanism, which includes a camshaft, is a rather complex unit and has some flaws.

In some researches are noted, that “line contact between existing cam and follower mechanism results in high frictional losses which results in low mechanical efficiency” [13].

In traditional engines cams are a type of lobe and as they spin the intake and exhaust valves are opened. But due to the design of the gas distribution mechanism, the phases of the intake and exhaust valves overlap. This causes the fresh portion to mix with the unburned mixture.

In Figure 11 presented displacement diagrams for valves (exhaust 1 and intake 2) in the traditional engine, in the proposed one (intake 3 or connecting 4) and an area of aperture 15 for exhaust in the proposed engine. In the traditional engines the valve opening area changes from 0 to maximum and from maximum to 0 during the piston movement. The exhaust starts from the end of the combustion stroke and finishes at beginning of the intake stroke. The intake starts from the end of the exhaust stroke and finishes at the beginning of the compression. In the proposed engine the valves (intake valve 3 and connecting valve 4) are opened by pressure instantly. The valve (intake or connecting) area in the proposed engine is about 1.35 times the intake valve area in the traditional one.

An exhaust gas releases through apertures 15 when piston of the main cylinder 1 is in the extreme low point. The effective aperture area 15 is many times the area of the exhaust valve in traditional engines (see Fig. 5).

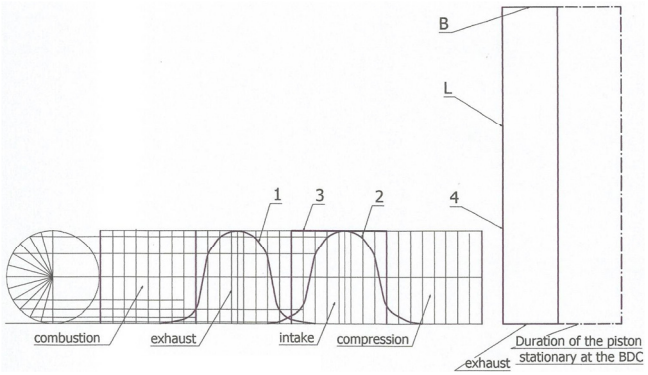

Fig. 11. Displacement diagram of valves: 1 – displacement diagram and an effective area of the exhaust valve in the traditional engines, 2 – displacement diagram and an effective area of the intake valve in the traditional engine, 3 – displacement diagram and an effective area of the intake (connecting) valve in the proposed engine, 4 – an affective area of aperture for exhaust and exhaust duration when the piston is stationary at the BDC, L – length of apertures, B – width of apertures

4. Conclusions

1. Fuel consumption is reduced due to two reasons:

a) Due to that the gear racks move linearly and provide the lever of tangential force on the drive shaft constant along the pistons entire travel path. In result, the arithmetic average of the moment in the proposed engine is 1.83 times the arithmetic average of the moment in the traditional engine.

b) Due to the time delay at the TDC, the pressure and temperature are significantly higher than in the traditional

one. It can be assumed that an optimization of the delay will increase the pressure by at least 20–30%. It means, that the HP of the new engine will be more than in the traditional one in the same scale using equal amounts of fuel for both engines.

2. Improved exhaust and fuel combustion process.

a) Due to delay at the BDC the time for exhaust increases many-fold. This means that fresh fuel-air mixture will not mix with the remnants of the combusted mixture.

b) The combustion stroke and the injection stroke are performed simultaneously, both strokes being isolated. More over the compression stroke is isolated also.

c) The absence of the gas distribution mechanism, including a camshaft, means that the pressures in cylinders 1 and 2 make "opening" and "closing" of the valves 3 and 4 and aperture 15. This design provides more efficient “intake” and “exhaust” compared to the gas distribution mechanism.

5. Perspectives

First of all, it is a huge step in the field of ecology. Reducing fuel consumption will reduce the water, land and air pollution on the same scale. As a result, we can anticipate a decrease in the number of diseases caused by poor environmental conditions, a lower risk of global warming, lower health care costs, an increase in life expectancy, etc. And second, but not last, for example, the new engines connected to generators will force out nuclear and thermal power stations working on coal. Small household electric generators will allow the cheap electricity to be used for heating the home, providing hot water and operation of home appliances, etc.

It is difficult to imagine a general picture of the consequences of using the new engine. Multiple correlations of causes and effects can be described in an economic/mathematical model.

Nomenclature

P	force acting on the piston
HP	horse power
F	pressure in the cylinder
M	torque on the shaft
n	engine speed
L	size of the lever on the shaft
S	area of the piston
T	tangential force
T_c	cooler temperature
T_h	heater temperature
η	coefficient efficiency

Bibliography

[1] Carbon dioxide. Latest measurement: July 2020. NASA. Global climate change. Vital Sings of the Planet. https://climate.nasa.gov/vital-signs/carbon-dioxide/

[2] Learn the facts: Fuel consumption and CO_2. Natural Resources Canada. Published 2014. https://www.nrcan.gc.ca/sites/www.nrcan.gc.ca/files/oee/pdf/transportation/fuel-efficient-technologies/autosmart_factsheet_6_e.pdf

[3] BP. Primary energy. 2019. www.bp.com/en/global/corporate/energy-economics/statistical-review-of-world-energy/primary-energy.html

[4] What is the United Nations Framework Convention on Climate Change? United Nations Framework Convention on Climate Change. 21 March1994. https://unfccc.int/process-and-meetings/the-convention/what-is-the-united-nations-framework-convention-on-climate-change

[5] REITZ, R.D., OGAWA, H., PAYRI, R. et al. IJER editorial: The future of the internal combustion engine. *International Journal of Engine Research*. 2019, **21**(1), 3-10. https://journals.sagepub.com/doi/10.1177/1468087419877990

[6] CARSTENSEN, J. Thermodynamics and kinetics. Lecture at the Faculty of Engineering University of Kiel. www.tf.uni-kiel.de/matwis/amat/td_kin_i/kap_1/backbone/r_se31.html

[7] What is Polytropic Process – Definition. Thermal Engineering. 2020. https://www.thermal-engineering.org/what-is-polytropic-process-definition

[8] GOTZ, A.N. Kinematics and dynamics of the crank mechanism of piston engines. *Vladimir State University*. Vladimir 2006. http://window.edu.ru/resource/807/65807/files/dinamika.pdf

[9] Engine combustion process explained. X-engineer. 2020. x-engineer.org/automotive-engineering/internal-combustion-engines/performance/engine-combustion-process-explained/

[10] Power and Torque. EPI Inc. Expertise + Integrity = Performance. 2020. www.epi-eng.com/piston_engine_technology/power_and_torque.htm

[11] The Carnot Efficiency. PennState. College of Earth and Mineral Sciences. www.e-education.psu.edu/egee102/node/1942

[12] RUDY, P.C., NOVIYANTO, T. Design and manufacture camshaft for Otto cycle modification to reducing fuel consumption. *International Journal of Development Research*. 2017, 7(12), 17398-174022017. https://www.journalijdr.com/sites/default/files/issue-pdf/9136.pdf

[13] MALI, M., MASKAR, P., GAWANDE, S. et al. Design optimization of cam & follower mechanism of an internal combustion engine for improving the engine efficiency. *Modern Mechanical Engineering*. 2012, **2**(3), 114-119. https://doi.org/ 10.4236/mme.2012.23014

Serguei Tikhonenkov – Advanced Training Department, Lifting and Building Machines. Belorussian-Russian University, Belarus (residence in the current time: Vaughan city, Ontario, Canada).

e-mail: *srgtikhonenkov@gmail.com*

Article citation info:
FĄFARA, J-M. Overview of low emission combustors of aircraft turbine drive units. *Combustion Engines*. 2020, **183**(4), 45-49. https://doi.org/10.19206/CE-2020-407

Jean-Marc FĄFARA

CE-2020-407

Overview of low emission combustors of aircraft turbine drive units

It is important to notice that aircraft turbine drive units are commonly used in the modern aviation. The piston engines are often reserved for small and/or sportive aircraft. The turbine drive units are also combustion engine. This paper presents the most popular combustors used in the aeronautical turbine engines. Firstly there are listed the requirements that a combustor has to achieve. Then are presented the combustor designs that permit to achieve the firstly presented requirements. In this work are presented the LPP, TAPS, RQL, graduated combustion zone, VGC, exhaust recirculation system combustors. For each combustor design is enlighten its principle of work, described the etymology of the given name to this design and shown a scheme. The work is closed by a briefly conclusion about the described combustor.

Key words: *aircraft, engine, low emission, combustors, design*

1. Introduction

Combustors are inseparable elements of turbine drive units. Their task is to transfer the energy contained in the fuel into the air stream flowing through the turbine engine. Improvement of the design of combustor can be done taking in consideration different criterion. The first of the criteria is to optimize the combustion process to improve the combustor efficiency. The second direction of improvement the combustors is to reduce the emissions. In order to perform the above-mentioned steps, a variety of engineering tools have been created to enable faster and simpler pre-verification of the modifications. Such tools include computer programs that enable simulation of mechanical loads, thermal loads and combustion processes. The use of these tools leads to minimization of manufactured and tested prototypes, saving time and financial resources, from where the ever-increasing effectiveness of the combustion chamber designing process.

The first criteria, that can be considered during designing turbine engine, is to increase the efficiency of combustor. When fuel is burned, a part of the fuel will not be consumed or will not be oxidized to the most stable chemical form. In most cases, this is simply due to imperfections of the air-fuel mixture, and in particular when the entire fuel is not well evaporated or when the mixture is not homogeneous in its entire volume. In order to prevent these adverse phenomena, design solutions of combustors have been developed such as: increasing the number of fuel injectors (which permits better fragmentation of the fuel), the use of developed methods to turbulence the air entering into the combustor liner and heating fuel before entering into the injectors using hot oil from the engine lubrication system.

The second criteria for the design of turbine drive units is to reduce atmospheric emissions. One of the more harmful substances emitted by this type of engine are nitrogen oxides (NO_x). This substance is responsible for numerous respiratory health problems, acid rains and destruction of the ozone layer [1]. This substance is naturally produced by combustion as a result of excessive combustion temperature. Its formation is largest when fuel is burned in stoichiometric proportions (Fig. 1 and Fig. 2). In order to avoid combustion in the stoichiometric proportion, lean or rich combustion may be designed. The combustion of a rich mixture promotes the reduction of nitrogen oxide (NO_x) emissions, but also results in higher carbon monoxide (CO) and hydrocarbons (HC) emissions. The combustion of a lean air-fuel mixture, in addition to reduce nitrogen oxide emissions (NO_x), also reduces carbon monoxide (CO) emissions, but leads to an increase in hydrocarbons emissions (HC). It is the way of designing the combustion process that permits the combustion of fuel outside the stoichiometric ratio; these solutions reduce nitrogen oxide (NO_x) emissions.

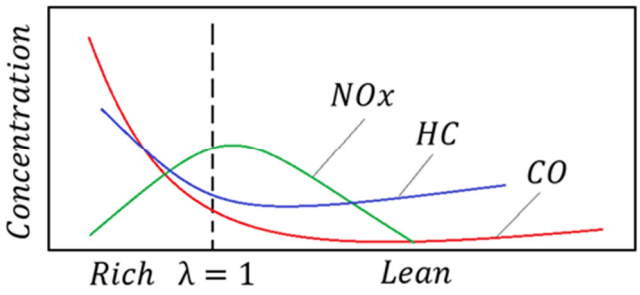

Fig. 1. Example of the effect of the air variation delivered to the combustion zone on the formation of nitrogen oxides (NO_x) and other atmospheric pollutants (on the example of the petrol combustion) (basing on [2])

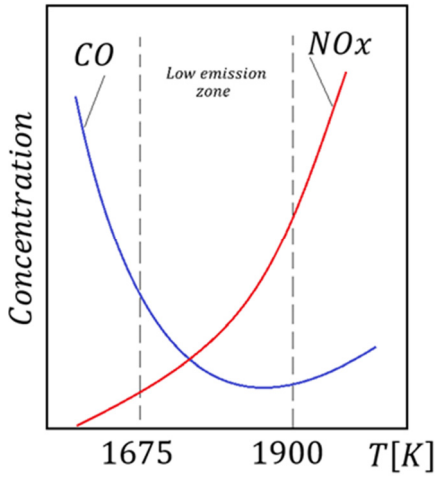

Fig. 2. Effect of combustion temperature on nitrogen oxide formation (basing on [3])

Received 4 September 2020; Received in revised form 3 November 2020; Accepted 4 November 2020
Available online 15 December 2020

2. Development direction of combustors in aircraft turbine engines

2.1. Optimization of the air-fuel mixture formation process

Combustors permit fuel energy transmission into the air stream flowing through the combustor. Depending on the degree of heating of the air in the combustor and the intensity of the air mass stream, a certain amount of fuel should be brought into the combustor. The same amount of fuel may be brought in different ways. It is important to note that, in order to create a air-fuel mixture with optimal parameters, it is necessary to ensure the best possible fuel spray and adequate turbulence of the forming mixture. The smaller is the size of the fuel droplets, the larger evaporation surface area is obtained, which permits for more intense reception of heat from the environment (from the air arriving behind the compressor, and from the combustion zone), and consequently leads to faster evaporation of the fuel. Properly evaporated fuel is not able to ensure the homogeneity of the air-fuel mixture. In order to ensure its homogeneity, swirled air must be delivered into the air-fuel mixture formation zone. Faster evaporation of fuel and uniformity of its distribution in the air stream, provide conditions for the lower temperature fluctuations in the combustion zone, which leads to a reduction in nitrogen oxide emissions (NO_x), and permits more complete combustion of the fuel, which permits a reduction in hydrocarbons (HC) and carbon monoxide (CO) emissions.

Fuel systems with more injectors may be used to ensure that the fuel evaporation processes are carried out and that the fuel is properly mixed with air, while maintaining an adequate fuel mass flow. In that system, each injector delivers less fuel, but with a higher degree of spraying. The work performed in Russia, presented by A.N. Markushin, A.V. Baklanov, and N.E. Tsyganov, indicates through experimental studies that the use of higher number of injectors makes possible to significantly reduce emissions of substances such as nitrogen oxides (NO_x) and carbon monoxide (CO) [4].

The temperature of the fuel supplied to the injector also affects the evaporation process of the fuel during the air-fuel mixture formation. Higher the fuel temperature at the injector's inlet is, lower amount of heat will be needed to evaporate the fuel outing from the injector. However, the evaporation temperature cannot be excessive in order to avoid the formation of fuel vapor "jams" in the fueling system. Fuel-oil heat exchangers are used to increase the fuel temperature arriving into the injector [5]. It permits the desired fuel temperature to be incurred before arriving into the injector, while cooling the oil from the lubrication system, which also partially permits the cooling of the sensitive drive unit zones (the bearing of the turbine shaft(s), gearbox components, etc.).

2.2. Stoichiometric combustion avoiding in the combustors

As it has already been shown, it is possible to reduce the emission of substances harmful for humans and the environment by avoiding the stoichiometric combustion of the air-fuel mixture. Avoiding stoichiometric combustion reduces the combustion temperature, resulting in lower nitrogen oxide (NO_x) emissions. There are therefore two fundamental ways to approach this problem. The first is the combustion of a lean air-fuel mixture, in which there is an excess of air compared to the theoretical air demand. This solution includes combustors such as LPP and TAPS. The second method is to burn a rich air-fuel mixture. For this solution, the RQL combustors may be assigned. There are also other solutions, combining the combustion of a rich and lean air-fuel mixture. In the latter category of technical solutions, variable geometry combustion chambers and graduated combustion zone combustors may be cited.

LPP combustors (lean premixed prevaporized) – LPP combustors adopt maximum evaporation of the fuel and its mixing with air, the quantity of which is greater than the theoretical demand. It is therefore possible to talk about the "Lean" combustor referring to the lean air-fuel mixture, "Premixed" for optimal mixing of fuel with air, and "Prevaporized" in reference to the rapid evaporation of fuel, from where comes the name of the LPP combustors (*Lean Premixed Prevaporized*). Burning a lean air-fuel mixture will reduce the combustion temperature, which in turn will reduce emissions of nitrogen oxides (NO_x). The LPP combustion chamber consists of three zones. The first zone is responsible for spraying fuel in the air stream, for evaporation of fuel and thus for the formation a lean air-fuel mixture. The second combustor zone is the place where the previously prepared air-fuel mixture is burned; the combustion zone is stabilized by a recirculation zone. The last combustor zone is the exhaust-air mixing and cooling zone. It can be concluded that throughout the combustion process in the combustor, the fuel-air mixture created and burned is in a lean state, which has a lower combustion temperature as a consequence, which permits to reduce the emissivity of the these combustors [6]. The LPP combustors must be adequately shaped to form a stable recirculation zone. This is very important because the combustion of a lean air-fuel mixture is generally unstable. The diagram of the LPP combustion chamber is shown in Fig. 3, on which the air-fuel mixture formation zone can be seen in particular.

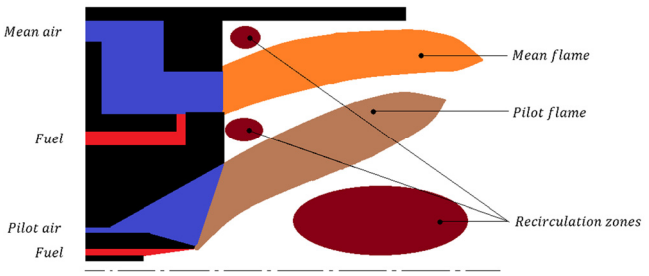

Fig. 3. LPP combustor scheme (basing on [7])

TAPS combustors (twin annular premixing swirler) – another combustor, which is also in the category of the combustors with lean air-fuel mixtures, are the TAPS combustors. This combustor has two air swirls, to which fuel is also delivered. The administered fuel, and the air from the central (internal) swirl, permits the formation of a rich air-fuel mixture. This is the combustion process that can be found in classical combustors. The presence of this central

rich combustion zone permits to generate a pilot flame, permitting partial stabilization of the remaining, lean, combustion zone. Part of the air from the central swirl and the air from the outer swirl permits an optimal mixing of air and fuel spray arriving from between the swirls, forming a lean fuel-air mixture. The combustion of a lean air-fuel mixture is not generally stable. In this type of combustor, the main, lean, combustion zone is stabilized by the centrally located pilot flame, and by the formation of recirculation zones. Thus, it is called a "Twin Annular Swirler" combustor, referring to the fact that the combustor contains a double ring (swirlers) permitting the "Premixing" of the fuel with air. On the low load of the turbine drive unit, fuel is fed only to the central system, which permit the formation of a rich pilot flame, ensuring the running of the turbine engine. As the engine power increases, the fuel begins to be fed into the perimeter combustion zone, where lean combustion takes place. At the same time, recirculation zones are being established, which are increasingly beginning to stabilize the lean combustion zone. After exceeding a certain power value of the engine, the recirculation zones are so significant that they are able to fully stabilize the lean combustion zone; the pilot flame is extinguished. The suppression of the pilot flame reduces hydrocarbons (HC) and carbon monoxide (CO) emissions. Compared to the LPP combustion chamber, the TAPS combustion chamber is characterized by greater flame stabilization safety by using a pilot flame on the low load of the drive unit. In addition, the combustion chamber is characterized by very low emissions of nitrogen oxides (NO_x); the third generation of TAPS combustors has reduced around 75% of nitrogen oxide (NO_x) emissions planned in the CAEP/6 [6]. Figure 4 shows the work principle of the TAPS combustor.

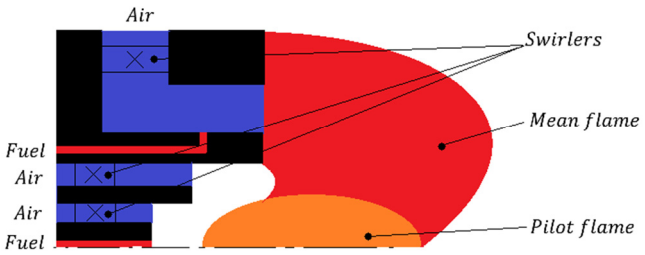

Fig. 4. TAPS combustor scheme (basing on [8])

RQL combustors (rich-burn, quick-mix, lean-burn) – another type of combustors is a combustor containing two combustion zones; the first with a rich air-fuel mixture and the second with a lean air-fuel mixture. The first part of the combustor includes the injection of fuels and air swirl. The amount of air supplied into the air-fuel mixture formation and combustion zone is less than under stoichiometric conditions. Due to the combustion of the rich mixture, the combustion temperature is lower than for stoichiometric conditions, which limits the amount of nitrogen oxide (NO_x) emissions. As a result of rich combustion, unfortunately, hydrocarbons (HC) and carbon monoxide (CO) are created. As a result of the presence in this combustion zone of an increased amount of radicals, the flame is relatively stable. Due to the presence of this first part of the combustor, the beginning of the combustor name is "Rich-Burn". In order to burn hydrocarbons (HC) and carbon monoxide (CO), while avoiding the transition to stoichiometric combustion, a significant amount of air is supplied behind the rich combustion zone. This rapid transition into the lean combustion process will minimize the stoichiometric combustion area; because of that comes the second part of the combustor name: "Quick-Mix". The mutation of the combustion process from rich into lean will, in addition to maintaining low levels of nitrogen oxide formation (NO_x), permit the achievement of hydrocarbon (HC) and carbon monoxide (CO) combustion. In reference to this last combustion zone, comes the last part of this combustor name: "Lean-Burn". Given the structure and principle of work, its name "Rich-Burn, Quick-Mix, Lean-Burn" (RQL) can be justified. The result of this combustion process design is the reduced nitrogen oxide emissions (NOx) [6]. Figure 5 shows the scheme of the described combustor.

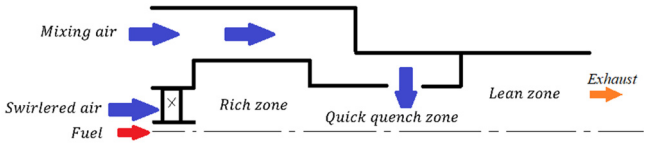

Fig. 5. RQL combustor scheme (basing on [9])

Combustors with graduated combustion zone – another combustor reducing atmospheric emissions is combustor with a graduated combustion zone. The work principle of this kind of combustor is similar to the RQL combustor, with the difference that the fuel is delivered into both combustion zones; into the rich and lean combustion zones. Air coming from the lean combustion zone quickly dissolve the rich combustion zone. The rich combustion zone permits to stabilize the combustion process of the lean combustion zone, but produces hydrocarbons (HC) and carbon monoxide (CO). In turn, the lean combustion zone permits the elimination of hydrocarbons (HC) and carbon monoxide (CO) coming from the rich combustion zone. The combustor is designed in the way that the combustion process is either rich or lean, in order to reduce the stoichiometric combustion zone, which causes a higher combustion temperature and therefore greater emissions of nitrogen oxides (NO_x) [6]. Figure 6 shows the combustor analyzed above.

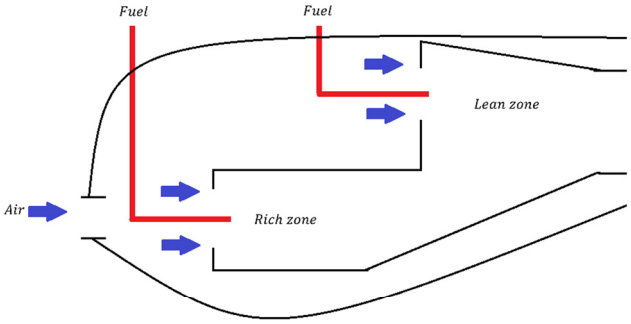

Fig. 6. Combustor with graduated combustion zone (basing on [10])

VGC combustors (variable geometry combustors) – as a result of the operation of the turbine drive unit at different ranges, the parameters of the air mass flowing through the combustion chamber also change. As a result of the air mass flux parameters change, a modification of the combustion process may happen and as for example a close-up to the stoichiometric combustion may occur. In order to prevent this phenomenon, it is possible to control the fuel system, but there is also the possibility of using combustors equipped with variable geometry liner. The change in the geometry of the liner consists primarily in the modification of the arrangement and the cross-sectional field of the air-supply holes, permitting to deliver air into the combustion zone. An actuator is placed outside the combustor to change the geometry of the liner. The actuator is controlled by a system that takes into account the operating range of the drive unit. The name of this combustor, "Variable Geometry Combustors" (VGC), is derived from the liner design [11]. Figure 7 shows the combustor discussed above.

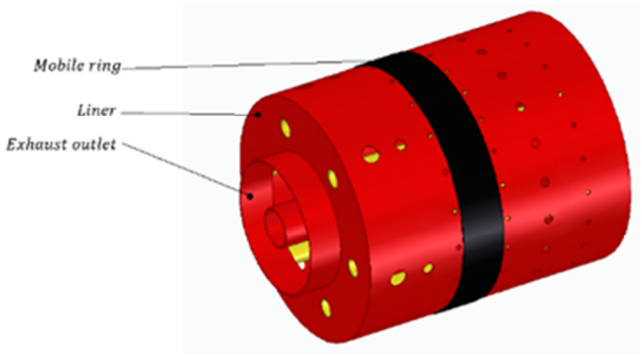

Fig. 7. VGC combustor scheme

Combustors with exhaust recirculation system – exhaust recirculation systems are today commonly used in car industry. Despite the apparent reservation of this technology for piston engines, it may be also used for aircraft turbine drive units. Exhaust gases would be collected in the combustor exhaust system, cooled, compressed to the appropriate pressure, and re-administered to the combustor. It could provoke the dilution of the air supplied to the combustion zone which in turn would reduce the peak combustion temperature. A lower combustion peak temperature would reduce the formation of nitrogen oxides (NO_x). This technical solution is not used in aircraft industry, but just described. Research into this solution could assess the usefulness of this technical solution. Figure 8 shows a combustor equipped with a exhaust recirculation system.

3. Conclusion

Since the creation of turbine drive units, engineers and scientists are constantly striving to improve them. In general, the turbine engines consist of an inlet, compressor, combustor, turbine and outlet system. Each of these components is of great importance for the proper and efficient work of turbine drive units. Combustors are designed in the way to improve the process of creating an air-fuel mixture and to improve the combustion process itself. These two directions of combustors development permit the reduction of atmospheric emissions and higher efficiency of these machinery. Striving for the reduction of the turbines' emissions, the use of catalytic combustors may be also interesting. The catalytic combustor permits for a flame-free fuel oxidation, which permits for a significant reduction in emissions of harmful substances into the environment. Regardless of the progress and development of the combustors, the use of the newest technologies for their development and testing was, is and will remain the standard. Increasingly improved numerical technologies permits for a better understanding of intra-combustor phenomena. Numerical technologies are intensively developed and applied to the science and technology.

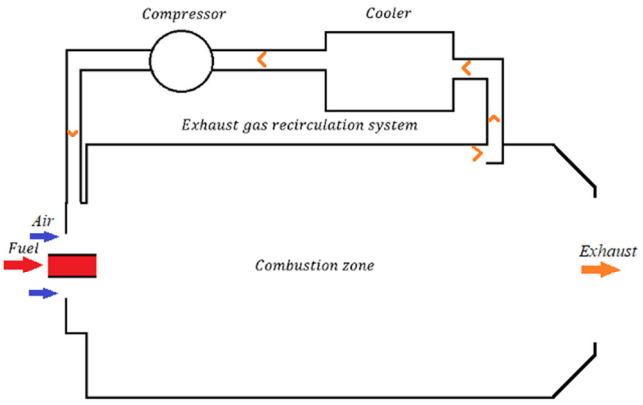

Fig. 8. Combustor with exhaust recirculation system (basing on [11])

Acknowledgements

This work is presented in order to compile contemporary designs of aircraft turbine engine combustors, linked to the reduction of their emissivity.

Nomenclature

CO	carbon monoxide
HC	hydrocarbons
LPP	lean premixed prevaporized
NO_x	nitrogen oxides
RQL	rich-burn, quick-mix, lean-burn
TAPS	twin annular premixing swirler
VGC	variable geometry combustors

Bibliography

[1] Les oxydes d'azote – Polluant atmosphérique surveillé en Nouvelle-Calédonie: origines, impacts et surveillance. New Caledonia, Printer *SCAL'AIR*, 2015.

[2] OCDE. Études de l'OCDE sur l'innovation environnementale – Invention et transfert de technologies environnementales. 2012. Printer OCDE, Paris. https://doi.org/10.1787/20743505

[3] GŁOWACKI, P., SZCZECIŃSKI, S. Turbinowy silnik odrzutowy jako źródło zagrożeń ekologicznych. *Prace Instytutu Lotnictwa*. 2011, **4**(213), 252-257.
[4] MARKUSHIN, A., BAKLANOV, A., TSYGANOV, N. Improvement of aircraft GTE emission characteristics by using the microflame fuel combustion in a shortened combustion chamber. *Russian Aeronautics* (Iz VUZ). 2014, **56**(4), 59-62.
[5] Royce Rolls. The jet engine. Derby, 1986. Printer Royce Rolls plc.
[6] GUELLOUH, N., SZAMOSI, Z., SIMENFALVI, Z. Combustors with low emission levels for aero gas turbine engines. *International Journal of Engineering and Management Sciences*. 2019, **4**(1), 503-514. https://doi.org/10.21791/IJEMS.2019.1.62.
[7] TEMME, J.E., ALLISON, P.M., DRISCOLL, J.F. Low frequency combustion instabilities imaged in a gas turbine combustor flame tube. *50th AIAA Aerospace Sciences Meeting including the New Horizons Forum and Aerospace Exposition*. 2012, Nashville, Tennessee.
[8] HERBON, J., AICHOLTZ, J., HSIEH, S.Y. et al. N+2 Advanced low NO_x combustor technology – Final Report. 2017NASA/CR-2017-219410, E-19298, GRC-E-DAA-TN35615.
[9] KHOSRAVY EL_HOSSAINI, M. Review of the new combustion technologies in modern gas turbines. In: BENINI, E. Progress in gas turbine performance. *Printer IntechOpen*, London 2013, 145-164. https://doi.org/10.5772/54403
[10] BAUDOIN, C., COMMARET, P., LE LETTY, E. et al. Canadian patent no 2 398 669. 2002, *Canadian Intellectual Property Office*.
[11] GIERAS, M. Miniaturowe silniki turboodrzutowe. *Oficyna Wydawnictwa Politechniki Warszawskiej*. Warszawa 2016.

Jean-Marc Fąfara, MEng. – Department of Mechanics, Machines and Energy Processes, Faculty of Mechanical and Power Engineering, Wroclaw University of Science and Technology,
e-mail: *jean-marc.fafara@pwr.edu.pl*

Article citation info:
SZAŁEK, A. Energy conversion in motor vehicles. *Combustion Engines*. 2020, **183**(4), 50-57. https://doi.org/10.19206/CE-2020-408

Andrzej SZAŁEK

CE-2020-408

Energy conversion in motor vehicles

The portfolio of the automotive market appears more and more low-emission and zero-emission propulsions in vehicles. This is the result of measures taken to limit or even eliminate the emission of harmful substances into the atmosphere generated by vehicles. The article covers issues related to energy conversion in automotive drive systems currently offered by automotive manufacturers. Standard, hybrid, hybrid plug-in, electric and fuel cells drive system were analyzed. Attention was drawn to the chain of energy transformations related to each of the analyzed drive systems. The efficiency of the presented vehicle drive systems was analyzed. General conclusions were formulated regarding the method of analyzing energy changes related to the operation of automotive propulsion systems. The article reviewed selected author's own works on hybrid and hydrogen propulsion.

Key words: *passenger vehicle propulsion systems, chain of energy transformations, efficiency of energy conversion*

1. Introduction

For over 130 years, heat engines have been the basic and practically dominant source of power for all types of vehicles. In the case of means of land and water transport, these are mainly piston internal combustion engines, while means of air transport are mainly driven by flow engines. The basic feature of the above-mentioned sources of propulsion is the necessity to use natural, non-renewable energy resources necessary for heat generation. This has specific consequences related to the consumption of air needed to release energy in the oxidation process and, consequently, its impact on the natural environment. It is important to use the same air resources, which are necessary both for the respiratory functions of humans and other living organisms, and for the implementation of many industrial processes, including the functioning of modern heat engines. The final effect is the transformation of the atmospheric air into combustion products containing components that are toxic to living organisms and greenhouse gases, and the average temperature value in areas of human activity is increased. Therefore, the mentioned processes are strictly dependent on the number of population and economic activity, including the number of used vehicles powered by heat engines. They are also dependent on the energy consumption of technological processes necessary to produce fuels from energy resources. Taking into account the mass scale of the use of means of transport, a lively discussion about the past sources of propulsion of motor vehicles has been going on in the world for several years. Its main areas are conducted, on the one hand, in terms of energy expenditure necessary to meet human transport needs, and on the other hand, in terms of environmental burden with direct and indirect effects of the use of propulsion sources of a certain type. It is well known that any type of energy use entails a change in the overall energy balance of the globe. Therefore, the aim of contemporary development works on the future of vehicle propulsion sources is to develop a new propulsion system considering the chain of energy transformations that directly and indirectly affect the environment. In this context, the electric drive of the vehicle, with the generator in the form of a stack of fuel cells, is currently a very advantageous and viable proposition in relation to standard propulsion sources. The most experienced in the construction of this type of vehicles is the Toyota company, which in 1992 started the first work on a FCV (*Fuel Cell Vehicle*) powered by fuel cells, launching a serial vehicle called Toyota Mirai in 2014. Currently, following Toyota, vehicles of this type are also offered by other vehicle manufacturers (Honda, Hyundai) [9].

It should be mentioned though that before starting work on this latest proposal from the automotive industry, work was carried out on the creation and implementation for mass production of vehicles with hybrid, hybrid plug-in propulsion and purely electric vehicles with traction batteries.

A hybrid propulsion system has three main configurations, namely serial, parallel, and serial-parallel. In a serial hybrid system topology, the internal combustion engine (ICE) drives a generator which electrical power output is combined with the power coming from the electrical storage and then transmitted through an electric DC-bus to an electric motor (EM) driving the wheels. In parallel hybrid system topology, the combined power is mechanical rather than electrical, in which the ICE and the EM are connected to a torque coupling such that their torque is combined and then transmitted to the wheels using a conventional driveshaft and possibly a differential gear. A serial-parallel hybrid system, also known as a power-split hybrid system, combines the complementary advantages of serial and parallel systems [17].

A plug-in hybrid propulsion system essentially possesses the same configuration as a hybrid propulsion system but with an external electric charging plug, bigger electrical components (i.e. an electric motor and a battery), and a downsized engine. Owing to the high capacity of the electrical components, vehicles with plug-in hybrid propulsion can run in full-electric mode for long periods [17]. The presented topography is based on a parallel hybrid system (Fig. 1).

The purely electric propulsions topology is represented by a battery and fuel cell propulsion. The battery electric propulsion is totally powered by electricity and it does not have any fuel tank to store the fuel. This powertrain consists of large rechargeable batteries to power the vehicles and do not release any harmful gasses to the environment. The battery can be recharged from the grid or from any other external power source by using a socket. In fuel cell propulsion hydrogen is used as fuel. The hydrogen power-

Received 11 November 2020; Received in revised form 30 November 2020; Accepted 30 November 2020
Available online 15 December 2020

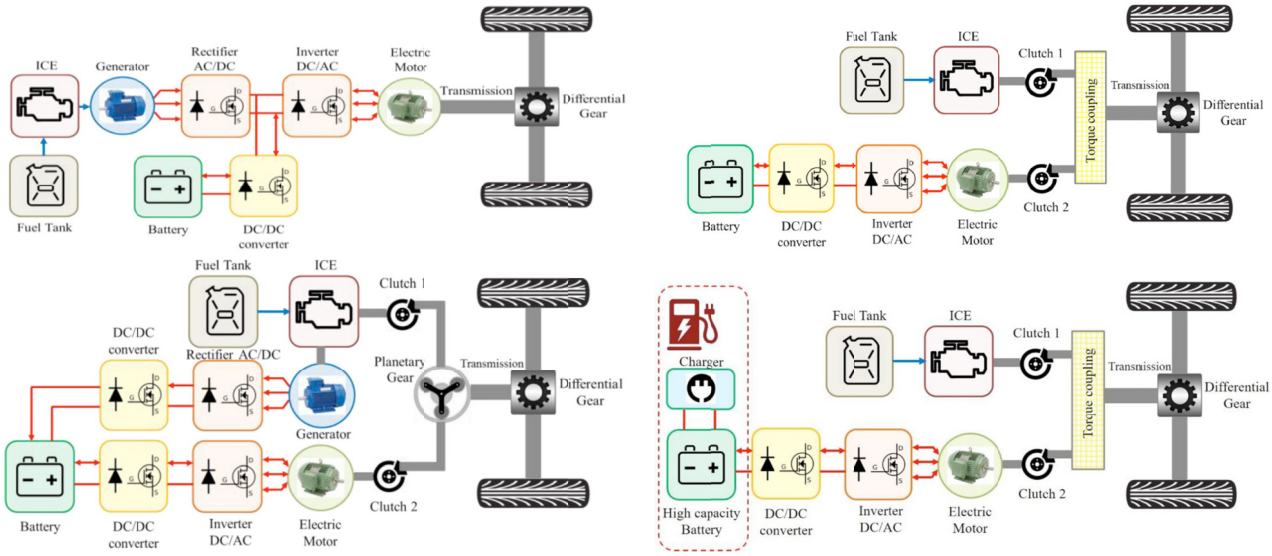

Fig. 1. Types of configuration of hybrid and hybrid plug-in propulsions [17]

train architecture is same as battery electric one. A fuel cell acts as a battery and generates electric power to the motor driving the vehicle [15].

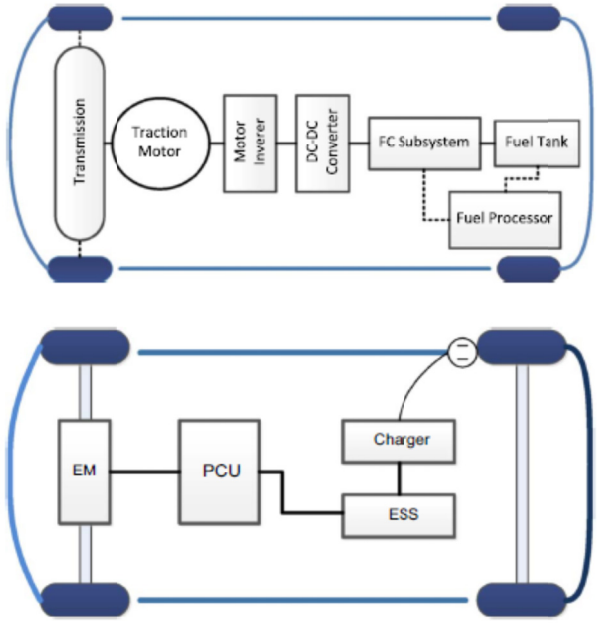

Fig. 2. Configuration battery and fuel cell electric propulsions [7]

2. Analysis of the energy consumption of modern vehicle drive systems

Correct analysis of energy consumption in transport should take into account all stages of its processing, starting from obtaining energy resources, transforming them into fuel, and then converting it into mechanical energy that drives the vehicle.

The first vehicles equipped with their own mechanical drive used a piston steam engine. This type of drive was used practically from the mid-nineteenth century to the 1960s, mainly in rail vehicles and water transport, where dimensions, weight of the drive unit and energy storage in the form of hard coal were not a key problem. The chain of energy transformations in this type of drive system was limited to the mining and transportation of hard coal, then the extraction of heat from it in the furnace of the boiler, in which steam was generated and directed to the engine cylinder, and then mechanically transferring the force of the expanding steam to the vehicle wheel drive. Despite the relatively short chain of these changes, the efficiency of energy conversion was very low, because the efficiency of the steam engine itself did not exceed a few percent. This was the main reason for the abandonment of this power source. Another reason was also environmental considerations, as the operation of steam engines usually generated a large amount of soot, which when mixed with water vapor formed a sticky pollutant for the environment. It was especially troublesome at stations and railway routes. It should be mentioned that the decisions to abandon steam engines were made at a time when hard coal resources were easily available and its price on the world markets was very low.

There is an analogy here with the current situation of a piston internal combustion engine, which is currently the dominant source of propulsion for land and water vehicles in the world, and the resources of liquid hydrocarbon fuels are still available at an acceptable price.

Combustion engines generate a third of the mechanical energy from the energy contained in the fuel. The main losses, beyond the effective operating point, are caused by exhaust gas emissions at high temperatures and energy losses in the cooling system. The remainder heat loss includes not only the heat-transfer caused by the convection and radiation on the surface of ICE, but also the heat storage of the system (body, coolant, oil) in the engine compartment during the cycle [5]. Since the internal combustion engine in mobile applications requires connection to a gearbox, its efficiency should also be considered in the energy conversion chain of this type of drivetrain.

Nevertheless, as in the case of the steam engine, the same reasons decided to take steps to seek new solutions for vehicle propulsion systems. The activities are carried out in two directions.

The first direction is the improvement of the efficiency of the propulsion containing the internal combustion engine through its simultaneous cooperation with the electric motor. Electricity is obtained either from the conversion of the mechanical energy produced by the internal combustion engine or from the conversion of the kinetic energy during vehicle braking. This extends the energy conversion chain and requires the use of additional devices in the form of electrical machines, high-voltage batteries such and voltage converters. Nevertheless, it increases the efficiency of the entire system. In addition, the plug-in system allows to use not only the energy stored in liquid hydrocarbon fuels, but also electricity from the power grid.

The second direction is the replacement of a heat engine as a mechanical energy generator in a vehicle with an electric motor. The source of electricity in this case is either a traction battery or a fuel cell. Energy conversion in a vehicle with a traction battery has a short energy chain. The energy taken from the power grid is stored in the battery and then, after conversion from direct current to alternating current, it is directed to the electric motor and from there through the mechanical transmission to the wheels. In a drive system with a fuel cell, the energy stored in the vehicle is compressed hydrogen. The hydrogen production process itself requires energy. Electricity is generated by a chemical reaction in a fuel cell. The further conversion of energy is identical to that in the battery drive.

3. Internal combustion engines

According to the definition, the overall efficiency of an internal combustion engine is the ratio of the effective work measured on the engine shaft to the sum of the supplied heat, which results from the supplied fuel stream and its calorific value.

The overall efficiency of a modern petrol-fueled spark-ignition (SI) engine can reach the maximum value of 36 to 40%, while when fueled with natural gas it can reach efficiency even above 40%. This is possible due to the high resistance of natural gas to knocking combustion, which allows the use of a higher compression ratio. The values given refer to the most favorable operating points of the engine, while the average efficiency of an SI engine driving the vehicle in road traffic usually does not exceed 30%.

Contemporary compression-ignition (CI) engine used in vehicle propulsion can achieve an overall efficiency of 42 to 45%, while some stationary engines can achieve efficiency up to 50%. This applies to the most favorable engine operating points, while the average efficiency of a diesel engine driving a vehicle in road traffic is usually up to 35% [9].

In the chain of energy transformations necessary to drive the vehicle, one should also take into account all energy losses caused by the transmission of torque to the wheels through the drive system components, as well as the energy expenditure related to the production and distribution of hydrocarbon fuels. In the case of motor gasoline and diesel oil, it is energy related to the extraction of crude oil, its transportation and processing in refineries, and then distribution of the finished fuel to filling stations. In this context, it is somewhat more advantageous to supply combustion engines with natural gas, the extraction, transportation and cleaning of which usually requires less energy than the production of liquid hydrocarbon fuels. In terms of energy consumption, the quality of the energy raw material is of great importance, because all types of pollution, e.g. contamination of crude oil with sulfur or phosphorus, significantly increase energy expenditure. The place and method of obtaining energy resources is of similar importance. For example, the production of finished fuel from crude oil obtained in Siberia, due to the climatic conditions and the contamination of the raw material, requires much more energy than from crude oil from Arab countries.

4. Hybrid drive systems

Regarding the use of internal combustion engines as a vehicle propulsion source, the introduction of hybrid propulsion systems brought about a significant improvement in energy conversion efficiency. These are usually HEV (*Hybrid Electric Vehicle*) drive systems, in which the internal combustion engine works with one or two electric machines that play the role of an electric drive motor and a power generator. Research has shown that in real city street traffic, almost 60% of the distance traveled by a vehicle equipped with a hybrid powertrain is with the combustion engine switched off (Fig. 3).

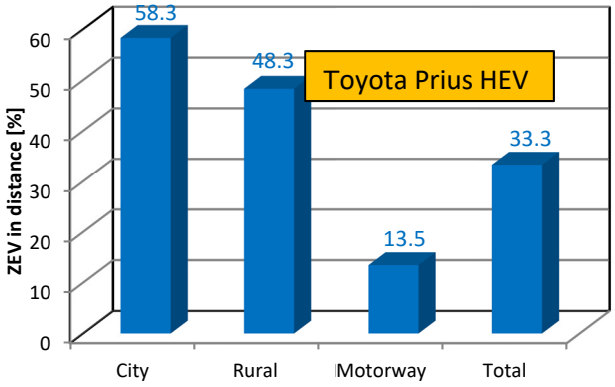

Fig. 3. Proportion of the drive with the combustion engine switched off (ZEV – Zero Emission Vehicle) in relation to the distance traveled in the Real Driving Emissions (RDE) test phases (Toyota Prius HEV) [9]

In some phases of the RDE test, the internal combustion engine is stopped for more than 50% of its operating time (Fig. 4).

The above results are possible to obtain thanks to the rationalization of the use of energy generated by the internal combustion engine. The braking energy recovery process, which takes place every time the direction of torque transmission changes, using the vehicle's kinetic energy to generate electricity and charge the battery, has the greatest share in this. In fact, only part of the braking energy is recovered due to the limitations resulting from the possibility of rapidly storing a large stream of generated electricity in the battery. For this reason, HEVs use special batteries, where the electric capacity is not the most important parameter, but the ability to frequently, cyclically receive and release a large stream of energy is important. Toyota has been using this type of nickel metal hydride (Ni-MH) battery for many years in its hybrid vehicles, and a new lithi-

um-ion (Li-Ion) battery with similar properties has been developed for the latest models.

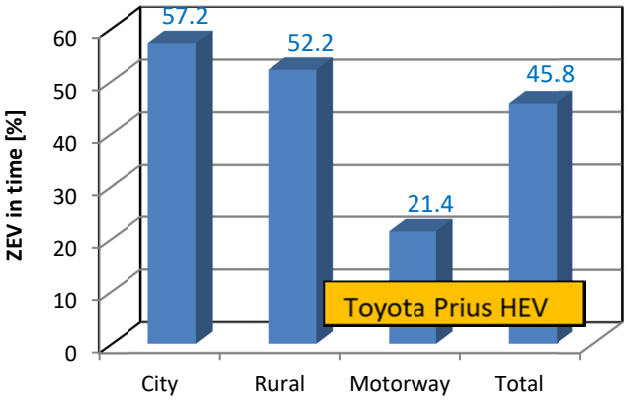

Fig. 4. Proportion of the drive with the combustion engine switched off (ZEV) in relation to the duration of the individual phases of the RDE test (Toyota Prius HEV) [9]

In the latest designs of hybrid drives, the energy recovered during braking accounts for up to 60% of the electric energy supplying the vehicle drive system. It should be emphasized here that the electricity collected in this way makes it possible to support the internal combustion engine with an electric motor, thanks to which the internal combustion engine can only work in the area of the part of characteristic, in which it develops the greatest efficiency. The support with an electric motor also allows the possibility of using a lower-power combustion engine, optimized for operation in the area of the highest efficiency, to drive the vehicle. Such a solution is e.g. the SI engine operating according to the Atkinson cycle, which allows the use of a high value of the compression ratio, which significantly increases the efficiency, which in this type of engine reaches over 40%.

The efficiency of the hybrid system used in passenger cars is primarily determined by the type of energy management system used. The parallel system is beneficial during city driving because the traction battery is able to support the work of the combustion engine thanks to the frequent possibility of recharging with energy recovered during braking.

The disadvantage of this solution is the inability to assist the internal combustion engine in the event of a low charge of the traction battery. In contrast, the serial arrangement is advantageous in steady travel where the vehicle speed varies within a narrow range. The combination of these two types of systems is a serial-parallel system that enables the internal combustion engine to operate in parallel with the electric motor at a low battery charge and, at the same time, to quickly recharge it. The optimal solution is a structure that connects all the systems and makes it possible to use them in any way depending on the speed and load of the vehicle.

Research using the HEV drivetrain [9] show that the average SOC (*State of Charge*) value in the drive test is independent of the initial battery state of charge. The battery charging time depending on the initial (differentiated) level of SOC is shown in Fig. 5.

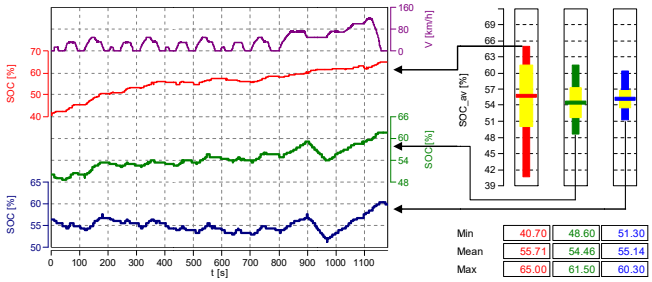

Fig. 5. Initial and average SOC values for various degrees of initial battery discharge and charging conditions during the NEDC test [14]

All the above-mentioned features of the hybrid drive system mean that the efficiency of energy conversion is significantly higher than in standard vehicles powered only by an internal combustion engine. The tests showed that the cost of operational fuel consumption by vehicles equipped with this type of drive system is usually lower by 20 to 40% compared to a standard vehicle of a similar class. Since the fuel used to power the engine is gasoline as in the case of standard vehicle drive systems, we must also take into account energy losses caused by the production and distribution of this fuel in the overall energy balance. Figure 6 shows the fuel consumption of the HEV (Toyota Prius) in the successive phases of the RDE test measured by the carbon balance method.

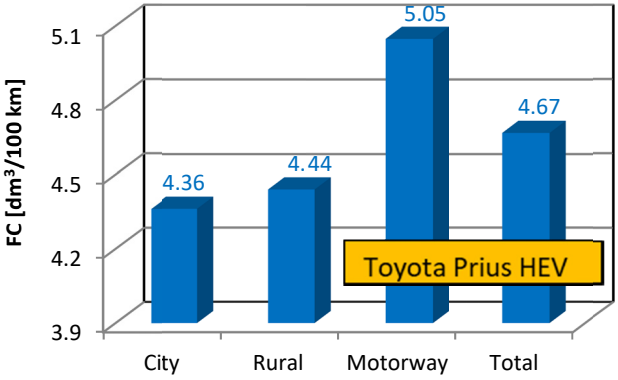

Fig. 6. Fuel consumption in the subsequent phases of the RDE test (Toyota Prius HEV) [9]

5. Plug-in hybrid drive systems

A more developed hybrid vehicle drive system is the PHEV (*Plug-in Hybrid Electric Vehicle*) system, which has a greater potential to increase the efficiency of energy conversion than in classic HEV hybrid vehicles. These vehicles use a Li-Ion battery with a much higher electrical capacity and the possibility of charging from the grid. They offer all the benefits of a hybrid powertrain, including brake energy regeneration. In addition, during proper operation, consisting in regular charging of the battery from the grid, the share of electricity in the vehicle drive is significantly greater than in the standard hybrid drive. This has a positive effect in the form of increasing the efficiency of the drive system and reducing the emission of toxic exhaust gas components, especially during urban operation. In operational tests, the PHEV hybrid drive system shows an advantage over the standard HEV system, but the necessary

condition is the systematic recharging of the electric battery from the power grid. Figures 7–10 show the results of the PHEV operational tests carried out in the context of fuel consumption and the share of time and distance in which the electric drive is used. The obtained test results are more favorable than for the standard hybrid HEV vehicle.

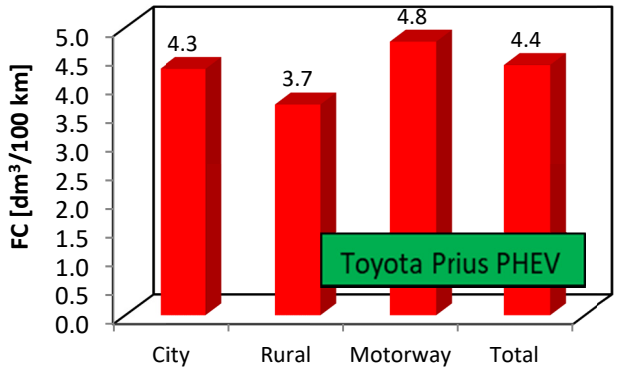

Fig. 7. Fuel consumption in the subsequent phases of the RDE test (Toyota Prius PHEV) [4]

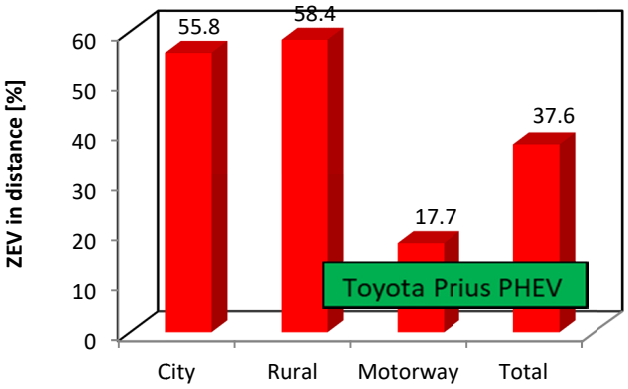

Fig 8. Proportion of the drive with the combustion engine switched off (ZEV) in relation to the distance traveled in the RDE test phases (Toyota Prius PHEV) [4]

An example of an analysis of the operating conditions of Prius plug-in hybrid drive (Fig. 9).

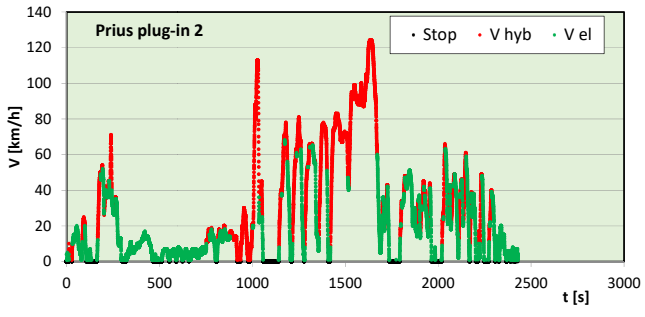

Fig. 9. Operational conditions of vehicles in electric (V el) and hybrid mode (V hyb) [11]

Statistical studies, however, have shown that only a minority of users regularly recharge the traction battery from the grid. The results of research in this area, conducted in three automotive markets, i.e. North America, Europe and Asia, showed that on average only 7.5% of users regularly charge their batteries from the power grid. Moreover, some of the vehicles with this type of drive are returned by users to the lessor with a factory-packed set of cables for charging the battery, which means that they operate the vehicle only with the internal combustion engine turned on.

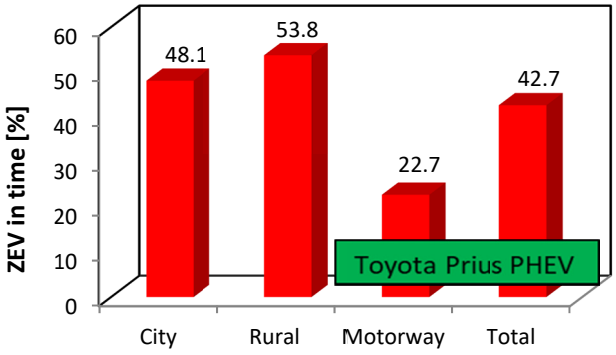

Fig. 10. Proportion of the drive with the combustion engine switched off (ZEV) in relation to the duration of the individual phases of the RDE test (Toyota Prius PHEV) [9]

In drive systems of the PHEV type, depending on the type of energy management used, vehicle operation has different effects in the event of irregular battery charging from the power grid. However, taking into account the large losses caused by energy transformations during this type of operation, the total energy balance of the drive system may turn out to be even less favorable than in standard vehicles powered only by an internal combustion engine.

In the case of a parallel hybrid system, a car with an uncharged traction battery consumes more fuel and generates more toxic exhaust gases compared to the same model with a conventional drive. This is due to the increase in weight of the vehicle by the weight of the traction battery and the inability to support the internal combustion engine by the electric motor. However, when we are dealing with a hybrid drive which, depending on the traffic conditions, works in a serial, parallel or serial-parallel mode, its operating parameters do not differ from a hybrid vehicle without the Plug-in option. The internal combustion engine (Fig. 11) and electric motor (Fig. 12) are running in range of high efficiency. The only downside is the greater weight and dimensions of the electric battery.

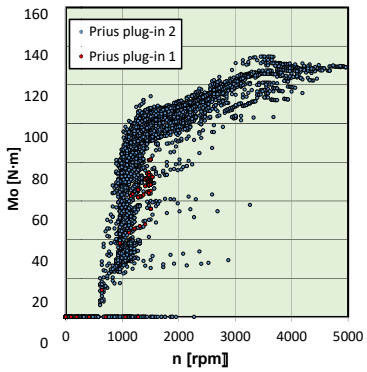

Fig. 11. Operational conditions of the combustion engines of tested hybrid vehicles in urban traffic conditions [3]

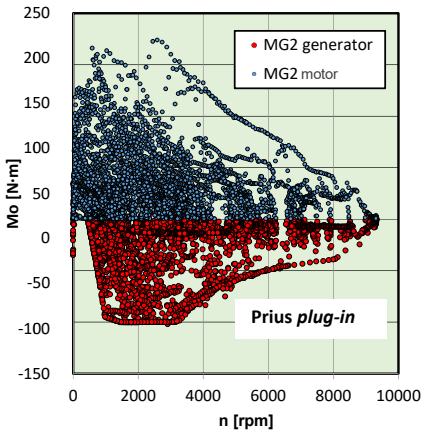

Fig. 12. Conditions of electric motors operation for engine and generator mode of operation [3]

6. Electric drive systems

The key problem of vehicles powered by electric motors (BEV – *Battery Electric Vehicle*), drawing energy only from a set of batteries, is the efficiency of charging the battery and the efficiency of consumption of the electricity stored in the battery by the motor. When charging the commonly used Li-Ion batteries from the power grid, heat losses occur due to the heating of the cells, which requires the use of cooling systems. A similar phenomenon occurs during the transfer of energy to the motor and to other electric devices in the vehicle. The total amount of losses, which is about 12% of the energy used for charging, depends on the value of the intensity of the flowing electric current, as well as weather conditions. In order to maintain the proper working cycle of the batteries in winter, they should be heated, and cooled intensively in summer. The losses in the electric motor amounting to 2–3% can be considered very small. Another problem that seriously limits the value of the vehicle is the long battery charging time. In addition, compared to conventional solutions using liquid hydrocarbon fuels, the currently used batteries, mainly of the Li-Ion type, have insufficient capacity to store energy needed to drive the vehicle, in relation to their dimensions and weight. Figure 13 shows the arrangement of the components of a BEV with an electric powertrain (Lexus UX).

Fig. 13. Arrangement of the components of the electric driveline (Lexus UX) [8]

When analyzing the energy consumption of electric drive systems, one should take into account the source and efficiency of obtaining electricity, as well as losses related to its transmission. When using electricity from thermal power plants that burn non-renewable fossil fuels, the energy balance of such a solution is not very favorable both in terms of energy consumption and environmental impact. Another unfavorable phenomenon is the inability to store electricity for charging the battery, which on a global scale creates problems with planning energy supply to the power grid.

7. Fuel cells

According to many opinions, the only real competition for an internal combustion engine is the Fuel Cell Vehicle system, which uses electricity generated on board the vehicle from a stack of hydrogen-powered fuel cells. Compared to an electric drive system that draws electricity from batteries, this type of drive system has much more advantageous features. In the case of fuel cells, there are no restrictions related to the range of the vehicle and the time to refuel hydrogen. The Toyota Mirai was the first FCV sedan to enter the market in series in 2014. It is a medium size car whose range, after fully refueling with hydrogen tanks, is estimated at around 500 to 700 km. The procedure of filling composite tanks with hydrogen is similar to the LPG (*Liquefied Petroleum Gas*) filling procedure and its time is comparable to the time of filling the tank with liquid fuel. The source of the vehicle's propulsion is a 114 kW electric motor, and this power level provides the performance typical for vehicles of the represented class. The maximum torque generated by the electric motor is 335 Nm, which is comparable to torque values achieved by CI engines, characterized by a high torque value compared to SI engines. It should be emphasized that in electric cars, thus also in the case of FCV, the maximum torque is achieved already starting from zero revolutions per minute. Moreover, with a smaller mass of the drive unit and without harmful emissions for the environment [16]. Figure 14 shows the arrangement of the individual components of the fuel cell driveline (Toyota Mirai).

Fig. 14. Arrangement of the components of the fuel cell driveline (Toyota Mirai) [8]

The only waste product discharged into the environment during the operation of the vehicle is water. This can be a problem during operation at negative ambient temperatures, while the developed procedures for washing and drying the cell surface protect the system against freezing. This was confirmed by tests carried out in a thermoclimatic chamber. Figure 15 shows a diagram of temperature changes in individual elements of the drive system with fuel cells (Fuel Cell Stack coolant and air) during tests in a thermoclimatic chamber.

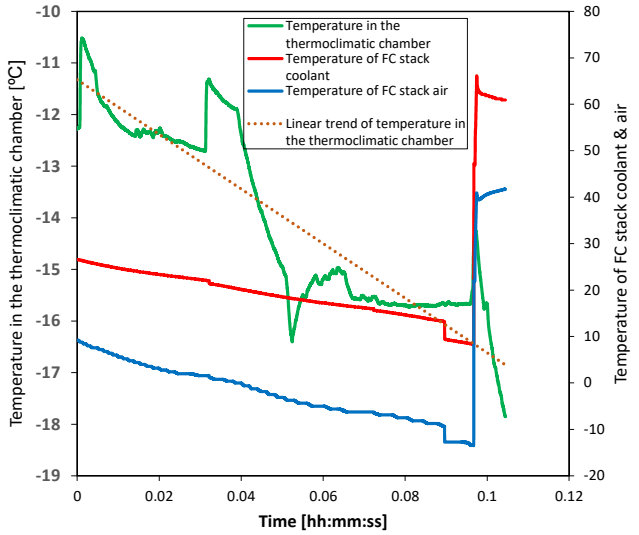

Fig. 15. Temperature of the cooling medium of fuel cells and air in the cell segments during vehicle tests in the thermoclimatic chamber [1, 2]

A significant advantage of using fuel cells to propel vehicles is the possibility of introducing them to a very wide range of vehicles, including lorries, buses, various types of rail vehicles and a wide range of industrial machinery, such as road, construction or mining machinery. In this context, battery operation for electric vehicles is in no way competitive.

The efficiency of the FCV drive system comes down to determining the efficiency of energy conversion in the fuel cell stack and the efficiency of converting energy transmitted to the electric motor. The fuel cell stack used in the Toyota Mirai model achieves a maximum energy conversion efficiency of 65%. Such high efficiency has been achieved by implementation of three main solutions i.e. reducing the thickness of the electrolyte membrane, humidifying the system using the moisture at the anode and reducing evaporation [6]. The transfer of the energy generated in the stack to the electric motor is achieved with the same efficiency as in the case of BEVs. As with hybrid or electric powertrain vehicles, FCVs use a Brake Energy Regeneration system in which the electrical energy accumulator acts as an energy buffer, storing the recovered energy and then using it to support the operation of the fuel cell stack.

A key issue in assessing the efficiency of energy conversion in FCVs is to consider the energy chain needed to produce hydrogen. This applies to both the method of obtaining hydrogen and its purification to the required purity parameters, amounting to approx. 99.97%.

Currently, hydrogen is available on the market and it is classified according to the method of production. For example, hydrogen, currently used in the refining and chemical industries, is mainly produced by steam reforming of natural gas or coal gasification. Both methods generate CO_2 emissions, which is why the hydrogen produced in this way is called gray hydrogen. A transient method for producing hydrogen is its production from fossil fuels, and the resulting carbon dioxide is captured and stored in underground reservoirs. The hydrogen obtained this way is called blue hydrogen. Hydrogen can also be produced by the methane pyrolysis process, in which natural gas is heated to high temperatures to generate hydrogen. The remainder of this process is solid carbon which can be used for other purposes. In this process, large energy expenditure is necessary, and the hydrogen produced by this method is called turquoise hydrogen. The mentioned methods of hydrogen production require a large energy input and generate emissions of carbon dioxide, and often also toxic gaseous components. In addition, they require the use of natural gas or coal, which are a non-renewable fossil fuel, and their extraction in developed countries requires import from distant extraction sites. For this reason, only so-called green hydrogen obtained from renewable energy sources is consider as ultimate fuel to be used in the power units of the FCV type vehicles. It is predicted that water electrolysis, among others, will be used for obtaining hydrogen, while assuming that the electricity required in this process comes exclusively from renewable energy sources.

Currently, the share of green hydrogen in the economy is very small due to high production costs. It is estimated that the current production costs are about three times higher than the costs of producing gray hydrogen, and technological advances in the development of renewable energy sources have reduced these costs by over 50% in the last decade. It is estimated that by 2040 the cost of producing green hydrogen in Europe will be similar to the cost of producing hydrogen currently used in industry. One should also consider a number of conditions affecting the costs of renewable energy and the investment outlays necessary to obtain it. In Europe, wind, hydro and photovoltaic farms have the largest share in obtaining renewable energy. In some parts of the world, climatic conditions may favor a significant reduction of these costs, such as obtaining energy from photovoltaic farms in countries in the subtropical zone. Taking into account the changing external conditions, which have a significant impact on the costs of electricity production from renewable energy sources and the local conditions and costs of producing green hydrogen directly resulting from it, quantification of the energy transformation chain for FCVs is not an easy task. Moreover, in the last decade, the market of electricity supply in the world from various sources has been changing very dynamically, not allowing for a reliable complete energy balance. Stabilizing this situation and creating a new global energy mix will make it possible to make a clear forecast about the future of vehicle propulsion sources.

8. Conclusions

Currently, despite the well-developed production of internal combustion piston engines, which are still characterized by sufficient utility values, and in view of the sufficient availability of liquid petroleum-derived fuels, an intensive search for a new type of drive for industrial vehicles and machines is underway in the world. This was due to a significant change in the criteria for assessing vehicle propulsion sources, which took place especially in the last decade. The basic conditions that currently play a key role and must be met are climate neutrality and high energy conversion efficiency. In this context, the unquestionable recent progress in the development of conventional internal combustion engine drive systems is no longer sufficient. A radical change in this respect, introducing an electric drive to vehicle propulsion, commonly powered by electric cells, is currently impossible, both due to the lack of appro-

priate infrastructure, limited resources of necessary materials, and clearly limited operational values. An important factor also taken into account are the sources of electricity, which on a global scale are associated primarily with the inefficient combustion process of non-renewable fossil fuels. According to current forecasts, the development of this type of vehicles will take place, but mainly in the sector of urban vehicles, operated in urbanized, richer regions of the world.

A rational, transitional stage in the development of vehicle propulsion sources, which retains all the operational values of standard vehicles, is the introduction of HEV and PHEV hybrid propulsion systems. Their main advantage is significantly greater efficiency of energy conversion and lower environmental impact. This stage of development will allow the gradual transformation of the car market towards completely new powertrains.

According to many opinions, the only source of propulsion that will replace the currently used internal combustion engines in the long run is a drive system equipped with hydrogen-powered fuel cells. As the operational tests have shown, the utility values and the scope of application of these drive systems are not inferior to modern piston engines. This type of propulsion gives the potential possibility of using renewable energy sources, processed with greater efficiency and guarantees climate neutrality.

Nomenclature

BEV	Battery Electric Vehicle
CI	Compression Ignition
FCV	Fuel Cell Vehicle
HEV	Hybrid Electric Vehicle
ICE	Internal Combustiom Engine
Li-Ion	Lithium-Ion Battery
LPG	Liquefied Petroleum Gas
Ni-MH	Nickel-Metal Hydride Battery
PHEV	Plug-In Hybrid Electric Vehicle
RDE	Real Driving Emissions
SI	Spark Ignition
SOC	State of Charge
ZEV	Zero Emission Vehicle

Bibliography

[1] BRZEŻAŃSKI, M., SZAŁEK, A., SZRAMOWIAT, M. Tests of the vehicle's power unit with fuel cells at a reduced ambient temperature. *Combustion Engines*. 2019, **179**(4), 65-69. https://doi.org/10.19206/CE-2019-410

[2] BRZEŻAŃSKI, M., SZAŁEK, A. Tests of the vehicle's powertrain with hydrogen fuel cells at a low temperature. *Proceedings of 8th International Conference on Hydrogen Safety* (ICHS2019), 2019 Adelaide, South Australia.

[3] CIEŚLIK, W., PIELECHA, I., SZAŁEK, A. Assessment of parameters of the hybrid drive system in vehicles in urban traffic conditions. *Combustion Engines*. 2015, **161**(2), 14-27.

[4] CIEŚLIK, W., PIELECHA, I., SZAŁEK, A. Indexes of performance of combustion engines in hybrid vehicles during the UDC test. *Combustion Engines*. 2015, **160**(1), 11-25.

[5] DONG, H., FU, J., ZHAO, Z. A comparative study on the energy flow of a conventional gasoline-powered vehicle and a new dual clutch parallel-series plug-in hybrid electric vehicle under NEDC. *Energy Conversion and Management*. 2020, **218**, 113019. https://doi.org/10.1016/j.enconman.2020.113019

[6] HASEGAWA, T., IMANISHI, H., NADA, M. et al. Development of the Fuel Cell System in the Mirai FCV. *SAE Technical Paper* 2016-01-1185, 2016. https://doi.org/10.4271/2016-01-1185

[7] HIMADRY, S.D., TAN, C.W., YATIM, A.H.M. Fuel cell hybrid electric vehicles: A review on power conditioning units and topologies. *Renewable and Sustainable Energy Reviews*. 2017, **76**, 268-291. https://doi.org/10.1016/j.rser.2017.03.056

[8] Materials Toyota Motor Corporation.

[9] Materials Toyota Motor Poland.

[10] MERKISZ, J., PIELECHA, J., BIELACZYC, P. et al. A comparison of tailpipe gaseous emissions from the RDE and WLTP test procedures on a hybrid passenger car. *SAE Technical Paper* 2020-01-2217. 2020. https://doi.org/10.4271/2020-01-2217

[11] PIELECHA, I., CIESLIK, W., SZALEK, A. Impact of combustion engine operating conditions on energy flow in hybrid drives in RDC tests. *SAE Technical Paper* 2020-01-2251. 2020. https://doi.org/10.4271/2020-01-2251

[12] PIELECHA, I., CIEŚLIK, W., SZAŁEK, A. Operation of hybrid propulsion systems in conditions of increased supply voltage. *International Journal of Precision Engineering and Manufacturing*. 2017, **18**(11), 1633-1639. https://doi.org/10.1007/s12541-017-0192-3

[13] PIELECHA, I., CIEŚLIK, W., SZAŁEK, A. The use of electric drive in urban driving conditions using a hydrogen powered vehicle – Toyota Mirai. *Combustion Engines*. 2018, **172**(1), 51-58. https://doi.org/10.19206/CE-2018-106

[14] PIELECHA, I., CZAJKA, J., WISŁOCKI, K. et al. Wpływ stopnia naładowania akumulatorów na warunki pracy napędu hybrydowego w teście NEDC. *Technika Transportu Szynowego*. 2013, **10**.

[15] REDDY, J., NATARAJAN, S. Energy sources and multi-input DC-DC converters used in hybrid electric vehicle applications – A review. *International journal of hydrogen energy*. 2018, **43**, 17387-17408. https://doi.org/10.1016/j.ijhydene.2018.07.076

[16] TOMAR, M., CHOUDHARY, M., JAIN, D. et al. Performance analysis and economic feasibility of fuel cell vehicles: a perspective review. *SAE Technical Paper* 2020-01-2256, 2020. https://doi.org/10.4271/2020-01-2256

[17] TRAN, D., VAFAEIPOUR, M., EL BAGHDADI, M. et al. Thorough state-of-the-art analysis of electric and hybrid vehicle powertrains: topologies and integrated energy management strategies. *Renewable and Sustainable Energy Reviews*. 2020, **119**, 109596. https://doi.org/10.1016/j.rser.2019.109596

Andrzej Szałek, DEng. – Toyota Motor Poland Company Limited, Warsaw.
e-mail: *andrzej.szalek@toyota.pl*

Article citation info:
SOKOLNICKA-POPIS, B., SZYMLET, N., SIEDLECKI, M. et al. The impact of particulate filter substrate type on the gaseous exhaust components emission. *Combustion Engines*. 2020, **183**(4), 58-62. https://doi.org/10.19206/CE-2020-409

Barbara SOKOLNICKA-POPIS
Natalia SZYMLET
Maciej SIEDLECKI
Dawid GALLAS

CE-2020-409

The impact of particulate filter substrate type on the gaseous exhaust components emission

The article presents ceramic and metal substrate filtration efficiency in the particulate filter of a spark-ignition engine with direct fuel injection. Gaseous exhaust components were taken into account. There are many publications on the solid particles mass and number reduction, so the authors examined the effect of catalytic carriers on gaseous compounds, such as CO, NO_x, THC, whose content also poses a threat to human health and life, and this issue is not often described in the literature dedicated to measurements of modern internal combustion engines. During the tests, the length and carrier material effect on the emission of harmful substances in exhaust gases was determined.

Key words: *filtration, emission, particulate filter, gaseous components, combustion*

1. Introduction

Vehicle engines are constantly improved and modernized as a result of the need to meet existing exhaust emissions standards. It is not possible to meet them without the advanced exhaust gas purification systems use. From 2018, the biggest changes concerned the introduction of a particulate filter for motor vehicles with SI engines. The development of a particulate filter dedicated to gasoline engines (GPF) includes meeting certain requirements: appropriate filtration quality, structural strength, high oxygen storage capacity, small dimensions and cost.

The particulate filter combined with the three-way catalytic converter must meet the requirements for both particulate mass and number, nitrogen oxides, hydrocarbons and carbon monoxide emission limits. The performance characteristics of filters adapted for gasoline-fueled engines are different than for diesel-fueled engines. The different composition of the air-fuel mixture and the combustion temperature in both engines affect the rate of ash accumulation and the frequency of filter regeneration. The brand new filter, in which there is still no soot accumulated inside, has an efficiency of 60%. To improve performance, a thicker catalytic layer is used. Increased efficiency was also noted as a result of the filtering properties of accumulated ash, as a result of which the filter efficiency increases to 80–90% [2].

Ceramic filters are the most commonly used solution in engine applications, which is associated with high temperature resistance. At the same time, the filter heating process is extended, which is also characterized by much lower resistance to mechanical damage compared to metal substrates [1, 2].

This does not change the number of vehicles with filters having a metal substrate, although the solution with a ceramic one is more widely described in the literature worldwide. The type of substrate, its geometrical configuration and technical parameters constitute the basic criterion for the selection of an element of the aftertreatment system for a given vehicle. Additional factors are currently being investigated, including low-ash oil and its effect on GPF [7].

The article compares the impact of the used substrate on the emission of gaseous exhaust components. Research centers around the world are focusing on mass emissions and particle numbers, although this is not the only criterion to be suggested when assessing the performance of a particle filter.

2. Methodology

2.1. Research stand

The test cycle was recorded during the drive in real traffic conditions according to RDE (*Real Driving Emissions*) test procedure introduced in September 2017. Real-world tests are an extension of the current WLTP (*Worldwide Harmonized Light Vehicles Test Procedure*) test [9]. During the actual drive, external factors such as weather conditions, congestion and the influence of the driving style are taken into account. The different colors are responsible for the type of route and the relevant speed regulations. (Fig. 1). The engine was located at the AUTOMEX engine dynamometer (Fig. 2). The engine used in laboratory test had the same technical parameters as the test vehicle (Table 1).

Fig. 1. Original research RDE route

The tests were carried out on a dynamic engine dynamometer equipped with an engine approved according to the Euro 5 standard with a displacement of 1197 cm^3. The test route was limited to an urban and extra-urban cycle as the exhaust gas temperature for the motorway cycle was too high to be reflected on the test bench. Performing the test for the full route corresponding to the RDE cycle could

Received 5 August 2020; Received in revised form 2 November 2020; Accepted 4 November 2020
Available online 15 December 2020

damage the measuring equipment due to insufficient cooling of the system. Reflecting the actual operation conditions with the use of a brake stand, it is possible to test many filters with the same equipment and configuration of the test stand which reduces the cost and time associated with the need to install each filter in the exhaust system of a real vehicle.

Table 1. Tested vehicle technical data

Engine type	Spark-ignition
Displacement [cm^3]	1197
Cylinders setup	inline
Number of cylinders	4
Power [kW]	77
Maximum torque [Nm]	160
Injection type	direct

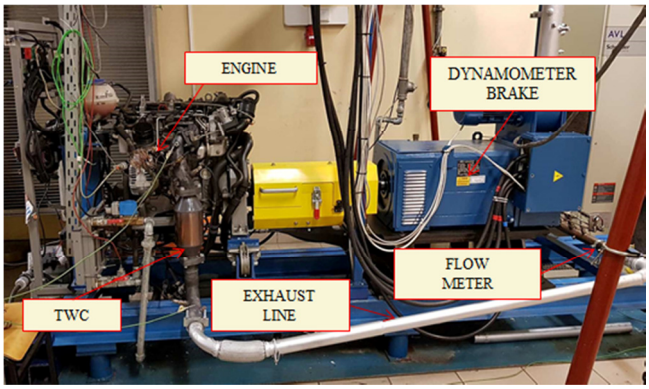

Fig. 2. View of the test stand

2.2. Measurement equipment

The tests were carried out using measuring equipment from the PEMS group – SEMTECH DS (*Portable Emissions Measurement Systems*), which is equipped with analyzers for measuring the content of harmful components in exhaust gases (Fig. 3). The exhaust mass flow probe takes a sample, which is then transported through a special tube that maintains a temperature of 191 degrees Celsius. This prevents the condensation of hydrocarbons that can cause device damage. Filtering the sample removes particulate matter. In such a sample prepared in this way, the hydrocarbon content is first determined. After the sample is cooled, it is sent to the analyzer with an ultraviolet detector, which measures the concentration of nitrogen oxide and dioxide. Carbon monoxide and carbon dioxide are tested using infrared (*Non-Dispersive Infrared Detector*). The last stage of the test is the measurement of the oxygen content in the exhaust gas. This is made possible by an electrochemical sensor. The SEMTECH DS analyzer has access to information contained in the vehicle's OBD system, such as rotational speed or engine load. With the help of the GPS system, it is possible to reflect the route using visualization tools. During both real and laboratory tests, the apparatus was zeroed and calibrated in accordance with the manufacturer's recommendations [4].

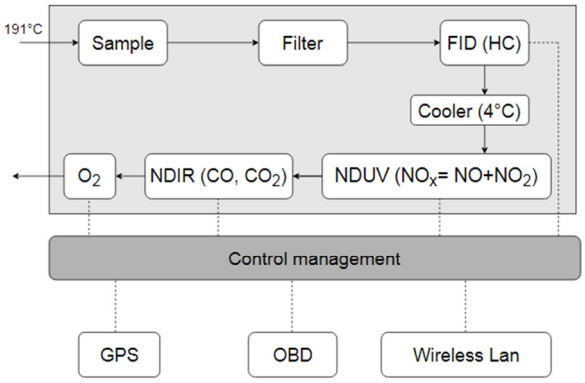

Fig. 3. SEMTECH DS – operation diagram

2.3. Research objects

Three configurations of the exhaust system equipped with a three-way catalyst, a particulate filter with a ceramic and a metal substrate were tested (Table 2). In addition to the material from which the interior of the filter was made, the elements differed in geometry, cell placement, length and thermal properties resulting from the material used [5]. The catalyst layer of each of the filters is the know-how of the manufacturer and has not been taken into account as a criterion for assessing filtration efficiency. The background for the research is the original three-way catalyst, which is the equipment of each approved vehicle (Fig. 5). It corresponds to exhaust emissions for a system not equipped with a particulate filter. TWC was used in each configuration of the system, initially only TWC, TWC + ceramic filter and TWC + metal filter.

Tab. 2. Basic characteristics of filters

Substrate feature		
Type	ceramic	metal
Length	120 mm	160 mm
Diameter	150 mm	130 mm
Flow type	wall-through	flow-through

The ceramic substrate has an even distribution and a constant number of cells per square inch over the entire diameter of the filter (CPSI) (Fig. 6). The metal substrate was formed as a result of rolling the material with a wavy structure (Fig. 4). A filter with a ceramic substrate is characterized by the flow of exhaust gases between the walls. This improves the filtration efficiency by distributing the exhaust gas inside the filter.

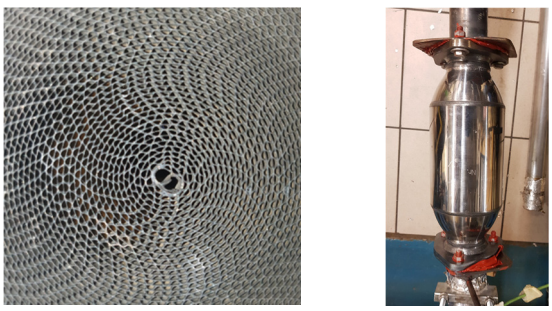

Fig. 4. View of the metal substrate inlet and particulate filter

Fig. 5. View of the TWC reactor used as a background results source

Fig. 6. View of the ceramic substrate inlet and particulate filter

3. Research results

The lowest CO_2 emission was recorded for the metal substrate, which may be due to lower flow resistance dictated by the largest actual cell size and reduced flow resistance in the central part (Fig. 7) [6].

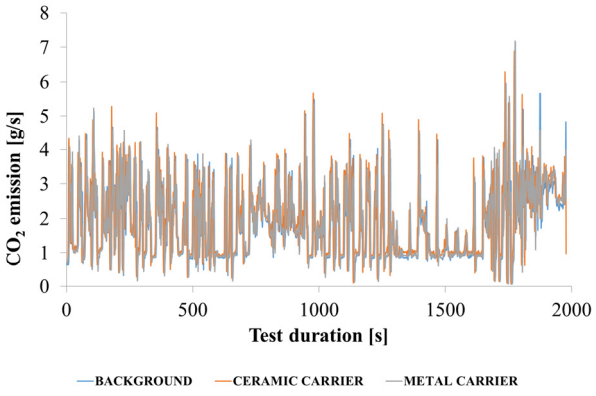

Fig. 7. Carbon dioxide emission intensity

In the case of carbon monoxide, an increased emission was recorded for a ceramic substrate, which may be caused by insufficient heating of the element and subsequent reaching the light-off temperature (Fig. 8) [10].

The phenomenon of incomplete combustion is reflected in hydrocarbon emissions (Fig. 9). The ceramic substrate has a long warm-up time, but also maintains temperature. Increased THC emission in the initial phase of the test results from the need to achieve the right temperature for more accurate combustion. The metal substrate is more susceptible to temperature fluctuations, and thus increased hydrocarbon emissions. Emission values are twice as high as for the ceramic substrate (Fig. 9).

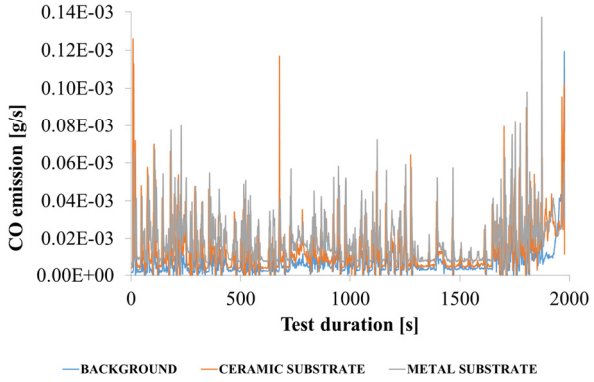

Fig. 8. Carbon dioxide emission intensity

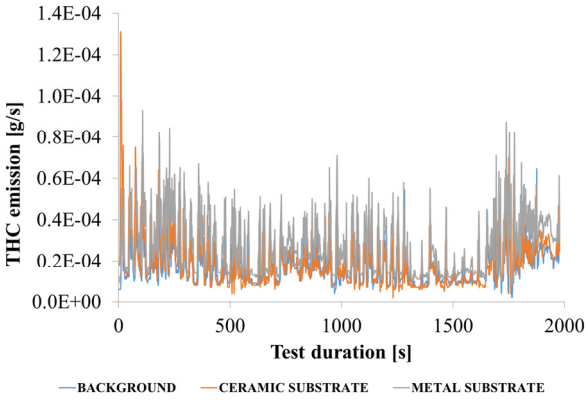

Fig. 9. Hydrocarbons emission intensity

High temperatures promote the formation of nitrogen oxides. The emission path for both substrates is similar. At the end of the test, the effectiveness of both solutions can be seen compared to a system that contains only a three-way catalytic converter (Fig. 10). Metal substrate has a greater impact on the reduction of nitrogen oxides, however, the total emission shows a greater efficiency of the ceramic substrate, which is not so susceptible to changes in thermal conditions.

The exhaust gas temperature was measured at the sampling point, i.e. at the end of the exhaust system. The first phase of the test corresponds to moving in urban conditions. Initially, the elements of the aftertreatment system absorbed the exhaust gas temperature, therefore the highest values were recorded for the system without particulate filters (Fig. 11).

In the extra-urban cycle, the temperature of all the systems was equalized, so that in the last part of the cycle, which reflects the conditions of traveling on the extra-urban route (vehicle speed between 60 km/h and 90 km/h), the highest values were achieved for the ceramic substrate and the system without filter. The metal substrate, due to its physicochemical properties, cools faster, so in the final phase of the test the temperature did not equalize with the ceramic substrate.

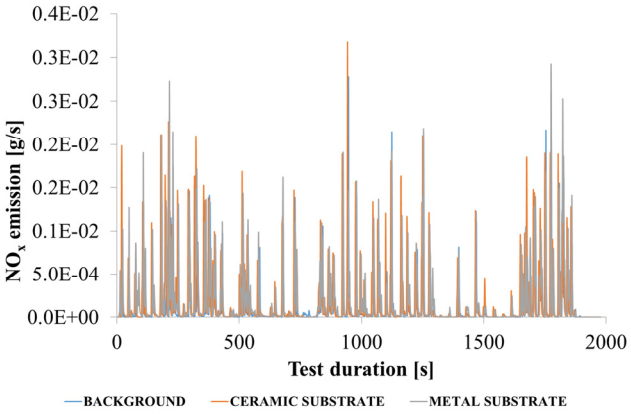

Fig. 10. Nitrogen oxides emission intensity

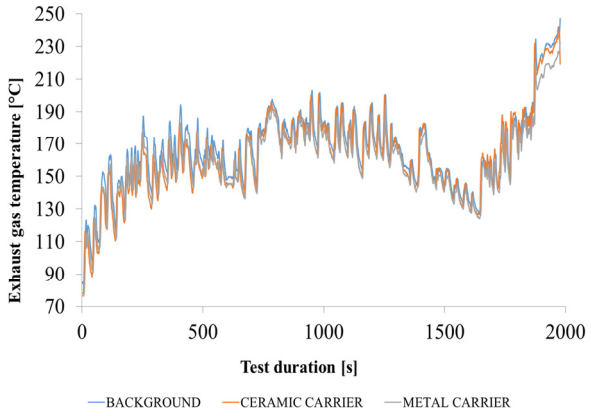

Fig. 11. Exhaust gas temperature during the test

4. Summary

The applicable regulations on pollutant emissions force vehicle manufacturers to use exhaust gas purification components. To achieve maximum efficiency, the solution has to be adapted to the specifics and operating conditions of the vehicle. The exhaust gas temperature of spark ignition engines is higher than for diesel fueled engines. This enables continuous filter regeneration, which ensures the removal of excess soot from the substrate during ongoing operation [3, 8].

The main purpose of gasoline particulate filters is their effect on reducing the content of solid particles in the exhaust gas, but it should be remembered that its operation does not remain indifferent to other exhaust gas components. Due to the small number of publications on this subject, the authors decided to conduct research in this area.

The research shows that, compared to the operation of the three-way catalyst, a filter with a ceramic substrate showed greater efficiency (Fig. 12). The exception was CO_2 emissions, which could have resulted from increased flow resistance. The time for the carrier to reach the light-off temperature (the appropriate operating temperature) is longer for the ceramic carrier, therefore its effectiveness at shorter distances is lower. Incomplete combustion of the mixture was more important in the case of a metal substrate filter. High susceptibility to temperature changes occurring in the system caused an increase in THC and CO emissions. The formation of NO_x is favored by the high combustion temperature of the mixture. The metal substrate undergoes temperature changes, caused for example by a sharp increase in vehicle speed.

The tests are also subjected to a combination of the ceramic filter substrate with a metal foam [6]. This is to combine the advantages of each solution, but so far no satisfactory results have been achieved due to pressure loss due to particle accumulation, therefore it is necessary to choose filters available on the market. Lack of guidelines and regulations determining the shape and other parameters of the carrier for individual treatment systems, manufacturers of particulate filters and catalytic reactors develop original technologies and designs. The freedom in choosing the shape, dimensions and density of the target results in the formation of carriers of different geometry and operational efficiency. The limitation of the test results is the difference between the performance of filters made of different materials, e.g. the type of catalytic layer. As part of further research, the authors will focus on comparing the filtration efficiency of elements made of the same materials in order to select the most effective configuration for a given type of engine.

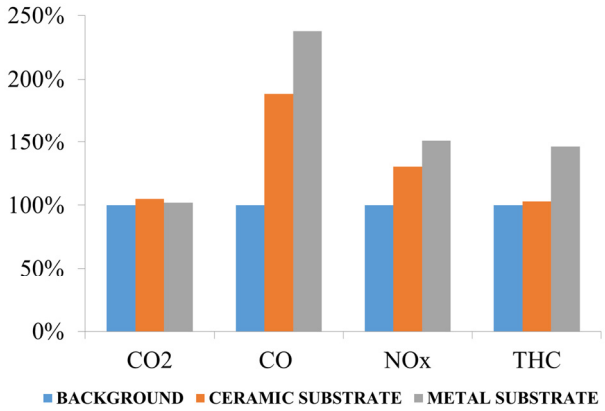

Fig. 12. Comparison of individual exhaust gas components emission related to TWC as a background values

Bibliography

[1] CUTTLER, W. Overview of ceramic materials for diesel particulate filter. *Ceramic Engineering and Science Proceedings Paper*. 2008. https://doi.org/10.1002/9780470291184.ch61

[2] LAMBERT, C., CHANKO, T., DOBSON, D. et al. Gasoline Particle Filter Development. *Emission Control Science and. Engineering*. 2017, **3**, 105-111. https://doi.org/10.1007/s40825-016-0055-x

[3] LEAHU, C., TARULESCU, R., TARULESCU, R. The exhaust gas temperature control through an adequate thermal-management of the engine. *IOP Conference Series Materials Science and Engineering*. 2018. https://doi.org/10.1088/1757-899X/444/7/072016

[4] MERKISZ, J., LIJEWSKI, P., FUĆ, P. et al. Measurement of exhaust emissions under actual operating conditions with the use of PEMS: Review of selected vehicles. *Improvement Trends for Internal Combustion Engines.* 2018. https://doi.org/10.5772/intechopen.70442

[5] PAVLOVIC, J., CIUFFO, B., FONTARAS, G. et al. How much difference in type-approval CO_2 emissions from passenger cars in Europe can be expected from changing to the new test procedure (NEDC vs. WLTP)? *Transportation Research Part A: Policy and Practice* 2018. https://doi.org/10.1016/j.tra.2018.02.002

[6] SARASAVADIYA, H., SHAH, M., SARKAR, I. et al. Performance of diesel particulate filter using metal foam combined with ceramic honeycomb substrate. *Springer.* 2018. https://doi.org/10.1007/978-981-13-2718-6

[7] SHAO, H., LAM, W., REMIAS, J. et al. Effect of lubricant oil properties on the performance of gasoline particulate filter (GPF). *SAE International Journal of Fuels and Lubricants* 2016, **9**(3), 650-658. https://doi.org/10.4271/2016-01-2287

[8] THAKRAL, N., PREMNATH, V., KHALEK, I. et al. Development of a burner-based test system to produce controllable particulate emissions for evaluation of gasoline particulate filters. *SAE Technical Paper* 2020-01-0389, 2020. https://doi.org/10.4271/2020-01-0389

[9] TSIAKMAKIS, S., CIUFFO, B., FONTARAS, J. et.al. Introducing a new emissions certification procedure for european light-duty vehicles: Monte Carlo simulation of the potential effect on fleet carbon dioxide emissions. *Transportation Research Record.* 2016, **2572**(1), 66-77. https://doi.org/10.3141/2572-08

[10] YANG, J., ROTH, P., DURBIN, T. et.al. Gasoline particulate filters as an effective tool to reduce particulate and PAH emissions from GDI vehicles: A case study with two GDI vehicles. *Environmental Science and Technology.* 2018, **52**(5), 3275-3284. https://doi.org/10.1021/acs.est.7b05641

Barbara Sokolnicka-Popis, MEng. – Faculty of Civil and Transport Engineering, Poznan University of Technology.
e-mail: *barbara.d.sokolnicka@doctorate.put.poznan.pl*

Natalia Szymlet, MEng. – Faculty of Civil and Transport Engineering, Poznan University of Technology.
e-mail: *natalia.r.szymlet@doctorate.put.poznan.pl*

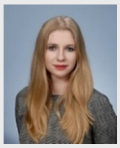

Maciej Siedlecki, MEng. – Faculty of Civil and Transport Engineering, Poznan University of Technology.
e-mail: *maciej.siedlecki@put.poznan.pl*

Dawid Gallas, MSc. – Faculty of Civil and Transport Engineering, Poznan University of Technology.
e-mail: *dawid.p.gallas@doctorate.put.poznan.pl*

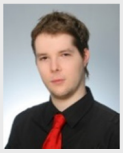

IX INTERNATIONAL CONGRESS ON COMBUSTION ENGINES

POLISH SCIENTIFIC SOCIETY OF COMBUSTION ENGINES

28th-29th June 2021

Lublin University of Technology
Faculty of Mechanical Engineering
Nadbystrzycka 36, 20-618 Lublin, Poland

IX INTERNATIONAL CONGRESS ON COMBUSTION ENGINES

POLISH SCIENTIFIC SOCIETY OF COMBUSTION ENGINES

28th-29th June 2021

The Polish Scientific Society of Combustion Engines and the Mechanical Engineering Faculty of the Lublin University of Technology cordially invite engineers and researchers to the 9th International Congress on Combustion Engines that will be held on June 28-29, 2021 in Lublin, Poland. This biennial event is a forum for the exchange of experiences between experts from science and industry, promoting and supporting the development of ICE science and engineering. The aim of the event is to present the latest achievements and state of the art in ICEs, also in a holistic and interdisciplinary context. Special attention will be given to new research results creating global trends that are important from the applicability perspective.

The Congress will host presentations and an exhibition, being a source of information and ensuring the dissemination of technical achievements and ideas related to ICEs. More and more frequently we observe that interdisciplinary teams, cooperating in various areas, participate in research works. Therefore, we invite participants not only from the field of ICE but also from related fields to share their experience and knowledge.

We encourage the ICE community to actively participate in thematic, interactive, problem and interdisciplinary sessions, and to attend meetings with experts and exhibitors. Participants will have an excellent opportunity to meet engineers and researchers from around the world and discuss current trends in the engine technology, share innovative ideas and promote collaboration.

CONGRESS TOPICS

- Engine combustion
- New engines, components, actuators and sensors
- Engine modelling
- Engine diagnostics and control
- Hybrid and electric powertrains
- Fuels and lubricants
- Exhaust emissions and aftertreatment

RESEARCH PAPERS

- All papers after positive review will be published in **Combustion Engines** journal (MNiSW: 20 pts).
- TOP 10 papers will be recommended for publication in a Congress special issue of the **International Journal of Engine Research** (IF: 2.382, MNiSW: 100 pts).

Deadline for submitting paper proposals (abstracts): ***February 28, 2021***

Lublin University of Technology
Faculty of Mechanical Engineering
Nadbystrzycka 36, 20-618 Lublin, Poland

INSTYTUT TECHNICZNY WOJSK LOTNICZYCH
ul. Księcia Bolesława 6, 01-494 Warszawa, skr. poczt. 96
tel.: 261 851 300; faks: 261 851 313
www.itwl.pl e-mail: poczta@itwl.pl

SYSTEM DIAGNOSTYKI TRIBOLOGICZNEJ

Pobieranie próbek oleju z silników, przekładni, skrzynek napędu, instalacji hydraulicznych	**Badania**	**Przekazanie informacji diagnostycznej**	
Użytkownik	Akredytowane laboratorium w ITWL	ITWL	Użytkownik

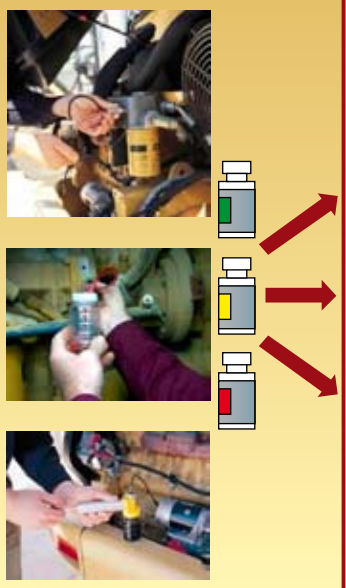

Analiza danych

Baza danych

Diagnoza

System Diagnostyki Tribologicznej (SDT), opracowany w Instytucie Technicznym Wojsk Lotniczych, przeznaczony jest do wspierania eksploatacji obiektów technicznych.

Na podstawie wyników badań próbek oleju pobranych z układów tribologicznych prowadzi się ocenę i prognozowanie stanu technicznego obiektów technicznych (statki powietrzne, pojazdy mechaniczne, statki wodne, maszyny robocze i inne).

PCA Polskie Centrum Akredytacji BADANIA AB 138

MON Akredytacja OIB JB 9/MON/2017

INSTYTUT TECHNICZNY WOJSK LOTNICZYCH
ZAKŁAD SILNIKÓW LOTNICZYCH
Akredytowane laboratorium:
Laboratorium Diagnostyki Systemów Tribologicznych

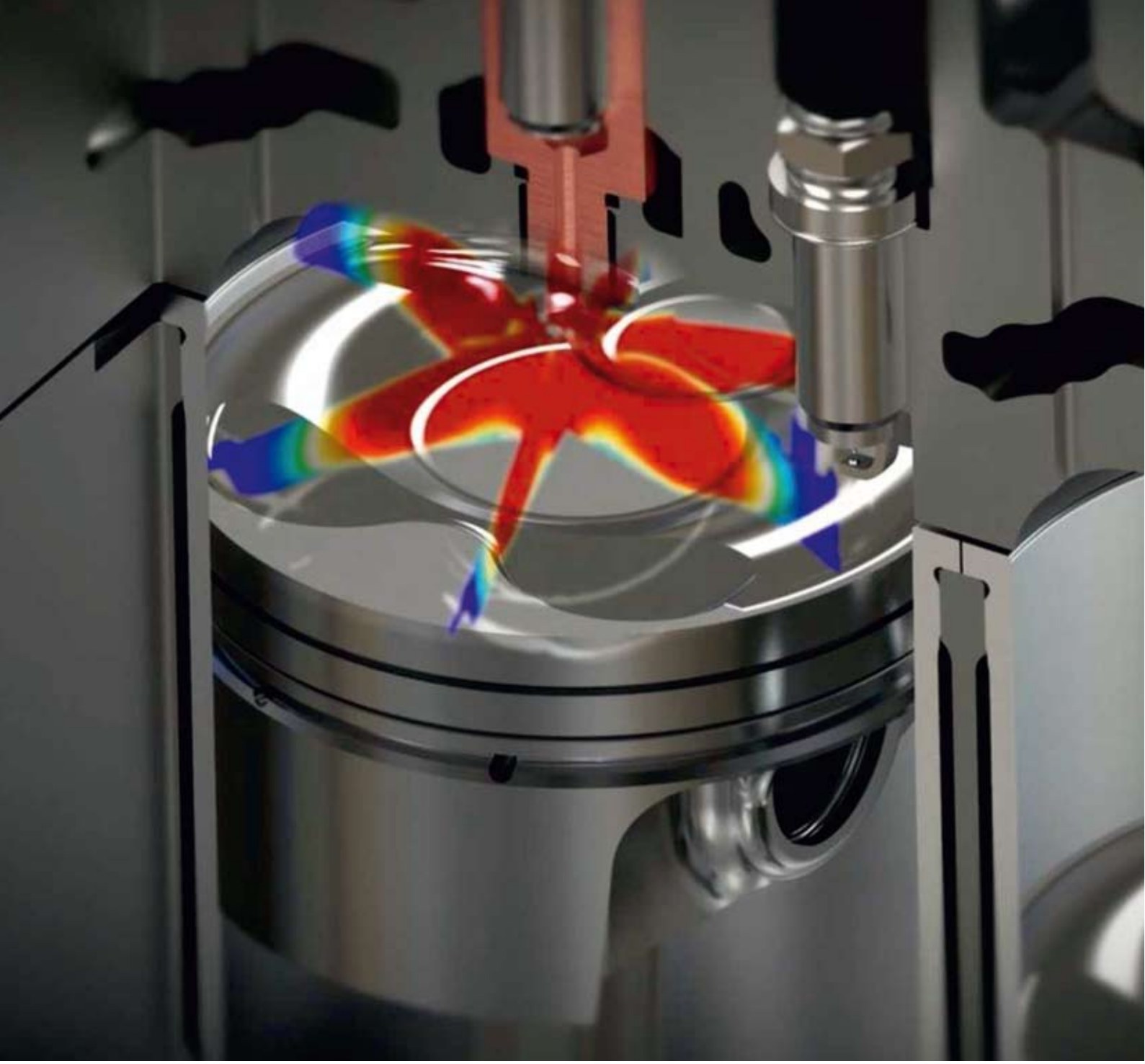

Publisher:

Polish Scientific Society of Combustion Engines

Combustion Engines

Polskie Towarzystwo Naukowe Silników Spalinowych

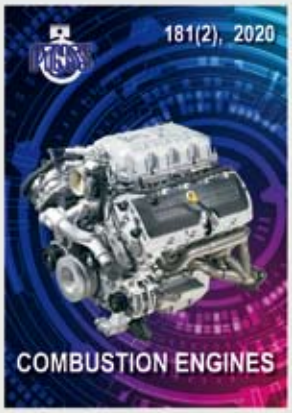

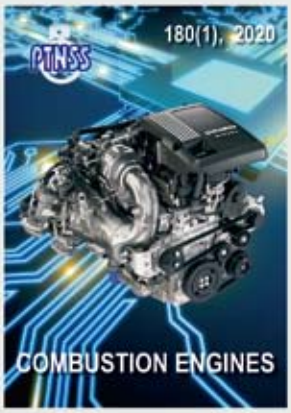

ISSN: 2300-9896
eISSN: 2658-1442

www.combustion-engines.eu